

Jo Søbstad Skjævesland and Joakim Horpestad

Quantifying the Impact of Integrating Wind Power on Composite Power System Reliability

Master's thesis in Energy and Environmental Engineering

Supervisor: Vijay Venu Vadlamudi

June 2021

Jo Søbstad Skjævesland and Joakim Horpestad

Quantifying the Impact of Integrating Wind Power on Composite Power System Reliability

Master's thesis in Energy and Environmental Engineering
Supervisor: Vijay Venu Vadlamudi
June 2021

Norwegian University of Science and Technology
Faculty of Information Technology and Electrical Engineering
Department of Electric Power Engineering



Quantifying the Impact of Integrating Wind Power on Composite Power System Reliability

J.S. Skjævesland and J. Horpestad

Abstract

Due to global efforts to combat climate change, renewable energy is currently seeing a boom in growth, with wind energy leading the way. Electric power generation from wind energy is different compared to that from conventional sources, due to the intermittent nature of the wind speed. Therefore, the operating characteristics of the wind energy facilities have a different impact on the reliability of the power system compared to that of conventional sources. The rapid development of wind energy installations can lead to increased pressure on electric power utilities. This thesis identifies and develops methods to evaluate and quantify the impact of significant wind power penetration on the reliability of composite power systems through probabilistic Monte Carlo Simulation methods.

Two fundamental Monte Carlo Simulation methods, the Sequential State Transition method, and the Non-sequential State Sampling method, are selected to include wind power penetration in composite system reliability assessment. Two different wind speed models, the auto-regressive moving average (ARMA) wind model and the Weibull distribution-based wind model, are included and compared in the composite system reliability assessment. The wind power modelling considerations are selected through an extensive literature review, which examines the state-of-the-art on the main topic of the thesis. The developed methods are applied to a DC-based contingency solver and an AC-based contingency solver for composite system state evaluation. The developed in-house software tools are tested on standard test systems suited for composite power system reliability evaluation through appropriate probabilistic indices and compared with selected corresponding benchmark results from the literature.

The thesis applies different wind speed regimes to case studies and compares the impact on the reliability of the system delivery points and the overall systems. Wind speed correlation between multiple wind sites is identified as an important parameter in the wind modelling process and is included in the wind speed models. The priority order load curtailment philosophy is used to control the load curtailments at the system delivery points. It is observed that the characteristics of the wind speed regime, transmission network, degree of wind speed correlation, and choice of load curtailment philosophy have a significant impact on the reliability of power systems with significant wind power penetration.

Sammendrag

Grunnet globale tiltak for å bremse klimaendringene har andelen installasjoner av fornybare energikilder i verden økt kraftig, med vindkraft som den ledende energikilden. Den leverte elektriske kraften fra vindkraftanlegg er svært annerledes fra tradisjonelle energikilder, grunnet de periodiske og tilfeldige egenskapene til vind. Derfor har driftsegenskapene til vindkraftanlegg en annen innvirkning på påliteligheten til kraftsystemer, sammenlignet med tradisjonelle energikilder. Den raske utviklingen av vindkraftinstallasjoner kan føre til et økende press for kraftselskaper. Denne avhandlingen identifiserer og utvikler metoder for å evaluere og beregne påliteligheten til sammensatte kraftsystemer som inkluderer kraftproduksjon og overføringsnett, gjennom Monte Carlo simuleringsteknikker.

To grunnleggende Monte Carlo simuleringsteknikker, den sekvensielle teknikken *state transition* og den ikke-sekvensielle teknikken *state sampling*, er valgt til å inkludere vindkraft i sammensatte kraftsystemanalyser. To ulike vindhastighetsmodeller, basert på autoregressiv-glidende gjennomsnittsmodell og Weibullfordelingen er utviklet og sammenlignet i analysen. Betraktninger i forhold til modelleringen av vindkraft er nøye utvalgt gjennom en grundig litteraturstudie, som undersøker ulike metoder og tilnærminger i litteraturen. De utviklede metodene er anvendt på systemtilstandanalyser basert på DC lastflyt og AC lastflyt, tilpasset sammensatte kraftsystemer. De utviklede programmene er testet på standardiserte testsystemer som er tilpasset sammensatte kraftsystemer, og sammenlignet med tilsvarende resultater fra andre studier.

Avhandlingen anvender ulike vindhastighetsregimer i ulike analyser, og sammenligner påvirkningen på påliteligheten til lastpunkter og hele systemer sett under ett. Korrelasjon mellom vindhastigheter fra ulike lokasjoner er identifisert som en viktig parameter i vindmodelleringen, og inkluderes i vindhastighetsmodellene. Lastreduksjonen i systemene kontrolleres ved å rangere lastpunktene etter en prioritetsliste. Det er observert at karakteristikken til vindhastighetregimene, graden av korrelasjon mellom vindhastighetene og valg av lastreduksjonsmetode har en betydelig innvirkning på påliteligheten til kraftsystemer med en betydelig andel vindkraft.

Acknowledgement

We would like to express our sincerest gratitude and appreciation to our supervisor, Associate Professor Vijay Venu Vadlamudi at the Department of Electric Power Engineering NTNU, for his guidance and support during the last year. Thank you for always helping us thoroughly and guiding us in the right direction.

Parts of the conducted work build on the existing work conducted at the Department of Electric Power Engineering at NTNU; especially the work of previous Master's student Øystein Stake Laengen has been very helpful.

Through this collaborative venture, we were able to rely on each other's strengths during all the highs and lows of the project phase; we got to be there together through the numerous challenges and discover the joys (and the occasional sorrows) and nuances of research, and the experience has left us humbled and hopefully, wiser. We gratefully acknowledge each other's role in our professional growth through this adventure.

Trondheim, 11 June 2021

Jo Søbstad Skjævesland
Joakim Horpestad

Contents

List of Figures	xi
List of Tables	xiv
1 Introduction	1
1.1 Background	1
1.2 Scope	2
1.3 Thesis Contribution	2
1.4 Thesis Structure	3
2 Conceptual Background and Literature Review	4
2.1 Basics of Power System Reliability	4
2.1.1 Defining Power System Reliability	4
2.1.1.1 Adequacy	4
2.1.1.2 Security	4
2.1.2 Hierarchical Levels	5
2.1.2.1 HL-I: Generation System	5
2.1.2.2 HL-II: Composite System	5
2.1.2.3 HL-III: Whole Power System	5
2.1.3 Evaluating the Adequacy Aspect of Power System Reliability	5
2.1.3.1 Loss of Load Events	6
2.1.4 The Load Model	6
2.1.5 The Generation System Model	7
2.1.5.1 Forced Outage Rate	7
2.1.5.2 COPT	8
2.1.6 Reliability Indices	9
2.1.6.1 Loss of Load Probability - LOLP	9
2.1.6.2 Loss of Load Expectation - LOLE	10
2.1.6.3 Expected Energy Not Served - EENS	10
2.1.7 Monte Carlo Simulation in Power System Reliability	12
2.1.7.1 State Sampling Approach	12
2.1.7.2 State Sampling Example	13

2.1.7.3	State Duration Approach	13
2.1.7.4	State Transition Approach	15
2.1.7.5	State Transition Example	16
2.1.7.6	Reliability Indices Using MCS	17
2.1.7.7	Reliability Index Example	18
2.1.8	Composite System Adequacy	19
2.1.9	Additional MCS Sampling and Data	20
2.1.9.1	Generator Data	20
2.1.9.2	Line Data	20
2.1.9.3	Bus Data	20
2.1.9.4	Selection of System States	21
2.1.9.5	Isolated Buses	22
2.1.10	AC-Based Load Flow Analysis	22
2.1.11	DC-Based Load Flow Analysis	22
2.1.12	DC Optimisation Problem Formulation	24
2.1.13	AC Optimisation Problem Formulation	25
2.1.14	General Approach	27
2.2	Literature Review and State-of-the-Art	29
2.2.1	The Need for New Reliability Criteria and the GARPUR Project	29
2.2.2	The Well-Being Analysis - Combining Deterministic and Probabilistic Methods	30
2.2.3	Concerns Related to Wind Power	31
2.2.4	The Concept of Capacity Credit	31
2.2.5	Wind Power Considerations	31
2.2.6	The Wind Speed	32
2.2.7	The Wind Turbine Generator	33
2.2.8	Developed Tools for HL-II Evaluation	34
2.2.9	Correlated Wind Speeds	35
2.2.10	Building a Comprehensive Framework for Conducting PSR Assessment at NTNU	36
2.3	Fundamental Knowledge of the Wind-Related Topics	36
2.3.1	Wind Speed Modelling	36
2.3.1.1	Weibull Distribution	37

2.3.1.2	ARMA	38
2.3.2	Wind Turbine Generator Modelling	39
2.3.3	Wind Speed Correlation	41
3	Methodological Approach	44
3.1	Load Model	44
3.2	Non-sequential State Sampling Approach	45
3.3	Sequential State Transition Approach	46
3.4	Wind Speed Correlation	48
3.4.1	Weibull Model	48
3.4.2	ARMA Model	50
3.5	Illustrative Example	52
3.5.1	The System Specifications	52
3.5.2	Initialisation and Pre-Calculation Work	53
3.5.3	Main Loop Calculations	54
3.5.4	First State Transition in Main Loop	54
3.5.5	Determining Available Generating Capacity	55
3.5.5.1	Determining Correlated Wind Speeds	55
3.5.6	Calculating the Reactance Matrix and the Distribution Factors	56
3.5.7	Calculating OPF Constraints	58
3.5.7.1	Cost Function	58
3.5.7.2	Equality Constraint	59
3.5.7.3	Decision Variable Bounds	59
3.5.7.4	Inequality Constraints	59
3.5.8	OPF Problem Formulation	60
3.5.9	OPF Results	61
3.5.10	Further Calculations	62
4	Case Studies and Results	63
4.1	Test Systems	63
4.2	Verifying the Developed Script: Swift Current Case Study	63
4.2.1	20MW WECS Added to the MRBTS	64
4.2.1.1	DC-based Load Flow Approach	65

4.2.1.1.1	State Sampling	65
4.2.1.1.2	State Transition	65
4.2.1.2	AC-based Load Flow Approach	66
4.2.1.2.1	State Sampling	66
4.2.1.2.2	State Transition	66
4.2.1.3	Benchmark comparison: DC-based State Sampling MCS	68
4.2.1.4	Benchmark Comparison: AC-based Sequential MCS	69
4.2.2	600 MW WECS Added to the RTS	70
4.2.2.1	State Sampling	70
4.2.2.2	State Transition	71
4.2.2.3	Benchmark Comparison: DC-based State Sampling MCS	72
4.2.3	Multiple WECS at RTS by Incorporating Wind Speed Correlation	73
4.2.3.1	300 MW WECS Added at Buses 1 and 3	74
4.2.3.2	Benchmark Comparison: DC-based State Sampling MCS with Correlation	75
4.2.4	Observations and Discussion	76
4.3	Ørland Case Study	80
4.3.1	The Wind Speed Data	80
4.3.1.1	The Weibull Model	80
4.3.1.2	The ARMA Model	81
4.3.2	RBTS	82
4.3.2.1	State Sampling	82
4.3.2.2	State Transition	83
4.3.3	RTS	84
4.3.3.1	State Sampling	84
4.3.3.2	State Transition	84
4.3.4	Observations and Discussion	85
4.3.5	Sensitivity Analyses	87
4.3.5.1	Degree of Wind Power Capacity	87
4.3.5.2	Single Site Location Analysis	88
4.3.5.3	Wind Speed Correlation Between Two Sites	89
4.3.5.4	Wind Turbine Generators Replacing Conventional Generators	90

4.3.5.5	Increasing the System Peak Load	91
4.3.5.6	Number of Wind Farms	93
5	Conclusions and Future Work	95
5.1	Conclusions	95
5.2	Future Work	96
	References	98
	Appendix	A-1
A	RBTS	A-1
A.1	The RBTS Generator Data	A-2
A.2	The RBTS Network Data	A-2
A.3	The RBTS Bus Data	A-3
B	IEEE-RTS	B-1
B.1	The RTS Generator Data	B-2
B.2	The RTS Network Data	B-3
B.3	The RTS Bus Data	B-5
C	Test System Load	C-1
D	MATLAB Codes	D-1
D.1	wtg-poweroutput	D-1
D.2	ARMAy	D-1
D.3	ARMAyCor	D-1
D.4	ARMAywind	D-2
D.5	unifrnd_corr	D-2
D.6	weibull	D-2
D.7	Solver_excerpt	D-3
D.8	WTGSamplingSS	D-3
D.9	WTGSamplingST	D-4
E	LOLE-estimates	E-1
E.1	MRBTS: 20MW WECS with the Swift Current wind-regime	E-1

E.1.1	DC	E-1
	E.1.1.1 State Sampling	E-1
	E.1.1.2 State Transition	E-1
E.1.2	AC	E-2
	E.1.2.1 State Sampling	E-2
	E.1.2.2 State Transition	E-2
E.2	RTS: 600MW WECS with the Swift Current wind-regime	E-3
	E.2.1 State Sampling	E-3
	E.2.2 State Transition	E-4
E.3	RBTS: 20MW WECS with the Ørland wind-regime	E-5
	E.3.1 State Sampling	E-5
	E.3.2 State Transition	E-5
E.4	RTS: 600MW WECS with the Ørland wind-regime	E-6
	E.4.1 State Sampling	E-6
	E.4.2 State Transition	E-7
E.5	Wind Speed Correlation	E-8
F	Standard Deviation of EENS-estimates	F-1
F.1	MRBTS: 20MW WECS with the Swift Current wind-regime	F-1
	F.1.1 DC	F-1
	F.1.1.1 State Sampling	F-1
	F.1.1.2 State Transition	F-1
	F.1.2 AC	F-2
	F.1.2.1 State Sampling	F-2
	F.1.2.2 State Transition	F-2
F.2	RTS: 600MW WECS with the Swift Current wind-regime	F-3
	F.2.1 State Sampling	F-3
	F.2.2 State Transition	F-4
F.3	RBTS: 20MW WECS with the Ørland wind-regime	F-5
	F.3.1 State Sampling	F-5
	F.3.2 State Transition	F-5
F.4	RTS: 600MW WECS with the Ørland wind-regime	F-6
	F.4.1 State Sampling	F-6

F.4.2	State Transition	F-7
F.5	Wind Speed Correlation	F-8
G	Standard Deviation of LOLE-estimates	G-1
G.1	MRBTS: 20MW WECS with the Swift Current wind-regime	G-1
G.1.1	DC	G-1
G.1.1.1	State Sampling	G-1
G.1.1.2	State Transition	G-1
G.1.2	AC	G-2
G.1.2.1	State Sampling	G-2
G.1.2.2	State Transition	G-2
G.2	RTS: 600MW WECS with the Swift Current wind-regime	G-3
G.2.1	State Sampling	G-3
G.2.2	State Transition	G-4
G.3	RBTS: 20MW WECS with the Ørland wind-regime	G-5
G.3.1	State Sampling	G-5
G.3.2	State Transition	G-5
G.4	RTS: 600MW WECS with the Ørland wind-regime	G-6
G.4.1	State Sampling	G-6
G.4.2	State Transition	G-7
G.5	Wind Speed Correlation	G-8

List of Figures

1.1	TWh Onshore wind power generation in the Sustainable Development Scenario, 2000-2030 [2]	1
1.2	TWh Offshore wind power generation in the Sustainable Development Scenario, 2000-2030 [2]	1
2.1	Division of reliability	4
2.2	Hierarchical levels in power system reliability studies	6
2.3	Illustration of the load models for a particular week	7
2.4	A visualisation of the state duration approach on a three-generator HL-I system. .	14
2.5	Visualisation of how the next state in the State Transition approach is obtained. .	16
2.6	A flowchart representing how to determine if a state in a HL-II analysis is a Loss-of-Load (LOL) situation, based on the methodology presented in [6].	28
2.7	The GARPUR Partners, consisting of 7 European Transmission System Operators, along with 12 universities and research centres [21]	30
2.8	The system well-being analysis model	30
2.9	Typical uncertainties in power systems [40]	32
2.10	Simplified, illustrative layout of an ANN model [48]	33
2.11	Example of a multi-state model for a wind unit [39]	34
2.12	The Weibull Probability Density Functions with selected Weibull scale and shape parameters.	38
2.13	The general shape of a power curve for a WTG.	39
2.14	Illustration of the intermittent nature of the wind speed and the corresponding output power from a wind turbine generator.	40
3.1	A flowchart detailing how the State Sampling algorithm works.	46
3.2	A flowchart detailing how the State Transition algorithm works.	48
3.3	Flowchart showing the algorithmic process of attaining correlated wind speeds with the Weibull model.	49
3.4	Scatter plots of correlated random numbers. Left: R=0.2. Middle: R=0.5. Right: R=0.8.	50
3.5	Scatter plots of correlated pairs of wind speed obtained from the Weibull wind speed model. Left: R=0.2. Middle: R=0.5. Right: R=0.8.	50
3.6	Flowchart showing the algorithmic process of attaining correlated wind speeds with the ARMA model.	51
3.7	Scatter plots of normally distributed correlated random numbers with mean $\mu = 0$ and variance $\sigma^2 = 0.52476^2$. Left: R=0.2. Middle: R=0.5. Right: R=0.8.	51

3.8	Scatter plots of correlated pairs of wind speed obtained from the Swift Current wind speed model. Left: $R=0.2$. Middle: $R=0.5$. Right: $R=0.8$	52
3.9	The system configuration used in the illustration example.	53
3.10	The system with calculated line flows.	61
4.1	Single line diagram of the MRBTS.	64
4.2	Comparison of the system-EENS in the MRBTS before and after the wind penetration, obtained by the State Sampling and State Transition techniques	66
4.3	Comparison of the system-EENS in the MRBTS before and after the wind penetration, obtained by the State Sampling and State Transition techniques	67
4.4	Benchmark comparison of the EENS at the buses in the MRBTS before and after wind penetration	68
4.5	Benchmark comparison of the system-EENS for the DC-State Sampling approach in the MRBTS before and after the wind penetration	69
4.6	Benchmark comparison of the system-EENS for the AC-State Transition approach in the MRBTS before and after the wind penetration	70
4.7	Comparison of the system-EENS in the RTS before and after the wind penetration, obtained by the State Sampling and State Transition techniques	72
4.8	Benchmark comparison of the EENS at the buses in the RTS before and after the wind penetration	73
4.9	Benchmark comparison of the system-EENS in the RTS before and after the wind penetration	73
4.10	The system-EENS of the RTSW-1&3-Swift Current and Regina Case with the ARMA and Weibull models	75
4.11	Benchmark comparison of the system-EENS of the RTSW-1&3-Swift Current and Regina Case	76
4.12	A plot of 2000 consecutive data points for the Ørland historical data.	80
4.13	A plot of 2000 consecutive data points for the Ørland Weibull model.	81
4.14	A plot of 2000 consecutive data points for the Ørland ARMA model.	81
4.15	A plot of the different wind models for Ørland against each other. Data is sampled for a 5 year period.	82
4.16	Comparison of the system-EENS in the RBTS before and after the wind penetration, obtained by the State Sampling and State Transition techniques	83
4.17	Comparison of the system-EENS in the RTS before and after the wind penetration, obtained by the State Sampling and State Transition techniques	85
4.18	The Weibull probability density functions for Ørland and Swift Current.	86
4.19	The system EENS for different levels of installed wind power capacity at bus 19 in the RTS.	87
4.20	The system EENS for addition of WECS at different single sites.	88

4.21	The system EENS for different levels of wind speed correlation between bus 1 and bus 3.	89
4.22	The Weibull probability density functions for Swift Current, Regina and Ørland. . .	90
4.23	The system EENS with removed existing conventional generators in the RTS. . . .	91
4.24	The system EENS for different levels of increased peak load.	92
4.25	The system EENS for different numbers of wind sites.	94
A.1	Single line diagram of the RBTS	A-1
B.1	Single line diagram of the RTS [70]	B-1

List of Tables

2.1	Simplified 3-unit example system units	8
2.2	Simplified 3-unit example system. The two 3MW units are in service	9
2.3	Simplified 3-unit example system. The 5MW unit is in service.	9
2.4	Simplified 3-unit example system. The 5MW unit is on outage	9
2.5	COPT for the simplified 3-unit example system.	9
2.6	Reliability standards in European countries [16]	11
2.7	Calculation of EENS for a simplified system	11
2.8	The randomly generated variables for the State Transition example.	17
2.9	λ values for the State Transition example.	17
2.10	The resulting states and durations for the State Transition example.	17
2.11	MCS data for reliability index calculation.	19
2.12	Input data for the generation model. State Sampling MCS AC-based approach . .	20
2.13	Input data for the AC-based contingency solver. State Sampling MCS.	20
2.14	Bus data for the AC based approach.	21
3.1	The generator parameters for the illustration example.	52
3.2	The bus parameters for the illustration example.	53
3.3	The line parameters for the illustration example.	53
3.4	The WTG and wind speed parameters for the illustration example.	53
3.5	The intervals corresponding to component transfer for the illustration example. . .	54
4.1	The wind speed data for Swift Current [53]	63
4.2	Estimated Weibull scale and shape parameters for the Swift Current wind-regime .	64
4.3	Obtained estimates for the MRBTSW-4 State Sampling DC-case study	65
4.4	Obtained estimates for the MRBTSW-4 State Transition DC-case study	65
4.5	Obtained estimates for the MRBTSW-4 State Sampling AC-case study	66
4.6	Obtained estimates for the MRBTSW-4 State Transition AC-case study	67
4.7	MRBTS-Swift Current case comparison against the State Sampling MECORE program benchmark results	68
4.8	MRBTS-Swift Current case comparison against the Sequential RapHL-II program benchmark results	69
4.9	Obtained estimates for the RTSW-19 State Sampling case study	71
4.10	Obtained estimates for the RTSW-19 State Transition case study	71

4.11	RTS-Swift Current case comparison against the State Sampling MECORE program benchmark results	72
4.12	The wind speed data for Regina and Swift Current, Canada [53]	74
4.13	Estimated Weibull scale and shape parameters for the Regina wind site	74
4.14	The system EENS for the RTS with different degrees of wind speed correlation . .	74
4.15	RTSW-1&3-Swift Current and Regina Case comparison against the State Sampling MECORE program benchmark results	75
4.16	Bus IEAR-values and priority order in the RBTS utilised in the MECORE Software [55].	77
4.17	Bus IEAR-values and priority order in the RBTS utilised in this thesis.	77
4.18	Bus IEAR-values and priority order in the RTS utilised in the MECORE Software [55].	78
4.19	Bus IEAR-values and priority order in the RTS utilised in this thesis.	78
4.20	The wind speed data for Ørland [53]	80
4.21	Estimated Weibull parameters for the Ørland wind-regime	80
4.22	Average output power from the WTGs using the different models for Ørland. . . .	82
4.23	Obtained estimates for the Ørland RBTSW-4 State Sampling case study	83
4.24	Obtained estimates for the Ørland RBTSW-4 State Transition case study	83
4.25	Obtained estimates for the Ørland RTSW-19 State Sampling case study.	84
4.26	Obtained estimates for the Ørland RTSW-19 State Transition case study.	85
4.27	System-EENS for wind speed correlation at RTS with the Ørland wind regime. . .	89
4.28	System-EENS while removing conventional generation from the RTS.	91
4.29	System-EENS for system load increases in RTS with the Ørland wind regime. . . .	92
4.30	System-EENS for the RTS with multiple, correlated wind sites with the Ørland wind speed regime	93
A.1	The generator data of the RBTS test system	A-2
A.2	The outage data of the RBTS network.	A-2
A.3	The RBTS network parameters.	A-2
A.4	The Bus data of the RBTS	A-3
B.1	The generator data of the IEEE-RTS	B-2
B.2	The outage data of the RTS network.	B-3
B.3	The RTS network parameters.	B-4
B.4	The Bus data of the RTS	B-5
C.1	The weekly peak load, used in the hourly peak load model for all simulations. . . .	C-1

C.2	The weekday peak load, used in the hourly peak load model for all simulations. . .	C-1
C.3	The hourly peak load, used in the hourly peak load model for all simulations. . . .	C-2
E.1	Obtained LOLE-estimates for the MRBTBW-4 State Sampling DC-case study, corresponding to Table 4.3.	E-1
E.2	Obtained LOLE-estimates for the MRBTBW-4 State Transition DC-case study, corresponding to Table 4.4	E-1
E.3	Obtained LOLE-estimates for the MRBTBW-4 State Sampling AC-case study, corresponding to Table 4.5.	E-2
E.4	Obtained LOLE-estimates for the MRBTBW-4 State Transition AC-case study, corresponding to Table 4.6.	E-2
E.5	Obtained LOLE-estimates for the RTBW-19 State Sampling case study, corresponding to Table 4.9.	E-3
E.6	Obtained LOLE-estimates for the RTBW-19 State Transition case study, corresponding to Table 4.10.	E-4
E.7	Obtained LOLE-estimates for the Ørland RBTWS-4 State Sampling case study, corresponding to Table 4.23.	E-5
E.8	Obtained LOLE-estimates for the Ørland RBTWS-4 State Transition case study, corresponding to Table 4.24.	E-5
E.9	Obtained LOLE-estimates for the Ørland RTBW-19 State Sampling case study, corresponding to Table 4.25.	E-6
E.10	Obtained LOLE-estimates for the Ørland RTBW-19 State Transition case study, corresponding to Table 4.26.	E-7
E.11	Obtained LOLE-results for wind speed correlation at RTS using Ørland wind data, corresponding to Table 4.27	E-8
F.1	EENS standard deviation for the MRBTBW-4 State Sampling DC-case study, corresponding to Table 4.3.	F-1
F.2	EENS standard deviation for the MRBTBW-4 State Transition DC-case study, corresponding to Table 4.4	F-1
F.3	EENS standard deviation for the MRBTBW-4 State Sampling AC-case study, corresponding to Table 4.5.	F-2
F.4	EENS standard deviation for the MRBTBW-4 State Transition AC-case study, corresponding to Table 4.6.	F-2
F.5	EENS standard deviation for the RTBW-19 State Sampling case study, corresponding to Table 4.9.	F-3
F.6	EENS standard deviation for the RTBW-19 State Transition case study, corresponding to Table 4.10.	F-4
F.7	EENS standard deviation for the Ørland RBTWS-4 State Sampling case study, corresponding to Table 4.23.	F-5

F.8	EENS standard deviation for the Ørland RBTSW-4 State Transition case study, corresponding to Table 4.24.	F-5
F.9	EENS standard deviation for the Ørland RTSW-19 State Sampling case study, corresponding to Table 4.25.	F-6
F.10	EENS standard deviation for the Ørland RTSW-19 State Transition case study, corresponding to Table 4.26.	F-7
F.11	EENS standard deviation for wind speed correlation at RTS using Ørland wind data, corresponding to Table 4.27	F-8
G.1	LOLE standard deviation for the MRBTSW-4 State Sampling DC-case study, corresponding to Table E.1.	G-1
G.2	LOLE standard deviation for the MRBTSW-4 State Transition DC-case study, corresponding to Table E.2	G-1
G.3	LOLE standard deviation for the MRBTSW-4 State Sampling AC-case study, corresponding to Table E.3.	G-2
G.4	LOLE standard deviation for the MRBTSW-4 State Transition AC-case study, corresponding to Table E.4.	G-2
G.5	LOLE standard deviation for the RTSW-19 State Sampling case study, corresponding to Table E.5.	G-3
G.6	LOLE standard deviation for the RTSW-19 State Transition case study, corresponding to Table E.6.	G-4
G.7	LOLE standard deviation for the Ørland RBTSW-4 State Sampling case study, corresponding to Table E.7.	G-5
G.8	LOLE standard deviation for the Ørland RBTSW-4 State Transition case study, corresponding to Table E.8.	G-5
G.9	LOLE standard deviation for the Ørland RTSW-19 State Sampling case study, corresponding to Table E.9.	G-6
G.10	LOLE standard deviation for the Ørland RTSW-19 State Transition case study, corresponding to Table E.10.	G-7
G.11	LOLE standard deviation for wind speed correlation at RTS using Ørland wind data, corresponding to Table E.11	G-8

List of Abbreviations

AC	Alternating Current
AI	Artificial Intelligence
ANN	Artificial Neural Network
ARMA	Auto-Regressive Moving Average
CC	Capacity Credit
COPT	Capacity Outage Probability Table
DCLF	Direct Current Load Flow
DC	Direct Current
DPL	Daily Peak Load
EENS	Expected Energy Not Served
ELCC	Effective Load Carrying Capability
FOR	Forced Outage Rate
GARPUR	Generally Accepted Reliability Principle with Uncertainty modelling and through probabilistic Risk assessment
HL	Hierarchical level
HPL	Hourly Peak Load
IEAR	Interrupted Energy Assessment Rate
IEEE-RTS	(Institute of Electrical and Electronics Engineer) Reliability Test System
LOLE	Loss of Load Expectation
LOLP	Loss of Load Probability
LOL	Loss of Load
MCS	Monte Carlo Simulation
MECORE	Monte Carlo Simulation and Enumeration Composite System Reliability Evaluation Program
MRBTS	Modified RBTS
MTTF	Mean Time To Failure

MTTR	Mean Time To Repair
MWh	Megawatt-hours
MW	Megawatt
NID	Normally Independent Distributed
OPF	Optimal Power Flow
PDF	Probability Density Function
PF	Power Flow
PSR	Power System Reliability
RapHL-II	Reliability analysis program for HL-II
RBTS	Roy Billinton Test System
RES	Renewable Energy Sources
TSO	Transmission System Operator
TTF	Time to Failure
TTR	Time to Repair
WB	Weibull
WECS	Wind Energy Conversion System
WTG	Wind Turbine Generator
YPL	Yearly Peak Load

1 Introduction

1.1 Background

Wind power is regarded as an important alternative to conventional electric power generating sources as it is a clean and renewable source of energy. Wind energy technologies have been developed rapidly, and are regarded as one of the lowest-priced renewable energy technologies.

Wind power has a vital role to play in achieving a rapid reduction in emissions of greenhouse gases to zero on a net basis over the coming decades, in line with the United Nations energy-related Sustainable Development Goals, including the climate goal of the Paris Agreement. To meet the long-term goals of the Paris Agreement, the share of Renewable Energy Sources (RES) in the world's primary energy supply must be raised to at least 65% by 2050 [1]. Wind power and solar energy are currently the fastest growing energy sources in the world, and are expected to play a vital role in the energy mix of the future. The onshore and offshore wind power generation in the Sustainable Development Scenario, developed by the International Energy Agency, is illustrated in Figure 1.1 and Figure 1.2.

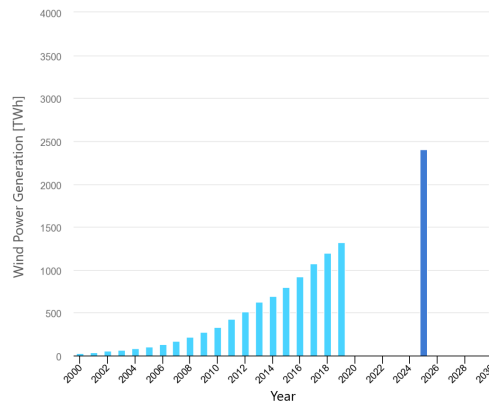


Figure 1.1: TWh Onshore wind power generation in the Sustainable Development Scenario, 2000-2030 [2]

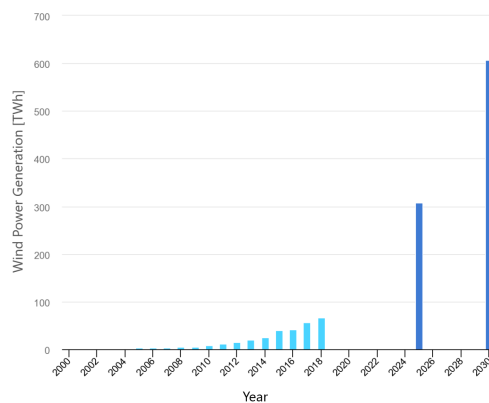


Figure 1.2: TWh Offshore wind power generation in the Sustainable Development Scenario, 2000-2030 [2]

Due to the intermittent nature of wind power, this rapid development leads to increased pressure on electric power utilities worldwide, as end-users expect the energy supply to be continuously available. Power System Operators need to quantify the impacts of the large increase in wind power on the reliability of the power systems, balancing reliability and costs.

Historically, composite power system reliability management has been relying on deterministic techniques, which are unable to capture the random nature of power systems. With increased generation from intermittent energy sources, the need for new techniques has increased further. Probabilistic methods have been highly developed and can provide relevant information about the behaviour of a system. Probabilistic techniques can be divided into analytical and simulation-based methods. The analytical models usually have to simplify the problems, and thus become inaccurate when the systems increase in size. Complex system effects and processes can be included to a higher degree in simulation-based methods. The simulation methods are usually based on Monte Carlo Simulation (MCS).

1.2 Scope

The thesis is a continuation of a specialisation project undertaken during Autumn 2020, where the main focus was to gain an understanding of the fundamental concepts in analytical power system reliability assessment (without wind), and further extend the concepts to include wind-power considerations and MCS. Based on this work, the thesis work conducted during Spring 2021 has the following main objective:

- Create a comprehensive framework for assessing the reliability of a composite power system that contains significant wind penetration, through MCS. Select/identify/create a suitable methodology for the PSR assessment, which will enable the quantification of the system reliability with the help of appropriate indices. Create in-house software tools for obtaining these reliability indices.

Reliability refers to its adequacy aspect.

The focus of the development of the scripts has been on the integration of new models and methods, and not every aspect of MCS such as variance reduction methods or computational efficiency, has been covered.

1.3 Thesis Contribution

The thesis is an addition to the computational tools in the ongoing project of building a comprehensive framework for conducting PSR assessment at the Department of Electric Power Engineering at NTNU. The objective is to evaluate the impact of integrating wind power on the reliability of composite power systems. The reliability metric Expected Energy Not Served (EENS) is selected as the most appropriate metric to quantify the impact of integrating wind power in composite system analysis by using MCS. The developed MCS scripts build on the composite adequacy studies presented in the Master's thesis [3] from the Department of Electric Power Engineering at NTNU.

A literature review of wind power considerations in composite power system reliability assessment is included in the thesis. Wind speed models based on ARMA and the Weibull distribution are developed and included in the modelling. The developed MCS scripts for wind sampling from the Weibull distribution are an extension of the scripts presented in [4]. Wind speed correlation is included in the developed wind speed models. The modelling of the wind turbine generator output

power is based on existing methods in the literature. The power system adequacy assessment is conducted by using Sequential and Non-sequential MCS techniques: the State Transition and State Sampling approaches. The conceptual background and applications of the concepts are presented and illustrated. The propositions made in this thesis are tested on three test systems: the RBTS, the MRBTS and the RTS. Real-life wind data from Ørland, Norway was adapted to obtain results in the case study. Existing wind data in the literature, from Canada, is also adapted to obtain results as the basis for validation.

The developed algorithm has both AC- and DC-optimal power flow options. The AC-based contingency solver is utilised for the MRBTS-Swift Current Case Study. All other case studies utilise the DC-based contingency solver, due to shorter computational time. The simulations were “capped” at 1000 simulation years for the State Sampling approach, and 7500 simulation years for the State Transition approach. Computational efficiency, accuracy and precision of the MCS approach have not been examined in the thesis.

The existing in-house MATLAB scripts have been extended to include the integration of significant wind power in composite systems, as presented in this thesis. MATLAB scripts that utilise the State Sampling and State Transition MCS techniques, ARMA- and Weibull distribution wind speed models, including wind speed correlation between multiple wind sites, and AC- and DC- load flows have been developed. The goal with the scripts was not to provide optimised scripts, but scripts that did a good basic job of obtaining reliability indices. All the developed scripts are released for further research and educational use at the Department of Electric Power Engineering at NTNU.

1.4 Thesis Structure

Chapter 1 - *Introduction*: provides the motivation, background, scope and contributions of the thesis.

Chapter 2 - *Conceptual Background and Literature Review*: presents the essential concepts of power system reliability (adequacy), a detailed literature review and the fundamental concepts required for executing the objectives of the thesis. The essential concepts include an introduction to reliability indices, MCS methods and composite system adequacy considerations. The literature review presents state-of-the-art methods and considerations related to the thesis work. Based on the conducted literature review, the selected fundamental methods for executing the objectives of the wind-related topics are presented.

For establishing narrative clarity and with an aim to make this thesis a complete and independent unit in and of itself, much of the content from chapter 2 is a replication of the specialisation project work, with suitable extensions where deemed necessary.

Chapter 3 - *Methodological approach*: presents an explanation of the proposed composite system assessment algorithms used for the implementation of MATLAB scripts in the thesis work, and highlights the unique contributions. A simple example illustrates the methodology.

Chapter 4 - *Case Studies and Results*: applies the developed scripts to different test systems. Presents and discusses various cases and methods for integrating wind power into power systems, including relevant sensitivity analyses and benchmark comparisons.

Chapter 5 - *Conclusion and Future Work*: summarises the results and work in the thesis and suggests future work.

2 Conceptual Background and Literature Review

2.1 Basics of Power System Reliability

This chapter addresses the fundamental aspects and concepts of PSR. To gain a thorough understanding of the field, the chapter examines elements of generation adequacy assessment before expanding to the more complex composite adequacy assessment. The chapter illustrates some of the concepts and indices analytically before these are included in Monte Carlo Simulation approaches.

2.1.1 Defining Power System Reliability

Power System Reliability has a wide range of meaning; various definitions exist. In a general sense, power system reliability concerns a system's ability to perform its function. It is often referred to as the probability of satisfactory provision of power and energy to meet load demand, as well as the ability to withstand disturbances. The power delivered to consumers must be within accepted standards and in the amount desired. The degree of reliability may be measured by the frequency, duration, and magnitude of adverse effects on consumer service [5].

To obtain a more concise picture, power system reliability can be divided into two basic aspects which are used for reliability assessment: adequacy and security [6].

2.1.1.1 Adequacy

Adequacy is the ability of the power system to supply the aggregate electric power and energy requirements of the customer at all times, taking into account scheduled and unscheduled outages of system components. The adequacy aspect includes facilities required for the generation of sufficient energy as well as facilities required for transport of the energy to the consumer load points. It is associated with static conditions, which implies that it does not include dynamic and transient disturbances.

2.1.1.2 Security

Security is the ability of the power system to withstand sudden disturbances such as electric short circuits or non-anticipated loss of system components. It is associated with dynamic conditions which may result in dynamic, transient or voltage instability of the system. An assessment typically examines whether a system can stay within its stability limits during a transient event.

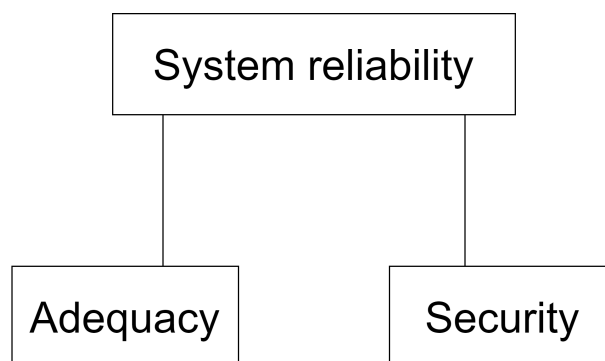


Figure 2.1: Division of reliability

In this thesis, power system reliability will refer to the adequacy aspect.

2.1.2 Hierarchical Levels

Electric power systems are immensely complex and large. Even high-tech computers cannot analyse a power system as a single entity in a completely realistic manner. Therefore, the system is divided into three distinguished subsystems that can be analysed separately. The concept of hierarchical levels has been developed to obtain a consistent means of identifying these subsystems [7]. The hierarchical levels consist of the generation system, transmission system and distribution system.

2.1.2.1 HL-I: Generation System

Hierarchical level 1 includes only the generation system. The total system generation is examined and compared to the total system load. The transmission system and the ability to move the generated energy to the system load points is not taken into account for this type of study.

2.1.2.2 HL-II: Composite System

Hierarchical level 2 includes both the generation system and the transmission system, often referred to as the bulk power system, or composite system. This study considers the ability of the system to provide sufficient supply to the system load points by including the network topology of the transmission system. Therefore, an assessment at HL-II is more complex than an assessment at HL-I, as it includes more parameters, such as limits for the power transmission, or voltage limits of the load buses. An HL-II assessment usually requires that some sort of load flow analysis is conducted. An HL-II assessment can be used to assess the adequacy of an existing or proposed system including the impact of various reinforcement alternatives at both the generation and transmission levels. Both individual bus indices and system indices may be evaluated. The system indices provide an assessment of the overall adequacy, while the individual bus indices provide the effect at individual buses [6].

2.1.2.3 HL-III: Whole Power System

Hierarchical level 3 includes the distribution facilities in addition to the two other systems which are included in HL-II studies. HL-III studies create large-scale models for most practical systems, and are therefore more complex to conduct [8]. This challenge may be overcome by performing isolated studies on the distribution system alone [9].

2.1.3 Evaluating the Adequacy Aspect of Power System Reliability

The adequacy of a system is evaluated by comparing a representation of a system to a criterion. The representation consists of a suitable index that quantifies the performance of the system. A variety of indices can be applied to assess the adequacy contribution of a system. Reliability evaluation can be done by deterministic and probabilistic methods. Deterministic indicators measure the historical performance of the power system, while probabilistic indicators forecast the performance of the power system over time [10]. The most common deterministic indices are the reserve margin and the largest set in the system. Deterministic methods do not account for the stochastic nature of system behaviour. As the share of renewable energy has increased and the demand side flexibility has

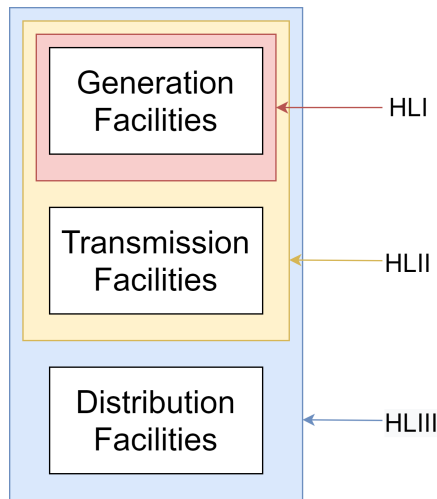


Figure 2.2: Hierarchical levels in power system reliability studies

increased, the probabilistic methods have prevailed as the most recognised and accurate methods. The deterministic methods will therefore not be emphasised in the thesis.

The probabilistic methods are divided into analytical and simulation-based methods. The analytical approach applies mathematical models and direct numerical calculation for reliability indices. The simulation-based approach utilises Monte Carlo Simulation. The advantage of the analytical approach is that the calculation time can be short compared to the simulation approach. The disadvantage with the analytical approach is that it simplifies the examined system in order to fit the analytical system model. This lowers the accuracy of the result. Therefore, as a system grows and becomes more complex, the simulation model becomes more advantageous.

2.1.3.1 Loss of Load Events

The most common probabilistic indices used today within the adequacy domain of PSR are related to loss of load events within power systems. For HL-I, this is associated with the insufficient generation, while HL-II also includes insufficient transfer capability. A generation model and a load model are needed to create a probabilistic risk model for an HL-I model. For an HL-II model, a network model is also needed. The results of LOL-indices are dependent on the chosen load model, and must be interpreted differently for each load model.

2.1.4 The Load Model

The load model is a representation of the system load demand and its variation in time. It is a prediction of the future load which is based on historical data. The time period is divided into increments of equal duration. Each increment consists of a load value. The Constant Yearly Peak Load (CYPL) model represents the entire year as one load increment equal to the annual peak load. In other words, the maximum load for the year is modelled to last for the entire year. The advantage of this model is that it gives a short computational time. However, it can give a very inaccurate and pessimistic result [11].

The Daily Peak Load (DPL) model represents the entire year as 365 load increments with a load equal to the daily peak load. In other words, the maximum load for each day is modelled to last for the entire day. Compared to the CYPL, this model gives a more accurate result. The drawback is that the computational time increases.

Lastly, the Hourly Peak Load (HPL) model represents the entire year as 8760 load increments with a load equal to the hourly peak load. The maximum load for each hour is modelled to last for the entire hour [12]. This model gives the most accurate representation of the system load demand and its variation. At the same time, the computational time increases compared to the DPL and CYPL.

A visualisation of the load variation for one week is provided in Figure 2.3. Note that the YPL is given for a different week than the one which is being presented.

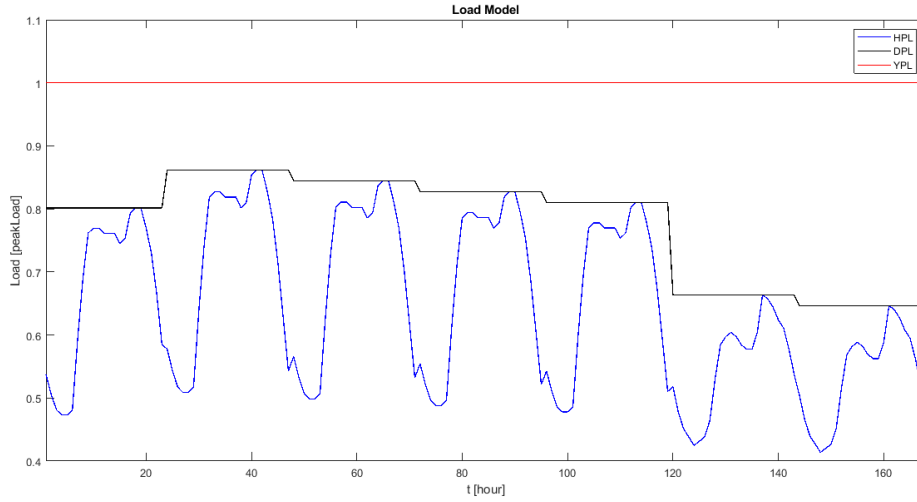


Figure 2.3: Illustration of the load models for a particular week

2.1.5 The Generation System Model

2.1.5.1 Forced Outage Rate

To represent the generation system in a realistic manner, an expression of the state of each generation unit is needed. A basic parameter used to do this is the probability of finding the unit on forced outage at some distant time in the future [13]. During the forced outage, the unit is unavailable and not performing its required function. It is classified to be in a “down”-state. FOR is the ratio of two time values, as illustrated in Equation 2.1.

$$\begin{aligned} \text{FOR} = U &= \frac{\lambda}{\lambda + \mu} = \frac{MTTR}{MTTF + MTTR} = \frac{MTTR}{T} \\ &= \frac{\sum [\text{down time}]}{\sum [\text{down time}] + \sum [\text{up time}]} \end{aligned} \quad (2.1)$$

- λ = expected failure rate
- μ = expected repair rate
- MTTF = mean time to failure = $1/\lambda$
- MTTR = mean time to repair = $1/\mu$
- T = cycle time

This model is directly applicable to a unit that is either operating or forced out of service. Scheduled outages must be considered separately. The model is associated with the two-state model consisting of a unit “up”- or “down”-state. Other multi-state models consisting of states such as “reserve shutdown” and “forced out but not needed” states can be represented as a Markov process. The reader is referred to [14] for elaboration on this.

2.1.5.2 COPT

For the loss of load approach, a basic, analytical generation model is known as the Capacity Outage Probability Table (COPT). It is a table that contains the possible outage states of the assessed generation system. Each of these outage states is represented by a cumulative probability of having an outage greater than, or equal to, the given number of MWs on outage(x_j), $P(X \geq x_j)$. This is illustrated in Equation 2.2.

$$P(X \geq x_j) = \sum_{X=x_j}^C p(X) \quad (2.2)$$

where:

- $p(X)$ = The individual probability
- C = The total installed capacity in the system

The individual probability in a COPT is the probability of exactly the indicated amount of capacity being out of service. Note that the individual probability associated with an outage state can be the sum of several system configurations that results in the same amount of capacity outage. The COPT is constructed by adding the generators one by one, convolving the capacity states of each unit with the outage states already added to the COPT [12]. A recursive algorithm can be utilised for this, as illustrated in Equation 2.3, assuming some units are added to the COPT already.

$$P^{new}(X \geq x_j) = (1 - FOR) \cdot P^{old}(X \geq x_j) + FOR \cdot P^{old}(X \geq x_j - g) \quad (2.3)$$

where:

- $p^{new}(X)$ = The new discrete cumulative probability probability distribution
- FOR = Forced Outage Rate
- g = Capacity

The calculation of the COPT by using the individual probabilities of a simple 3-unit system, shown in Table 2.1, is provided for clarification.

Table 2.1: Simplified 3-unit example system units

Unit capacity	Unit FOR
3 MW	0.02
3 MW	0.02
5 MW	0.02

A FOR of 0.02, yields an Availability of 0.98. First consider the probabilities of outages for the two 3MW-units, while the 5MW unit is out of service, as illustrated in Table 2.2.

Table 2.2: Simplified 3-unit example system. The two 3MW units are in service

Capacity out of service	Probability
0 MW	$p(x) = (0.98)(0.98) = 0.9604$
3 MW	$p(x) = (0.98)(0.02) + (0.98)(0.02) = 0.0392$
6 MW	$p(x) = (0.02)(0.02) = 0.0004$

Now consider that the 5MW unit is in service ($A = 0.98$). The probabilities are given in Table 2.3.

Table 2.3: Simplified 3-unit example system. The 5MW unit is in service.

Capacity out of service	Probability
0+0 MW	$p(x) = (0.9604)(0.98) = 0.941192$
3+0 MW	$p(x) = (0.0392)(0.98) = 0.038416$
6+0 MW	$p(x) = (0.0004)(0.98) = 0.000392$

If the 5MW-unit, however, is out of service, the probabilities are illustrated in Table 2.4.

Table 2.4: Simplified 3-unit example system. The 5MW unit is on outage

Capacity out of service	Probability
0+5=5 MW	$p(x) = (0.9604)(0.02) = 0.019208$
3+5=8 MW	$p(x) = (0.0392)(0.02) = 0.000784$
6+5=11 MW	$p(x) = (0.0004)(0.02) = 0.000008$

Finally, these scenarios are combined to form the COPT, as illustrated in Table 2.5.

Table 2.5: COPT for the simplified 3-unit example system.

State (j)	Capacity out of service, x_j	Individual probability	Cumulative probability
1	0 MW	0.941192	1.000000
2	3 MW	0.038416	0.058808
3	5 MW	0.019208	0.020392
4	6 MW	0.000392	0.001184
5	8 MW	0.000784	0.000792
6	11 MW	0.000008	0.000008

2.1.6 Reliability Indices

2.1.6.1 Loss of Load Probability - LOLP

As the name implies, this probabilistic index displays the probability of a LOL situation for a certain time period. The load demand may exceed the available capacity for different reasons such as generation unit outages or an unexpected increase in demand. To calculate LOLP analytically, the load model is compared to the generation model (COPT). The LOLP-value in time increment t is mathematically represented as shown in Equation 2.4, where X is the capacity outage, C is the installed capacity of the system that is not on scheduled outage and L_t is the load at a specific time increment.

$$LOLP_t = P(L_t > C - X) = P(X > C - L_t) \quad (2.4)$$

Here, $P(L_t > C - X)$ is the probability of demand exceeding the available capacity, while $P(X > C - L_t)$ is the probability of having an outage capacity that is larger than the installed capacity minus the load at that particular time increment. It should be noted that these are the same.

2.1.6.2 Loss of Load Expectation - LOLE

LOLE is one of the most used indices by power system planners and operators. LOLE displays the expected number of days or hours on which a load loss or deficiency will occur. It can be viewed as an extension of LOLP, as LOLE calculations consist of the summation of all $LOLP_t$ values over a time period. It should be noted that this is only possible if the time increment is equal to one day for the DPL-model, and one hour for the HPL-model.

During off-peak load periods and times when there is excess generating capacity available, LOLE-values will typically be zero. Non-zero values occur during peak periods and near-peak periods, or during periods that large amounts of capacity are undergoing scheduled maintenance and is, therefore, unable to provide capacity [15]. It does not indicate the severity of the deficiency and neither does it indicate the frequency nor the duration of loss of load [9]. A mathematical representation is presented in Equation 2.5 and Equation 2.6, where LOLE is calculated in terms of days/year using a DPL model and hours/year using an HPL model.

$$LOLE = \sum_{t=1}^{365} P(X > C - L) \Delta T \left[\frac{\text{days}}{\text{year}} \right] \quad (2.5)$$

$$LOLE = \sum_{t=1}^{8760} P(X > C - L) \Delta T \left[\frac{\text{hours}}{\text{year}} \right] \quad (2.6)$$

- $P(X > C - L)$ = Probability that the peak load will not be met
- ΔT = Time period for which a given peak load exists
- C = Total installed generation capacity in the system not on outage
- L = System load for a given time

LOLE analysis is used to determine the level of installed generation that is needed to achieve a given level of resource adequacy. In North America, this level of adequacy has traditionally been 0.1 day/year, but different regions or different entities can choose the appropriate target [15]. For this given level of adequacy, a DPL-model was utilised. This index can not be converted to hours/year since a different load model has been used. According to [16] the European reliability regulation is not uniform, and some countries do not have any reliability standards at all. LOLE-standards for certain European countries are presented in Table 2.6. As seen from the unit of measurement, an HPL-model has been used for these countries.

2.1.6.3 Expected Energy Not Served - EENS

A shortcoming of LOLE is that it does not take into account the severity of an outage. LOLE only denotes the expected average number of days or hours per year during which the system is being on outages. A system with a deficit of 5MW can have the same LOLP as a system with a deficit of 500MW. If the periods of deficits are equal, the systems also achieve the same LOLE.

Table 2.6: Reliability standards in European countries [16]

	LOLE [hr/yr]
Belgium	3
France	3
Great Britain	3
Ireland	8
The Netherlands	4

EENS overcomes this weakness in the LOLE index by including the size of the capacity deficit. It expresses the amount of electricity demand, measured in MWh, that is expected not to be met by generation in a given time period. The index is obtained by summing all the capacity outage states that give a capacity deficit and a summation over all the time increments. Usually, this is all hours in a year. This is illustrated in Equation 2.7.

$$EENS = \sum_{t=1}^{t=8760} \sum_{X_j=C-L_t}^C [x_j - (C - L_t)] \cdot p(X = x_j) [\text{MWh/year}] \quad (2.7)$$

- $p(X = x_j)$ is the probability of having a specific number of MW on outage
- $x_j - (C - L_t)$ is the energy that is curtailed at that specific number of MW outage capacity.

A simple example is provided for clarification. Assuming the generation model is presented by the COPT presented in Table 2.5. A single time increment where $L_t = 7\text{MW}$ is considered. Four out of the six outage states cause a capacity deficit, as illustrated in Table 2.7.

Table 2.7: Calculation of EENS for a simplified system

State (j)	Capacity out., x_j	Individual probability	Cumulative probability	Capacity deficit [$x_j - (C-L_t)$]	E_j
1	0 MW	0.941192	1.000000	0	0
2	3 MW	0.038416	0.058808	0	0
3	5 MW	0.019208	0.020392	1	$1 \cdot 0.019208 = 0.019208$
4	6 MW	0.000392	0.001184	2	$2 \cdot 0.000392 = 0.000784$
5	8 MW	0.000784	0.000792	4	$4 \cdot 0.000784 = 0.003136$
6	11 MW	0.000008	0.000008	7	$7 \cdot 0.000008 = 0.000056$

By using Equation 2.7, the EENS is calculated as $EENS = 0.019208 + 0.000784 + 0.003136 + 0.000056 = 0.023184$ MWh/hour, assuming the duration of the time increments is one hour. If this calculation is done for 8760 hourly time increments in a year, the EENS can be expressed as MWh/year.

2.1.7 Monte Carlo Simulation in Power System Reliability

In the previous sections, analytical approaches for how to calculate different metrics have been presented. As a system grows in complexity, finding analytical approaches to solving the system becomes more and more cumbersome, and calls for alternative methods. HL-II and HL-III systems are part of this category, systems that are often too complex to be analysed analytically. Monte Carlo Simulation (MCS) is a stochastic simulation utilising random numbers and can be used to solve both deterministic and stochastic problems [6]. When applied in PSR, MCS is used to sample the states of the components in the system. It is usual to represent the system as a vector of component states S , as shown in Equation 2.8. For an HL-I study, component states sampled are the generators, while an HL-II study will also include the states of the transmission components.

$$S = \{S_1, S_2, \dots, S_m\} \quad (2.8)$$

When a system state is obtained, the total capacity not on outage can simply be calculated by Equation 2.9.

$$C = \sum_{i=1}^m x_i C_{i, \text{rated}} \quad (2.9)$$

Where C is the total available capacity for the whole system, m is the total number of generators, $C_{i, \text{rated}}$ is the rated capacity for component i and x_i is a number in the range $[0,1]$ denoting how much of the rated capacity is available for component i . In a two-state representation $x_i = 1$ for the up-state and $x_i = 0$ for the down-state.

In PSR, MCS is often categorised into two main categories, Sequential and Non-sequential methods. A Sequential method implies that the next calculated state depends on the previous state. This is also called chronological MCS. A Non-sequential MCS method does not take into account previous states.

There exist three main simulation approaches when using MCS for PSR [6], the State Sampling approach, the State Duration approach and the State Transition approach. These three methods will be introduced.

2.1.7.1 State Sampling Approach

In this approach, every component in the system is represented with a state variable. For simplicity, only the up-and down-state will be considered, but the method can be extended to account for component representations with more than two states. Assume the i -th component has state variable S_i and a distribution of how likely the component is to be in the up-or down-state. Then S_i can be represented as:

$$S_i = \begin{cases} \text{Up state} & \text{if } U_i \geq p_{i, \text{down}} \\ \text{Down state} & \text{if } U_i < p_{i, \text{down}} \end{cases}$$

where $p_{i, \text{down}}$ is the probability of component i to be in the down state, and U_i is a randomly uniformly distributed variable in the range $[0,1]$.

In a two-state representation of each component, where the component is either in the up-or down-state, the FOR value will be a natural choice for the probability of the down-state. When

determining the system state, for each component in the system, a random uniformly distributed variable U between $[0,1]$ will be generated, and used to determine the state of each component.

Based on the state representation, the capacity on outage can be calculated according to Equation 2.9. The reliability indices can then be calculated according to the hierarchical level of the study.

This approach is Non-sequential, as it does not take into account previous states when determining the next state. As a consequence, frequency indices cannot be calculated.

2.1.7.2 State Sampling Example

For a given system that consists of five generating units with a capacity of 40 MW and a FOR of 0.01, one state of the system is sampled using the State Sampling approach. As the system consists of five units, a vector of five uniformly distributed random variables in the range $[0,1]$ is generated, as illustrated in Equation 2.10.

$$R = (0.7223 \quad 0.3422 \quad 0.9549 \quad 0.0043 \quad 0.2984) \quad (2.10)$$

The system matrix S is then found by comparing the elements of R against the FOR value of the generators. The resulting system matrix is then given by Equation 2.11 (where 0 indicates the up-state).

$$S = (0 \quad 0 \quad 0 \quad 1 \quad 0) \quad (2.11)$$

Employing Equation 2.9 yields that this state has a capacity not on outage of 160 MW, and a capacity on outage of 40 MW.

2.1.7.3 State Duration Approach

Instead of focusing on the chance of a given component to be in a state at one time, the state duration approach rather looks at the state duration distribution functions. When looking at a component with two states, the distributions are operating and repair. In this example, these are assumed exponentially distributed, but can follow any distribution.

Due to the exponential distribution, the time each component stays in one state is given by Equation 2.12. The equation is found by using the inverse transform method (described by [6]) on the cumulative probability function of an exponential distribution.

$$T_{TTF,i} = -\frac{1}{\lambda_i} \ln U_i \quad (2.12)$$

$$T_{TTR,i} = -\frac{1}{\mu_i} \ln U_i \quad (2.13)$$

Where $T_{TTF,i}$ is the time to failure, $T_{TTR,i}$ is the time to repair, λ_i is the failure rate and μ_i is the repair rate. U_i is a randomly uniformly distributed variable in the range $[0, 1]$.

The state duration approach is conducted according to these steps:

- Determine the initial state for each component. According to [6] setting each component to the up (success) state is a normal assumption.

- For each component, determine the time it stays in the initial state, and record it. Then determine how long it takes for the component to change state again. Repeat this process until the chronological component state is found for the wanted observing time.
- Combine the individual component chronological state to obtain the total system chronological state. An illustration of this is shown in Figure 2.4.
- From the chronological state the system state vector S can be found for a given time, and used to calculate the wanted reliability indices.

One important thing to note is that when a component is in the down-state, the next time constant is found from the Time-to-Repair distribution, while in the up-state the next time constant is found from the Time-to-Fail distribution. Due to this dependency on the current state for determining the time to the next state, this approach is a Sequential Monte Carlo Method.

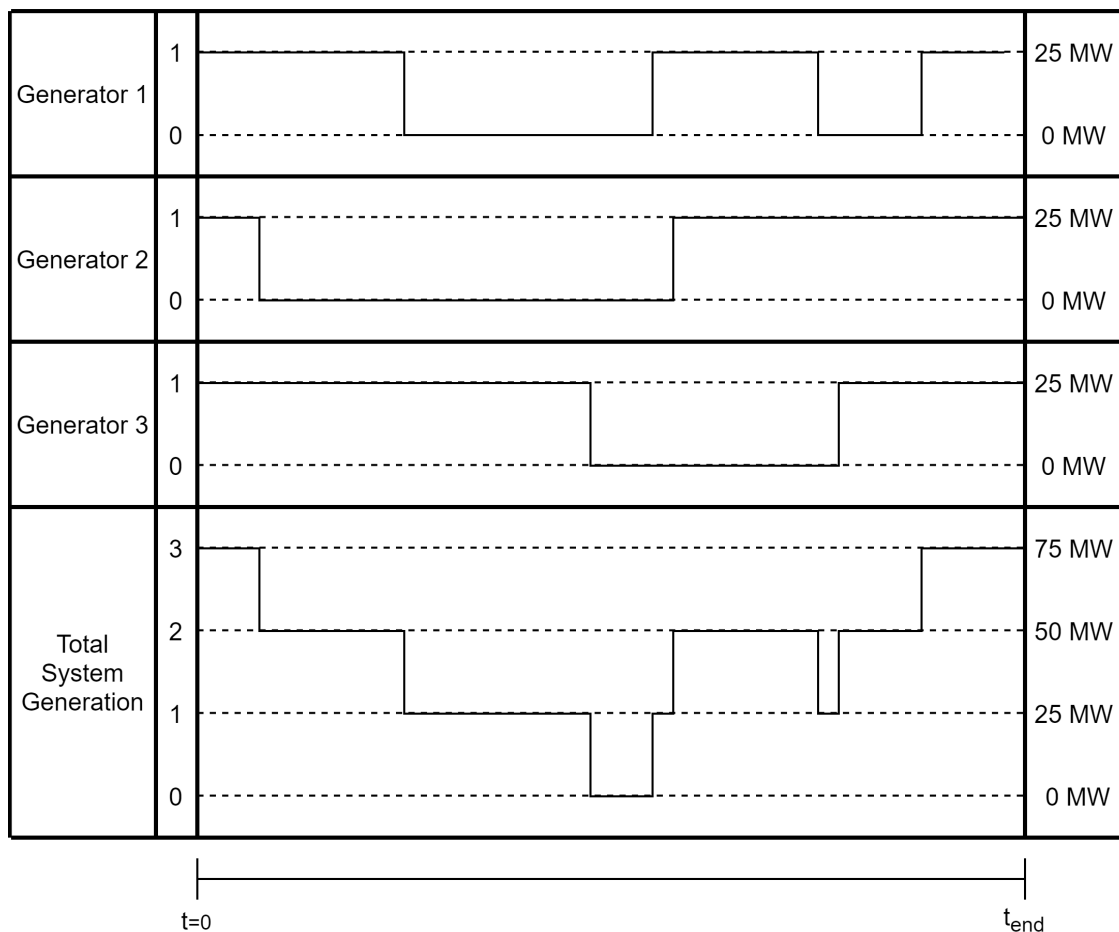


Figure 2.4: A visualisation of the state duration approach on a three-generator HL-I system.

In Figure 2.4, each generator has the same generation capacity of 25 MW and is either in the up-or down-state. The chronological data from each component is added for the whole system giving rise to the system generation data. It should be noted that the state distributions in the figure are unrealistic for real generators and only used to visualise the concept.

Since the state duration method is a Sequential method, it allows for the calculation of frequency indices. The state duration method is more computationally intensive compared to both the State Sampling and State Transition approach.

2.1.7.4 State Transition Approach

In this approach, the focus is on how the whole system transitions from one state to another, instead of how each component individually transitions. Only the main points of the proof are discussed. This section is based upon [6]; the reader is encouraged to see [6] for a more thorough proof of the approach.

For this approach, all the system components are assumed to follow an exponential distribution. Assume a state S consisting of m components, each with a transition rate λ_i . It should be noted that in this section, λ can refer to both failure rate and repair rate. By the assumption that all components are exponentially distributed, the transition rate for the whole system (λ) with a given system state is given by the sum of all the components' transition rate and is also exponentially distributed.

$$\lambda = \sum_{i=1}^m \lambda_i \quad (2.14)$$

The system transfers from one state to the next when any one component transitions. As such, the random time to transition, T , for the whole system can be expressed as in Equation 2.15.

$$T = \min\{T_i\} \quad (2.15)$$

The time between transitions can be sampled from equation Equation 2.16, which follows from T being exponentially distributed.

$$T = -\frac{1}{\sum_{i=1}^m \lambda_i} \ln U \quad (2.16)$$

It can be shown that since T_i and T follow exponential distributions, the probability for the transition from the current state due to a change in state at component j is given by Equation 2.17 [6].

$$P_j = P(T_j = t_0/T = t_0) = \frac{\lambda_j}{\sum_{i=1}^m \lambda_i} \quad (2.17)$$

$$\sum_{j=1}^m P_j = 1 \quad (2.18)$$

- P_j is the probability that the next component to change is component j
- t_0 is the time at which the change occurs
- λ_j is the transition rate for component j
- $\sum_{i=1}^m \lambda_i$ is the transition rate for the system.
- $P(T_j = t_0/T = t_0)$ is the probability that the transition in component j coincides with the transition of the whole system, which equates to P_j

Due to the results arrived at in Equation 2.17, sampling the next system state becomes rather simple. A random variable U in the interval of $[0,1]$ can be generated, and the probabilities from

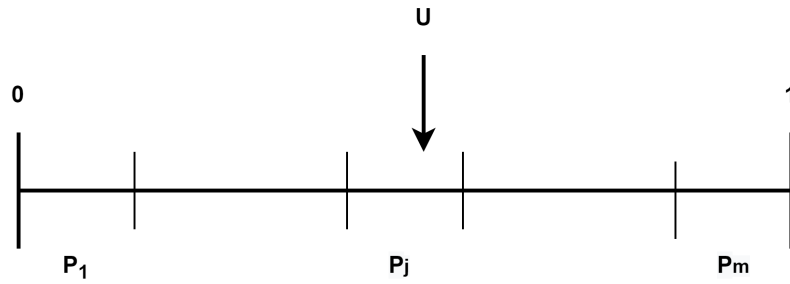


Figure 2.5: Visualisation of how the next state in the State Transition approach is obtained.

Equation 2.17 will give intervals for each component. When U is in the interval for component j , this implies that the system state transitions due to a transition in component j . Figure 2.5 visualises this process. In this illustration U falls in the interval for P_j , indicating that state P_j is the next state for the system.

As in the state duration approach, once a component transition, the λ_i for that component must be updated before the next state calculation is done.

The step-for-step approach is then:

1. Determine the initial state S_0 for the system, usually, this is the up-state for all components.
2. Determine and record the time to the next system state by generating a random variable U_1 and using Equation 2.16.
3. Determine and record the next system state by generating a random uniformly distributed variable U_2 in the range $[0,1]$ and use Equation 2.17.
4. Update λ_j for the component that transitioned.
5. Repeat from the second step until the wanted observing time is found.
6. Extract the system states and use that to calculate the wanted reliability indices.

A benefit of this approach is that it is a Sequential approach, allowing frequency indices to be obtained. It is also less computationally expensive compared to the state duration approach, since it needs to generate fewer random variables and store less information. A disadvantage of this approach is that Equation 2.17 requires T and T_j to be exponentially distributed, and as such this becomes a requirement for the method. However, this is a normal assumption in PSR studies [6].

2.1.7.5 State Transition Example

For a system with five generators of 40 MW, an expected failure rate of 2 and a repair rate of 100, the two next system states and the duration to those states using State Transition are obtained. The system state is set to $S_0 = (0 \ 0 \ 0 \ 0 \ 0)$. The λ values for the components for state S_0 are given in the first column in Table 2.9. It can be observed that for this system state, the next states intervals, used to determine which component transitions, are given by Equation 2.19 (following from Equation 2.17).

$$R = (0.2 \ 0.4 \ 0.6 \ 0.8 \ 1) \quad (2.19)$$

Table 2.8: The randomly generated variables for the State Transition example.

	State 0	State 1
U_1	0.4256	0.9721
U_2	0.1890	0.7269

The randomly generated variables are given in Table 2.8.

Using $\lambda_{sys} = 10$ and $U_1 = 0.4256$ in Equation 2.16, the time until next transition was found to be $T_0 = 0.0854$ (years). From $U_2 = 0.1890$ and Equation 2.19, gen. 1 is found to transition.

Table 2.9: λ values for the State Transition example.

Component	λ State 0 [incidents/year]	λ State 1 [incidents/year]
Gen 1	2	100
Gen 2	2	2
Gen 3	2	2
Gen 4	2	2
Gen 5	2	2
Sys	10	108

This gives system state $S_1 = (1 \ 0 \ 0 \ 0 \ 0)$. The λ values for S_1 are found in the second column of Table 2.9. This gives the intervals shown in Equation 2.20 for the next State Transition.

$$R = (0.9259 \ 0.9444 \ 0.9630 \ 0.9815 \ 1) \quad (2.20)$$

The time to the next transition is found by using $\lambda_{sys} = 108$ and $U_1 = 0.9721$, which yields $T_1 = 0.00026$. From $U_2 = 0.7269$ and Equation 2.20, gen. 1 is found to transition. This gives the system state $S_2 = (0 \ 0 \ 0 \ 0 \ 0)$.

The results from this example are summarised in Table 2.10.

Table 2.10: The resulting states and durations for the State Transition example.

	i = 0	i = 1	i = 2
S_n	$(0 \ 0 \ 0 \ 0 \ 0)$	$(1 \ 0 \ 0 \ 0 \ 0)$	$(0 \ 0 \ 0 \ 0 \ 0)$
T_n [years]	0.0854	0.00026	

2.1.7.6 Reliability Indices Using MCS

As MCS is a stochastic and not an analytical approach, it is impossible to arrive at a definite answer. Instead, the MCS is run for many simulated years, and the indices for each year are stored. From this, the mean and variance of the results can be calculated, by use of Equation 2.21 and Equation 2.22.

$$E[x] = \bar{x} = \frac{1}{N} \sum_{i=1}^N x_i \quad (2.21)$$

$$Var[x] = \sigma^2 = \frac{1}{N-1} \sum_{i=1}^N (x_i - \bar{x})^2 \quad (2.22)$$

By the law of large numbers, as the number of sampled years increases to infinity, the mean and variance of the MCS approach the true expectation value μ_x and true variance σ_x for the system, as shown in Equation 2.23. Therefore, the mean of the yearly indices is used to calculate the MCS indices. The resulting equation for LOLE and EENS is shown in Equation 2.24 and Equation 2.25, following from Equation 2.21 combined with Equation 2.6 and Equation 2.7 respectively.

$$\lim_{N \rightarrow \infty} \bar{x} = \mu_x \quad (2.23)$$

$$LOLE_{MCS} = \frac{\sum_{i=1}^N \left(\sum_{j=1}^M x_j \cdot \Delta t \right)}{N} \quad (2.24)$$

$$EENS_{MCS} = \frac{\sum_{i=1}^N \left(\sum_{j=1}^M x_j \cdot C_j \cdot \Delta t \right)}{N} \quad (2.25)$$

- N is the number of years simulated.
- M is the number of time steps per year, this is usually 364 if the timescale is days per year, or 8736 if the time scale is hours per year.
- x_j is a variable that is either 0 or 1 and represents if a LOL situation occurred at a time step j .
- Δt is the time increment per step, either 1 hour or 1 day.
- C_j is the severity of the outage in MW.

As it is practically impossible to run an infinite amount of simulations, it is impossible to attain the true indices with 100 % certainty. It is however possible to calculate the possible error of the indices. By the central limit theorem, the calculated mean values from the MCS generates a population that follows a normal distribution. This distribution is given as $\mathcal{N}(E[\bar{x}], Var[\bar{x}])$. The expectancy-value of the average ($E[\bar{x}] = \bar{x}$) is just the average, and the variance becomes $Var[\bar{x}] = \sigma^2/N$. As can be observed, the variance of this normal distribution decreases with N . In other words, the obtained average will be increasingly more likely to be located close to the true mean as N increases. Due to this, the variance of this distribution is often used to determine the accuracy of a MCS [3], see Equation 2.26.

$$Var[\bar{x}] = \frac{1}{N(N-1)} \sum_{i=1}^N (x_i - \bar{x})^2 \quad (2.26)$$

2.1.7.7 Reliability Index Example

A 5-generator system where each generator has a capacity of 40 MW and a constant yearly peak load of 130 MW is considered. Based on the simulated states, as seen in Table 2.11, the LOLE and EENS indices are obtained. The states are only simulated once per year.

The average value for LOLE and EENS is found as seen in Equation 2.27 and Equation 2.28.

$$LOLE = \frac{0 \cdot 4 + 1 \cdot 4}{8} = 0.5[\text{years/year}] \quad (2.27)$$

Table 2.11: MCS data for reliability index calculation.

Simulation year nr	System State Vector	LOL [year]	ENS [MWh]
1	$\begin{pmatrix} 0 & 0 & 0 & 0 & 0 \end{pmatrix}$	0	0
2	$\begin{pmatrix} 1 & 0 & 1 & 0 & 0 \end{pmatrix}$	1	87 360
3	$\begin{pmatrix} 0 & 0 & 0 & 1 & 0 \end{pmatrix}$	0	0
4	$\begin{pmatrix} 0 & 1 & 1 & 1 & 0 \end{pmatrix}$	1	436 800
5	$\begin{pmatrix} 1 & 0 & 1 & 0 & 0 \end{pmatrix}$	1	87 360
6	$\begin{pmatrix} 0 & 0 & 0 & 0 & 0 \end{pmatrix}$	0	0
7	$\begin{pmatrix} 1 & 0 & 0 & 0 & 1 \end{pmatrix}$	1	87 360
8	$\begin{pmatrix} 0 & 0 & 0 & 1 & 0 \end{pmatrix}$	0	0

$$EENS = \frac{0 \cdot 4 + 87360 \cdot 3 + 436800 \cdot 1}{8} = 87450[MWh/year] \quad (2.28)$$

The corresponding standard deviation is found by taking the root of the obtained results from Equation 2.26. The standard deviation of the LOLE- and EENS indices are shown in Equation 2.29 and Equation 2.30

$$SD_{LOLE} = 0.267[years/year] \quad (2.29)$$

$$SD_{EENS} = 52207[MWh/year] \quad (2.30)$$

2.1.8 Composite System Adequacy

As previously explained, HL-II, or composite system PSR studies include the transmission system in addition to the generation system. This means that not only does the available generation capacity need to fulfil the load, but the limitations of the transmission system need to be included. Therefore, to conduct HL-II studies, some sort of load flow analysis is needed. The load flow analysis can be both DC-based and AC-based. An AC-based model has higher accuracy, but requires longer computational time. The DC-based model is a simplified model compared to the AC-model, but requires less computational time. In addition to the data required in HL-I studies, network data must be supplied as input. Since the systems become much larger and complex for assessment at HL-II compared to assessment at HL-I, the simulation-based approach is often preferred over the analytical approach. Through MCS sampling, the system state at a specific time can be obtained and handed to the contingency solver, based on either AC-load flow analysis or DC-load flow analysis. The two most popularly used MCS methods for composite systems are the State Sampling method and the State Transition method [17]. Therefore, these methods will be emphasised. For both methods, network topology, impedances and current limits of the lines must be supplied to the MCS sampling and evaluation step, in addition to the generation data.

The additional elements for the HL-II algorithm, compared to the HL-I algorithm will be highlighted in this section, focus is on the theoretical basis for the algorithms. The explanation and presentation of matter on composite power system reliability in this Chapter are based on our understanding of the work of Laengen [3], and is a condensed paraphrasing of some work presented in his thesis.

2.1.9 Additional MCS Sampling and Data

Depending on the type of load flow study to be conducted, different data will be required. Since the DC-based approach is a simplification of the AC-based approach, the necessary data for an AC-based approach will be emphasised more.

2.1.9.1 Generator Data

Compared to an HL-I assessment, the generation model for the AC-based approach also has to take into account the reactive power capabilities of the generators. The input data for the generation model are illustrated in Table 2.12. A DC-based approach does not consider the reactive power, and would therefore disregard the reactive power limits.

Table 2.12: Input data for the generation model. State Sampling MCS AC-based approach

Generator	Capacity	Bus	Reactive min	Reactive max	FOR
1	$P_{cap,1}$	N_1	$Q_{min,1}$	$Q_{max,1}$	FOR_1
\vdots	\vdots	\vdots	\vdots	\vdots	\vdots
n	$P_{cap,n}$	N_n	$Q_{min,n}$	$Q_{max,n}$	FOR_n

As explained in the preceding section, the State Transition utilises TTF and TTR instead of FOR. The generator data required for the State Transition AC-based contingency solver is therefore given by Table 2.12 with the FOR-column replaced by the respective TTFs and TTRs.

2.1.9.2 Line Data

For the MCS sampling in an HL-II assessment, the states of the lines need to be sampled as well. To include the transmission system in the assessment, the network data is represented as illustrated in Table 2.13 for the AC-analysis, using the State Sampling approach. For the DC analysis, the resistance and susceptance are excluded. If the State Transition approach is utilised, the FOR column is replaced by the respective TTFs and TTRs.

Table 2.13: Input data for the AC-based contingency solver. State Sampling MCS.

Line	From Bus	To Bus	FOR	R [p.u]	X [p.u]	Half of shunt susceptance [p.u]	Current limit [p.u]
1	1	2	FOR_1	R_{12}	X_{12}	y_{10}	$I_{lim,1}$
\vdots	\vdots	\vdots	\vdots	\vdots	\vdots	\vdots	\vdots
n	k	l	FOR_n	R_{kl}	X_{kl}	y_{k0}	$I_{lim,n}$

2.1.9.3 Bus Data

In addition to these parameters, specific bus data for the system is required. The specific bus data concerns the allocation of loads in the system and the cost of load curtailment at each bus. Also, the minimum and maximum voltage magnitude limits of the buses need to be included. For the DC analysis, the voltage magnitudes would not be included, as these are assumed to be equal to 1 p.u. The bus data for the AC analysis is presented in Table 2.14.

Table 2.14: Bus data for the AC based approach.

Bus	Share of load	Curtailement cost [\$/KWh]	V_{min} [p.u]	V_{max} [p.u]
1	$Load_1$	$Cost_1$	$V_{min,1}$	$V_{max,1}$
\vdots	\vdots	\vdots	\vdots	\vdots
n	$Load_n$	$Cost_n$	$V_{min,n}$	$V_{max,n}$

2.1.9.4 Selection of System States

Each component in the composite system can be categorised by a binary value $[0,1]$, representing its state. If the component state is 0, the component is in its normal state. If the component state is 1, the component is in a contingency state due to component outage(s). States of the generators and lines are given as two vectors. For a system with n generators, and m lines, the vector of the generator states are illustrated in Equation 2.31, and the line states are illustrated in Equation 2.32 [3].

$$P_g = [X_1, \dots, X_n]^T \quad (2.31)$$

$$L = [X_1, \dots, X_m]^T \quad (2.32)$$

To represent each bus in a system, the generation state vector given in Equation 2.31 and the rated capacity of each bus is combined to form the generation capacity matrix. For an AC-based approach, the matrix gives the active power, reactive minimum and reactive maximum capabilities of the buses in the system. The generation capacity matrix for a system with k buses is illustrated in Equation 2.33.

$$G_{lim,AC} = \begin{bmatrix} P_{cap,1} & Q_{min,1} & Q_{max,1} \\ \vdots & \vdots & \vdots \\ P_{cap,k} & Q_{min,k} & Q_{max,k} \end{bmatrix} \quad (2.33)$$

For a DC-based approach, the reactive capabilities in Equation 2.33 are excluded, and the generation capacity matrix becomes a vector as illustrated in Equation 2.34.

$$G_{lim,DC} = [P_{cap,1}, \dots, P_{cap,k}]^T \quad (2.34)$$

Similar to the generation capacity matrix, a matrix that represents the load requirement among the buses is needed. The load requirement for a system with k buses, using an AC-based approach is given by Equation 2.35.

$$S_{load,AC} = \begin{bmatrix} P_{load,1} & Q_{load,1} \\ \vdots & \vdots \\ P_{load,k} & Q_{load,k} \end{bmatrix} \quad (2.35)$$

For a DC-based approach, the load requirement matrix becomes a vector, as illustrated in Equation 2.36.

$$S_{load,DC} = [P_{load,1}, \dots, P_{load,k}]^T \quad (2.36)$$

2.1.9.5 Isolated Buses

For the State Sampling and State Transition approaches, multiple lines can be on outage simultaneously. Parts of the system being assessed might therefore become islanded. The algorithm must have a way to solve this event, to make sure the load flow problem is solvable. A step-for-step guide to handle the possibility of isolated buses is proposed in [17].

2.1.10 AC-Based Load Flow Analysis

The classic load flow problem considers four variables at each bus, i , of a power system:

- P_i - Active power injection
- Q_i - Reactive power injection
- V_i - Voltage magnitude
- θ_i - Voltage angle

The load flow equations are given as illustrated below.

$$P_i = \sum_{j=1}^N |Y_{ij}| |V_i| |V_j| \cos(\theta_i - \theta_j - \delta_{ij}) \quad (2.37)$$

$$Q_i = \sum_{j=1}^N |Y_{ij}| |V_i| |V_j| \sin(\theta_i - \theta_j - \delta_{ij}) \quad (2.38)$$

- Y_{ij} - Mutual admittance, equal to the negative sum of the admittances between bus i and j
- N - Number of system buses

Since each bus has four variables, n buses have $4n$ variables in total. To solve the load flow equations, two of the four variables for each bus have to be specified prior to the assessment. For PQ-buses, or load buses, P_i and Q_i are known, while for PV-buses, or generator buses, P_i and V_i are known. V_i and δ_i must be specified for one bus in the system, and this bus is called the slack bus. The slack bus adjusts the power balance of the whole system.

2.1.11 DC-Based Load Flow Analysis

DCLF is a method that gives estimations of power flows on AC systems. The method simplifies the non-linear AC model to a linear form through the following assumptions:

- Line resistances (active power losses) are negligible, $R \ll X$
 - Voltage angle differences are assumed to be small, $\sin(\theta) = \theta$ and $\cos(\theta) = 1$
 - Magnitudes of bus voltages are set to 1 p.u.
-

The AC load flow equations Equation 2.37, Equation 2.38 are now only represented by Equation 2.39 since only active power flows are considered.

$$P_i = \sum_{j=1}^k B_{ij} \delta_{ij} \text{ where } \delta_{ij} = \delta_i - \delta_j \quad (2.39)$$

- B_{ij} - Mutual susceptance, the imaginary part of Y_{ij} .
- $B_{ij} = b_{ij} = -\frac{1}{X_{ij}}$. $B_{ii} = -\sum_{j=1, j \neq i}^k b_{ij}$

As in AC power flow, one of the buses needs to be defined as the slack bus. It is assumed that the slack bus compensates the system by either generating or consuming power, such that the total power equals zero ($\sum_{i=1}^n P_i = \sum P_{gen} - \sum P_{load} = 0$). This gives rise to Equation 2.40

$$P_{slack} = \sum_{i=1, i \neq slack}^n P_i \quad (2.40)$$

By grouping all the mutual susceptances into a matrix, see Equation 2.41, the DC power flow equations can be written on matrix form, as in Equation 2.42.

$$\mathbf{B} = \begin{bmatrix} B_{11} & B_{12} & \cdots & B_{1n} \\ B_{21} & B_{22} & \cdots & B_{2n} \\ \vdots & \vdots & \ddots & \vdots \\ B_{n1} & B_{n2} & \cdots & B_{nn} \end{bmatrix} \quad (2.41)$$

$$\boldsymbol{\delta} = (\mathbf{B})^{-1} \mathbf{P} \quad (2.42)$$

Where:

$$\mathbf{P} = \begin{bmatrix} P_1 \\ P_2 \\ \vdots \\ P_n \end{bmatrix}, \boldsymbol{\delta} = \begin{bmatrix} \delta_1 \\ \delta_2 \\ \vdots \\ \delta_n \end{bmatrix} \quad (2.43)$$

It should be noted that in 2.41, the elements of the columns and rows corresponding to the slack bus need to be zero. This is due to the aforementioned characteristics of the slack bus, as it compensates for the rest of the system.

The power flow between two buses in a DC system can be expressed as seen in Equation 2.44.

$$P_{ij} = \frac{\delta_i - \delta_j}{X_{ij}} \quad (2.44)$$

Where P_{ij} is the power flow on the line between bus i and j , δ_i is the angle at the corresponding bus and X_{ij} is the line reactance for the lines between bus i and j .

By use of Equation 2.42, the power flow on the lines can be expressed as in Equation 2.45.

$$P_{ij} = \frac{x_{i1} - x_{j1}}{X_{ij}} P_1 + \frac{x_{i2} - x_{j2}}{X_{ij}} P_2 + \cdots + \frac{x_{in} - x_{jn}}{X_{ij}} P_n \quad (2.45)$$

Introducing the distribution factors into the equations, the line flows can further be represented as in Equation 2.46.

$$P_{ij} = a_{ij,1}P_1 + a_{ij,2}P_2 + \cdots + a_{ij,n}P_n \quad (2.46)$$

A sensitivity matrix of each of the distribution factors, \mathbf{A} , can then be assembled. The line flows \mathbf{T} are given by Equation 2.47.

$$\mathbf{T} = \mathbf{A}\mathbf{P} \quad (2.47)$$

$$\mathbf{P} = \mathbf{P}_{gen} + \mathbf{C}_P - \mathbf{P}_{load} \quad (2.48)$$

\mathbf{P} can be represented as in Equation 2.48. \mathbf{P}_{gen} is a column vector of all generation, \mathbf{C}_P is the column vector of load curtailment and \mathbf{P}_{load} is the column vector of the load. Since the \mathbf{P}_{gen} cannot increase above the maximum capacity available at a bus, and \mathbf{P}_{load} is set for a given time, the introduced \mathbf{C}_P allows the equation to be solved for cases where available generation is lower than the load, by introducing load curtailment.

2.1.12 DC Optimisation Problem Formulation

An optimisation problem formulation can be defined for the system, as seen in 2.49. The formulation is found by the following criteria:

- Minimise load curtailment, a load curtailment of 0 means there is no loss-of-load.
- Active power consumption and generation must be equal, $\sum \mathbf{P} = 0$, see Equation 2.48.
- The power flows on the lines must stay within the rated values for the lines.
- The generation at each bus cannot exceed its maximum capacity, nor be negative.
- The load curtailment at each bus cannot exceed the load at that bus, nor be negative.

$$\min \quad \mathbf{c}_{curtail}^\top \cdot \mathbf{C}_P + \mathbf{c}_{reschedule}^\top \cdot \mathbf{P}_{gen}; \quad (2.49)$$

$$\text{subject to} \quad \sum_{i=1}^n P_{gen,i} + \sum_{i=1}^n C_{P,i} = \sum_{i=1}^n P_{load,i} \quad (2.50)$$

$$|[\mathbf{A}] \cdot [\mathbf{P}]| \leq \mathbf{T}_{max} \quad (2.51)$$

$$0 \leq \mathbf{P}_{gen} \leq \mathbf{P}_{gen,max} \quad (2.52)$$

$$0 \leq \mathbf{C}_P \leq \mathbf{P}_{load} \quad (2.53)$$

- $\mathbf{c}_{curtail}$: Cost column vector the load curtailment.
 - \mathbf{C}_P : column vector of load curtailment.
 - $\mathbf{c}_{reschedule}$: Cost column vector for the generation.
 - \mathbf{P}_{gen} : column vector of generation.
-

- $P_{gen,i}$: generation at bus i .
- $C_{P,i}$: load curtailment at bus i .
- $P_{load,i}$: load at bus i .
- \mathbf{A} : matrix of distribution factors.
- \mathbf{P} : column vector of total power as described by Equation 2.48.
- \mathbf{T}_{max} : column vector of line transfer limits.
- $\mathbf{P}_{gen,max}$: column vector of maximum generation limits.
- \mathbf{P}_{load} : column vector of loads.

By passing the problem to an optimisation problem solver, it can be determined if and where load curtailment arise, and by extension if a LOL situation has arisen.

2.1.13 AC Optimisation Problem Formulation

The first thing to consider when performing AC OPF is which network model to use for the system. There exist two main methods, the branch and the injection method [17]. This thesis will proceed to present the injection based OPF method. How to attain the network model is explained in [17]. The model has the corresponding active and reactive power equations as already presented in Equation 2.37 and Equation 2.38.

As an AC system considers reactive power, a reactive load curtailment C_Q is introduced, defined similarly to the active load curtailment C_P . This gives rise to Equation 2.54.

$$\mathbf{Q} = \mathbf{Q}_{gen} + \mathbf{C}_Q - \mathbf{Q}_{load} \quad (2.54)$$

Compared to DC, when using AC in an optimal power flow solver, there are more limits to consider. The following is a definition for an AC OPF minimisation problem for use in HL-II PSR.

- Minimise active and reactive load curtailment, a load curtailment of 0 means there is no loss-of-load.
 - Active and Reactive power consumption and generation must be equal, $\sum \mathbf{P} = 0$ and $\sum \mathbf{Q} = 0$, see Equation 2.48 and Equation 2.54.
 - The current flows on the lines must stay within the rated values for the lines.
 - The active power generation at each bus cannot exceed its maximum capacity, nor be negative.
 - The reactive power generation must stay within their given limits.
 - The active load curtailment at each bus cannot exceed the active load at that bus, nor be negative. The same is true for the reactive load curtailment.
 - The voltage at each bus must stay within their given limits.
-

When looking at line overloading, in the AC case the maximum current is considered rather than the transferred power as in DC. The absolute value of the line current is given by 2.55.

$$|I_{ij}| = |V_i - V_j| |y_{ij}| \quad (2.55)$$

Where I_{ij} is the current flowing from bus i to bus j , V_i is the voltage phasor at bus i , V_j is the voltage phasor at bus j and y_{ij} is the admittance for the line.

Different variables can be considered when looking at what to minimise in the objective function. These are called the decision variables. Reference [17] suggests using a vector W as defined in Equation 2.56, where the decision variables are active and reactive power, active and reactive load curtailment, bus voltage, and bus angle. It is also mentioned by [17] that other decision variables can be included.

$$\mathbf{W} = P_{gen,1} \cdots Q_{gen,1} \cdots C_{P,1} \cdots C_{Q,1} \cdots V_1 \cdots \delta_1 \cdots \quad (2.56)$$

An optimisation problem can then be defined as in Equation 2.57.

$$\min \quad \mathbf{k}^\top \cdot \mathbf{W}; \quad (2.57)$$

$$\text{subject to} \quad \mathbf{P}_{gen} + \mathbf{C}_P - \mathbf{P}_{load} - \mathbf{P}(\mathbf{V}, \boldsymbol{\delta}) = 0 \quad (2.58)$$

$$\mathbf{Q}_{gen} + \mathbf{C}_Q - \mathbf{Q}_{load} - \mathbf{Q}(\mathbf{V}, \boldsymbol{\delta}) = 0 \quad (2.59)$$

$$|\mathbf{I}| \leq |\mathbf{I}_{max}| \quad (2.60)$$

$$0 \leq \mathbf{P}_{gen} \leq \mathbf{P}_{gen,max} \quad (2.61)$$

$$\mathbf{Q}_{gen,min} \leq \mathbf{Q}_{gen} \leq \mathbf{Q}_{gen,max} \quad (2.62)$$

$$0 \leq \mathbf{C}_P \leq \mathbf{P}_{load} \quad (2.63)$$

$$0 \leq \mathbf{C}_Q \leq \mathbf{Q}_{load} \quad (2.64)$$

$$\mathbf{V}_{min} \leq \mathbf{V} \leq \mathbf{V}_{max} \quad (2.65)$$

$$-\pi \leq \boldsymbol{\delta} \leq \pi \quad (2.66)$$

$$\mathbf{H}_{load} \cdot \mathbf{C}_P - \mathbf{C}_Q = 0 \quad (2.67)$$

- \mathbf{k} : Cost column vector corresponding to the elements of \mathbf{W} .
- \mathbf{W} : column vector of decision variables to minimize.
- \mathbf{P}_{gen} : column vector of active generation.
- \mathbf{C}_P : column vector of active load curtailment.
- \mathbf{P}_{load} : column vector of active load.
- $\mathbf{P}(\mathbf{V}, \boldsymbol{\delta})$: column vector of active power injection calculated from Equation 2.37.
- \mathbf{Q}_{gen} : column vector of reactive generation.
- \mathbf{C}_Q : column vector of reactive load curtailment.
- \mathbf{Q}_{load} : column vector of reactive load.
- $\mathbf{Q}(\mathbf{V}, \boldsymbol{\delta})$: column vector of reactive power injection calculated from Equation 2.38.
- \mathbf{I} : column vector of line currents.

- \mathbf{I}_{max} : column vector of maximum line currents.
- $\mathbf{P}_{gen,max}$: column vector of maximum generation limits.
- $\mathbf{Q}_{gen,max}$: column vector of maximum reactive power generation.
- $\mathbf{Q}_{gen,min}$: column vector of minimum reactive power generation.
- \mathbf{V}_{max} : column vector of maximum bus voltage.
- \mathbf{V}_{min} : column vector of minimum bus voltage.
- \mathbf{H}_{load} : a column vector of relation between active and reactive load.

Equation 2.67 is added to ensure the load at a bus maintains the same power factor if load curtailment arises [17].

By passing the problem to a non-linear optimisation problem solver, it can be determined if and where load curtailment arise, and by extension if a LOL situation has arisen.

2.1.14 General Approach

By combining the elements presented in the preceding chapters, a general approach to conduct HL-II analysis can be formulated.

In Figure 2.6, a flowchart for determining Loss-of-Load situations in HL-II is presented, but will be more thoroughly explained in the following section. It is important to note that this approach assumes that the state to be investigated is already sampled, as shown in section 2.1.9.4.

The first check which is done is to ascertain if the given system state S is a contingency case. By definition, a contingency case is a system representation where one or more components are on outage. If the current system state is a contingent system state, contingency analysis is conducted.

Contingency analysis is the use of an AC load flow solver, as detailed in section 2.1.10, or DC load flow solver, as detailed in section 2.1.11. When the contingency analysis is finished, the line loading needs to be checked. If one or more lines carry more power than their rating, a rescheduling of power generation is conducted. This is done by the use of an optimisation problem solver, with the formulations for the optimisation problems as defined in section 2.1.12 for DC or section 2.1.13 for AC.

If there is a load curtailment after the generation rescheduling, then the current system state is a Loss-of-Load situation.

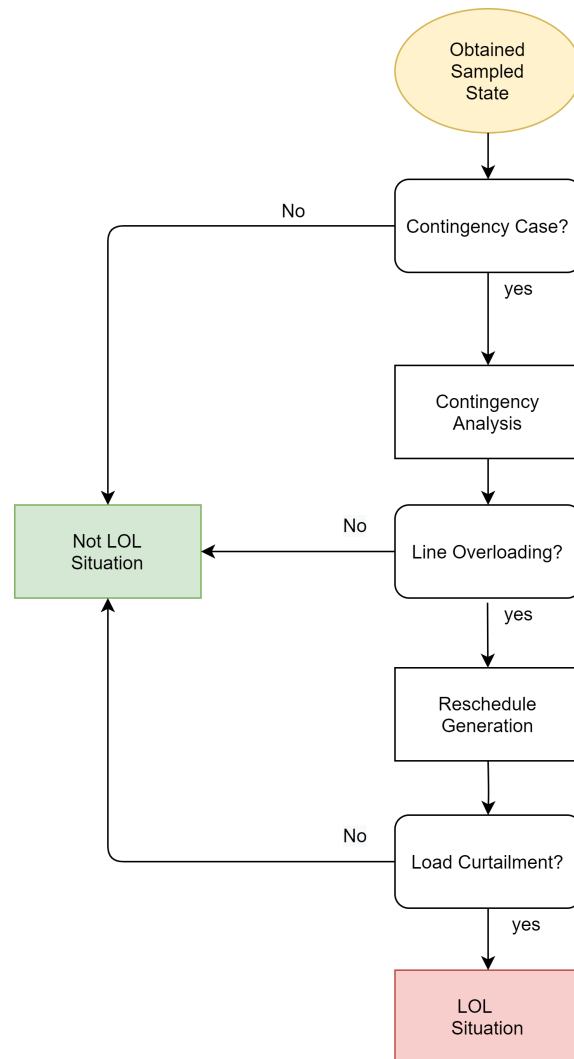


Figure 2.6: A flowchart representing how to determine if a state in a HL-II analysis is a Loss-of-Load (LOL) situation, based on the methodology presented in [6].

2.2 Literature Review and State-of-the-Art

As the interest and need for more large-scale WECS installations have increased, several different methods for PSR assessment with significant wind power penetration have been developed. A vast amount of literature exists on the assessment of PSR for cases with wind penetration. There are many considerations that have to be considered when integrating WECS, since they behave very differently from conventional generating units. One of the challenges for assessment with wind energy penetration is to provide an accurate representation of the variability and intermittency of the WTG power output. Many different indices, approaches and methods exist for PSR assessment, but there is no established methodological approach. This can make it confusing to find the optimal approaches. Naturally, there exists more literature for reliability at HL-I, compared to the more complex HL-II. Probabilistic reliability assessment is usually divided between two main approaches: analytical and Monte Carlo Simulation methods [14, 18]. The difference lies in how the contingencies are selected. In analytical methods, like the contingency enumeration approach, the contingencies are first selected by screening techniques and then based upon a failure criteria. Monte Carlo Simulations select the contingency based upon random sampling [14]. Hybrid models have also been constructed [19, 20].

2.2.1 The Need for New Reliability Criteria and the GARPUR Project

Historically in Europe, composite power system reliability management has been relying on the deterministic N-1 criterion. This criterion requires that the system should be able to withstand, at all times, an unexpected failure or outage of a system component in such a way that the system is capable of accommodating the new operational situation without violating its limits. Today, the increasing uncertainty of generation due to intermittent energy sources, and the growing complexity of the pan-European power system, further the need for new reliability criteria. Reliability criteria that show a better balance between reliability and costs [21]. The N-1 criterion is becoming increasingly expensive, which also means more expensive electricity for consumers. Besides, the probabilities of occurrence of single-component failure events are usually ignored, and multiple component failures are excluded from consideration in the N-1 criterion. It is difficult to deal with all the uncertainty factors using deterministic methods, including uncertainties in load forecast and the location of the future generation [18]. New approaches which can take advantage of new possibilities such as demand flexibility, energy storage and advanced grid monitoring could allow the power system to operate closer to its optimum. The GARPUR project, a 4-year EU project coordinated by SINTEF Energy Research with a budget of approximately 10.9 million euro, has developed a new methodology that allows TSOs to assess the probability and consequences of failures in their power system, expressed as the potential cost of power interruptions to consumers [21].

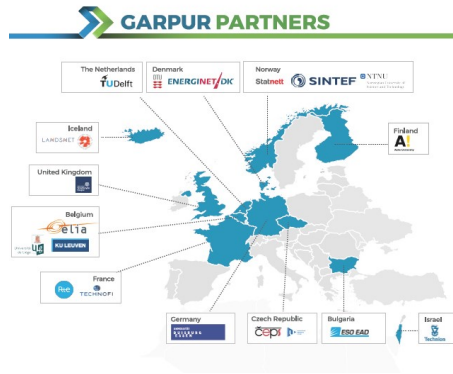


Figure 2.7: The GARPUR Partners, consisting of 7 European Transmission System Operators, along with 12 universities and research centres [21]

2.2.2 The Well-Being Analysis - Combining Deterministic and Probabilistic Methods

The basic probabilistic techniques, as presented in section 2.1, are quite widely utilised in the actual generation planning area. However, for transmission planning, most utilities currently utilise the deterministic N-1 criterion approach due to its complexity [22]. The well-being analysis, illustrated in Figure 2.8, was developed to create a bridge between the deterministic and probabilistic methods and create an effective framework for adequacy assessment [22–26].

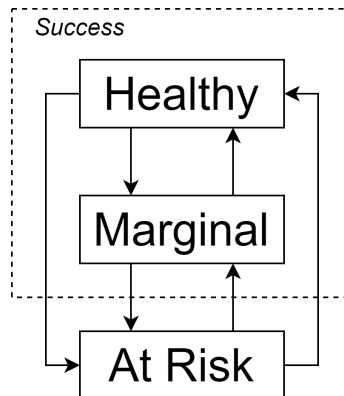


Figure 2.8: The system well-being analysis model

The well-being analysis method consists of system operating states which are categorised as being either healthy, marginal or at-risk. A system operating in the healthy state yields that it has enough capacity reserve to meet a deterministic criterion, like the loss of the largest online generating unit. The marginal state yields that the system is not in any trouble, but does not have sufficient margin to meet the predefined deterministic criterion. Lastly, the at-risk state yields that the load exceeds the available capacity. This state is equal to the LOLP, explained in section 2.1. The well-being indices are given as probabilities, frequencies, and durations of the healthy, marginal and risk states. The system well-being analysis has been used for assessment with wind penetration, such as in [23, 25]. The analysis can give an extended viewpoint of the effects of adding WTGs to a system, due to the different system operating states. References [26, 27] provide more details of the system well-being analysis methodology.

2.2.3 Concerns Related to Wind Power

According to [10], modelling considerations concerned with topics such as protection systems, cascading, weather effects and remedial control actions are well covered in the literature. Renewables and market modelling, however, is not. Renewable generation, and wind, in particular, is an emerging issue as it presents operational and transmission planning challenges. Correlations of wind energy output across geographically separated sites can cause significant changes in power flow and corresponding challenges in voltage control, line congestion and frequency regulation. Tools that allow consideration of stochastic variables to assess such impacts are needed [28]. In general, MCS is the most recognised probabilistic approach at HL-II with significant wind penetration, due to the immense complexity for HL-II systems. Another important aspect is that it is difficult to build analytical models of wind farms considering wind power correlation [29].

Another issue with wind energy is that the fuel source is not transportable, so the developer needs to be able to make an economic case for investing in generating facilities at the site of the energy source, with the ability to transmit the power electrically to load centres. In most regions, the ideal locations for wind plants are often both remote from load centres and from major transmission corridors. As a result, many transmission owners are facing challenges in trying to justify transmission investments in the face of uncertain generation commitment [28].

2.2.4 The Concept of Capacity Credit

To quantify the impact of wind penetration on the reliability of the power systems, the concept of capacity credit is often utilised [4, 11, 30]. Capacity Credit, or Capacity Value, is a value that quantifies how much new generation contributes to the reliability of a system. Effective Load Carrying Capability (ELCC) is the preferred CC index since it is an independent value with only load and generation as input [11]. It is used as the standard measure in evaluating the contribution of intermittent generation, providing the additional load to the system while keeping the same LOLE level of the system [30]. The ELCC of new wind power generation is often computed by using the multi-state unit representation of the wind plant, and includes the wind generation in a COPT calculation [11]. A major concern associated with this approach is the loss of information on wind speed correlation and correlation between load and wind [30]. ELCC is a measure of the generation system reliability (HL-I), and cannot be directly integrated into composite power systems [31]. To get an evaluation of the adequacy of a composite system, both load point indices and system indices are needed. The most common single index in composite adequacy assessment is the EENS. The EENS combines the frequency and magnitude of outages into one single index. The EENS can be combined with an appropriate interrupted energy assessment rate (IEAR) to estimate the customer outage costs at a load point or for the overall system [14]. Various other indices also exist, which can be specific for both load points or the entire system.

2.2.5 Wind Power Considerations

There is no consensus on how to treat wind power in composite adequacy evaluations [31]. Due to its intermittent nature, the wind power must be treated very differently compared to conventional generators. No other energy source used on a large scale has intermittency as significant as the wind [32]. Considerable work has been done on developing methods for generating capacity adequacy evaluations and reliability assessment of conventional generating systems incorporating wind power [4, 11, 33–37]. However, most studies focus on HL-I. Relatively little work has been done on the integration of wind power in composite generation and transmission system reliability analysis [31, 38]. An applicable model for wind power needs to be able to incorporate the randomness

and the intermittent characteristics of the wind speed for any wind unit. Probabilistic reliability techniques are able to do this [39]. Some of the models seen in the literature are: utilising the observed wind speed data directly, mean observed wind speed, ARMA model, normal distribution, Markov models and the multi-state WECS model. The modelling of wind power can be divided between the modelling of the wind speed and the modelling of the WTG output power.

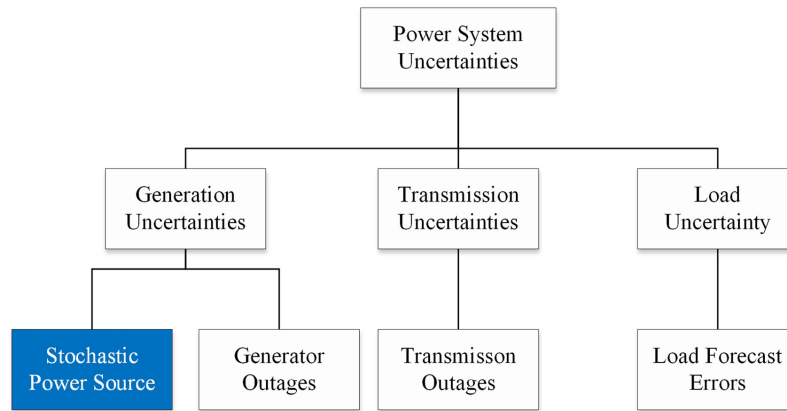


Figure 2.9: Typical uncertainties in power systems [40]

2.2.6 The Wind Speed

The power produced by a WTG at a particular site is highly dependent on the wind regime at that location. Wind speed can be modelled in a number of ways in power system reliability evaluation [41]. Some models contain much more information than other models and therefore have the potential to provide more accurate adequacy assessment [42]. The observed wind speed method uses an observed hourly wind speed data set repetitively in the reliability evaluation sequential simulation process. Typically, the hourly wind speed data then lasts for one year. If the mean of the observed wind speed is to be used, there must be existing wind speed data for several years. The mean for each hour is then calculated based on different annual wind speed data sets. The hourly mean wind speed is then used repetitively in the sequential simulation process [4].

According to [25], observed wind speed data cannot fully represent the wind speed variations from year to year. Using mean values, the reliability indices can be lower than those obtained using other models if the mean wind speed is close to the rated wind speed, and higher than those obtained using other models if the mean wind speed is much lower than the rated wind speed. A reason for this can be the nonlinear shape of the WTG power curve. The ARMA method, which uses the autoregressive moving average (ARMA) model to predict wind speeds, is based on the observed wind speed data and incorporates the yearly wind speed variations. If only a small number of years of data are used, the formed ARMA model tends to produce reliability indices that are closer to those obtained based on a large number of years of data [25]. According to [25], the ARMA model “provides a more comprehensive representation of wind speeds” and is more suitable for the Sequential MCS. Drawbacks of the ARMA model involve heavy computation overhead and large amounts of data are required for training the ARMA parameters [40].

Wind speed can also be simulated using a normal distribution approach. Weibull distributions are often used to characterise wind speed distributions [4, 43, 44]. This statistical tool expresses how often winds of different speeds will be observed at a location with a certain average (mean) wind speed. From given data sets, parameters describing the distributions of wind speeds can be extracted. It is generally agreed that the Weibull probability density function adequately represents the wind speed probability distribution for most sampling times [45]. By using the inverse transform

method, an algorithm can generate Weibull distribution random variates. This method is able to model the random behaviour of the wind speed [46]. A drawback with this approach is that, unlike the ARMA model, the autocorrelation between the wind speed at a particular and the previous hours is not considered. Therefore, yearly wind speed variations are not incorporated.

There also exist some new, interesting methods which are being developed to model the wind speed, like the Artificial Neural Network (ANN) [47, 48]. AI methods are promising alternatives to predict wind speed and to understand the wind behaviour for a region. This computational tool consists of simple parallel elements known as neurons, which consist of connected input, output and hidden layers. Each neurone in the input layer represents a unique attribute in the data set, like wind speed, earth temperature, relative humidity and elevation [48]. By using concepts of AI, a training process is executed, which obtains the weights of each connection between the layers and the neurons threshold value [47].

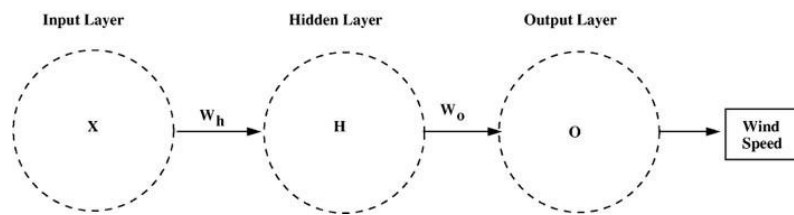


Figure 2.10: Simplified, illustrative layout of an ANN model [48]

Another promising tool to forecast the wind speed is the Wind Power Scenario Tree Tool [24, 49]. Reference [49] claims that the reliability of systems with high wind penetrations is impacted by the uncertainty associated with wind forecasting error. To solve this, the authors came up with a tool to examine the impact of wind forecast error statistics on unit commitment for high wind penetration test systems. A detailed representation of the tool is given in [49].

2.2.7 The Wind Turbine Generator

The WTG power curve can be used directly to calculate the output power when the wind speed is given. The power curve is dependent on different quantities, and can vary between different types of WTGs. This approach can involve much calculation, due to the non-linear relationship between wind speed and output power. It is the most popular approach for the Sequential MCS when wind speed is sampled chronologically.

A capacity outage probability table of a WTG can be created by applying the hourly wind speed to the power curve. Output states for a WTG are then defined as segments of the rated power, and the total number of times that the wind speed results in a power output falling within one of the output states is calculated. The probability of each state is then determined by dividing the total number of occurrences for each output state by the total number of data points.

A multi-state WECS model is often utilised when wind power is to be included in a calculation process using an analytical technique or a Non-sequential Monte Carlo approach [41, 42]. One method to obtain a multi-state WECS model is to use some sort of hourly wind speed data to obtain the probability density of the wind for different wind speeds. This can subsequently be compared with the power curve of the WTG unit to calculate the probability of different power outputs, as illustrated in Figure 2.11.

The number of states can be critical for a reliability assessment, because more states usually mean a better modelling accuracy as well as a higher computation overhead [40]. A five-state COPT model can achieve a trade-off between accuracy and computation overhead, and is used in many

reliability assessment cases [50].

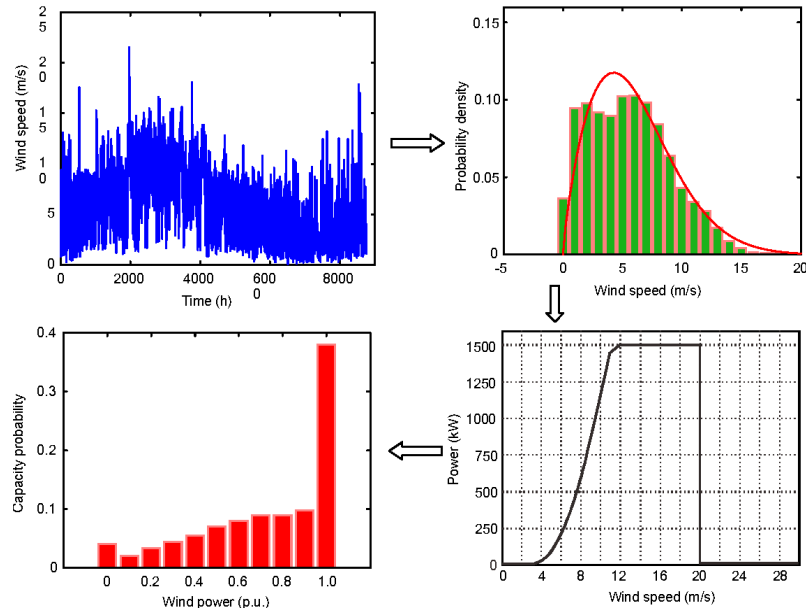


Figure 2.11: Example of a multi-state model for a wind unit [39]

Multi-state Markov models is another approach to model the WTGs. In this approach, the chronological wind power fluctuations are modelled by state transitions of a Markov model. A Markov model is a stochastic method for randomly changing systems where it is assumed that future states do not depend on past states. By this model, not only the state probabilities but also the frequency and duration indices are able to be calculated and evaluated [40]. The wind speed is represented by a Markov chain with a finite number of states. The wind model parameters can be calculated using the available observed wind speeds. The transition rates between wind speed states are needed in order to simulate wind speeds in the reliability evaluation process [41]. The drawback with this method is the computational overhead during reliability evaluation. The method is therefore not suitable to be applied to large scale systems [40].

The unavailability of the WTG can be expressed by the unit forced outage rate. According to [51], the changes in the FOR of the WTG units do not have a significant impact on the calculation of system reliability indices. The WTG FOR can therefore be neglected in many practical situations without creating unreasonable errors in the calculated reliability indices [52].

2.2.8 Developed Tools for HL-II Evaluation

Since composite system reliability assessment is complex, considerable efforts have been devoted to developing risk-based or probabilistic tools for power system planning and operation studies [28]. References [10, 28] provide lists of existing probabilistic planning tools, which are both commercial and research-grade tools. Among the presented tools, which are both aimed at long-term system development and short-term operational planning, the number of tools capable of performing analytical assessment and Monte Carlo simulation is approximately the same. With regards to the power flow solution algorithm, there is a slight overweight of tools capable of performing AC power flow compared to DC [10]. Among the most used programs in HL-II assessment with wind penetration is the MECORE program [38, 50, 52–54]. MECORE was developed at the University of Saskatchewan, Canada, and has been subsequently enhanced and applied by BC Hydro, Canada [28, 55]. This program is based on a combination of Monte Carlo simulation (State Sampling technique) and enumeration techniques, and utilises linear programming methods to arrive at optimal power

flows and optimal load curtailment [28]. The program can include appropriate multi-state renewable energy models, and is therefore suited for wind integration [55].

A program that utilises Sequential MCS in composite assessment with wind penetration is the RapHL-II program [56]. RapHL-II uses the fast decoupled AC load flow technique to calculate load flows and line loadings and to check the system operating constraints. An OPF approach is used to conduct corrective actions to alleviate operating constraints [57]. It should be noted that the program can utilise different load curtailment policies. Instead of using the priority order policy, which is based on ranking the bulk delivery points using a reliability worth index such as the IEAR, assessment often utilises the Pass-1 policy, where loads are curtailed at the delivery points that are closest to the elements on the outage [58]. If this load shedding policy is utilised, the end results can be very different from those obtained by the priority order policy. This illustrates the complexity of HL-II assessment. The RapHL-II program utilises the WTG power curve directly, instead of creating multi-state WECS models. HL-II assessment which has utilised the MECORE and RapHL-II programs utilise the ARMA wind speed model.

2.2.9 Correlated Wind Speeds

Correlation between wind speeds at different locations has been identified as an important factor when examining the reliability contribution of wind power in a power system. Correlations of wind energy output across geographically separated sites can have a significant impact on the power flow [28]. Multiple WECS can relatively easily be added to power systems in reliability assessment by simulating completely identical wind speeds, or by simulating totally independent wind speeds [35]. The latter is perhaps a reasonable assumption when the distances between the various wind farms are large. However, the assumption of site wind independence could be extremely optimistic if the sites are in reasonably close proximity. Studies show that the degree of wind speed correlation between two wind farms has a considerable impact on the resulting reliability indices [59].

Other factors that can influence the reliability benefit of WECS is the degree of hourly wind speed variation and the degree of correlation between wind energy output and load demands. Correlation of a time series with its own past and future value can be referred to as autocorrelation [59]. Only the ARMA wind speed model can incorporate autocorrelation. Also, the degree of correlation between period wind power output and load demands can influence the reliability benefit of adding WECS to a power system. Reference [54] developed seasonal and monthly WECS models which considered variation in wind speed and load models. The summation of seasonal system EENS obtained using the seasonal WECS model were similar to those obtained using the annual models. It was therefore concluded that the annual wind profile is an acceptable representation. Variations in the system reliability indices for different time periods are obviously dependent on the system conditions [54].

A power system containing multiple wind farms will generally have higher generating capacity adequacy than a system having only a single wind farm, even though the total installed WECS capacity in both cases are identical. The reliability benefit is, however, highly dependent on wind regimes, geographical dispersions, and the distances between wind farms. For composite assessment, potential reliability benefits are also dependent on the properties of the transmission system. The degree of the benefit can be measured in terms of the degree of wind speed correlation between the different wind locations [52, 59].

The previously presented HL-II reliability programs, MECORE and RapHL-II, have been modified to include wind site correlation [59]. In both programs, the ARMA models are adjusted to simulate correlated wind speeds with a specified wind speed cross correlation coefficient [53]. Little work is

done regarding the multisite problem using the Weibull wind speed model. However, reference [60] developed an analytical approach to model two-site WECS using the Weibull distribution.

2.2.10 Building a Comprehensive Framework for Conducting PSR Assessment at NTNU

In the last few years, as a part of building a comprehensive framework for conducting PSR assessment at the Department of Electric Power Engineering at NTNU, a few master theses regarding the assessment of PSR with wind penetration have been written. Reference [11] developed an analytical approach to assess the capacity credit of wind at HL-I. Historical wind speed data was used directly in the wind speed model. In [4], an assessment of the contribution of energy storage to PSR at HL-I with wind power penetration was conducted. This assessment utilised Sequential MCS using the State Transition method, which was based on the work of [3]. The wind speed model was obtained utilising Weibull distributions based on average historical wind speed data. Reference [3] created scripts for MCS using the State Sampling and State Transition for both HL-I and HL-II. To expand on the work that has been conducted thus far, this thesis attempts to further develop the HL-II MCS scripts developed in [3] to include wind power penetration. The ARMA and Weibull wind speed models have been identified as suitable wind speed models and will be included in the wind speed modelling. If multiple wind farms are added to a system, the degree of correlation between wind speeds can have a significant impact on the reliability benefit of adding WECS. Correlation between multiple wind speeds will therefore be included in both the Weibull and ARMA wind speed models.

2.3 Fundamental Knowledge of the Wind-Related Topics

The following section is an extension of the literature review as it presents the fundamental knowledge of the selected wind-related topics required for executing the objectives of the thesis.

Modelling conventional generators in MCS PSR assessment is a relatively straightforward task given their respective generator capacity, FOR or time to repair and time to breakdown. The Wind Energy Conversion System (WECS) model, however, is dependent on the site-specific wind speed regime, as well as the Wind Turbine Generator (WTG) model. There exist different methods to model both the wind speed and the WTGs, and the chosen methods can have a large impact on the final results of a PSR assessment when wind penetration is considered. The subsequently presented methods were selected and used in the developed HL-II MCS reliability assessment.

2.3.1 Wind Speed Modelling

The power of an air mass that flows at speed v through an area A can be calculated as illustrated in Equation 2.68. The power depends on the cube of the wind speed. This means that even small changes in wind speed can have large impacts on power generation. At the same time, wind speed fluctuates randomly with time. This illustrates the importance of accurate wind speed models to attain accurate results.

$$P_{wind} = \frac{1}{2}\rho Av^3 \quad (2.68)$$

Wind speed is usually modelled in hourly wind speed series. The wind speed data can be modelled using actual wind speed data for a lengthy period of time or by wind speed time series models

developed from the actual data [53]. When using historical data, several years of data from the same location is often utilised to give better predictive accuracy [11]. The subsequent chapters present sampled wind speed utilising the Weibull distribution and the Auto Recursive Moving Average (ARMA) time-series model.

2.3.1.1 Weibull Distribution

Weibull distributions are often used to characterise wind speed distributions [4, 43]. It is generally agreed that the Weibull probability density function adequately represents the wind speed probability distribution for most sampling times [45]. The parameters defining the behaviour of the PDF is extracted based on historical data, and a random number generator is then used alongside the PDF to sample wind speeds. The Weibull PDF is given by Equation 2.69.

$$f(v) = \frac{\beta}{\alpha} \left(\frac{v}{\alpha}\right)^{\beta-1} e^{-\left(\frac{v}{\alpha}\right)^\beta} \quad (2.69)$$

where:

- v : wind speed
- α : scale parameter
- β : shape parameter

The scale parameter, which is similar to the mean wind speed, indicates how windy the site is, on average. The shape parameter expresses how peaked the distribution is. If the wind speeds always tend to be very close to a certain value, the distribution will have a high shape parameter and be very peaked. This is illustrated in Figure 2.12.

The cumulative probability function for the Weibull distribution is illustrated in Equation 2.70.

$$F(v) = 1 - e^{-\left(\frac{v}{\alpha}\right)^\beta} \quad (2.70)$$

By using the inverse transform method [6], as illustrated in Equation 2.71, a way to randomly sample the wind speed from the Weibull distribution is illustrated in Equation 2.72. The randomly generated variable U is uniformly distributed in the range $[0,1]$.

$$v = F^{-1}(U) \quad (2.71)$$

$$v = \alpha(-\ln(U))^{\frac{1}{\beta}} \quad (2.72)$$

Where F^{-1} is the inverse cumulative probability function, U is a randomly generated uniformly distributed variable in the range $[0,1]$, α and β are the Weibull scale and shape parameters.

Examples of Weibull probability density functions with varying values of the scale parameter and the shape parameter is provided in Figure 2.12.

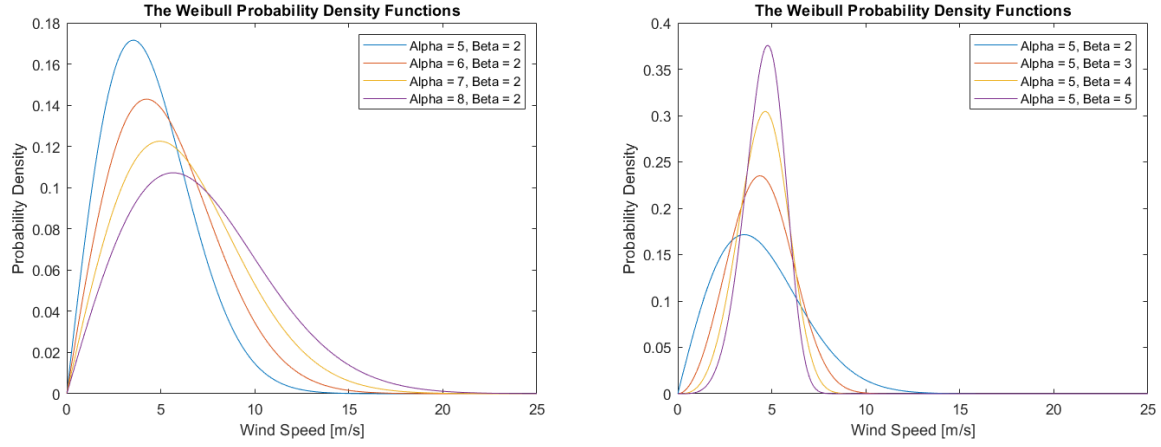


Figure 2.12: The Weibull Probability Density Functions with selected Weibull scale and shape parameters.

2.3.1.2 ARMA

Future hourly data can be predicted by using the time series model, which is based on historical wind speeds. This method incorporates the chronological nature of the actual wind speed. In the time series model, the simulated wind speed, SW_t , can be obtained from the observed mean wind speed and its standard deviation, as illustrated in Equation 2.73 [33].

$$SW_t = \mu + \sigma \cdot y_t \quad (2.73)$$

where:

- μ = Mean wind speed for the wind site
- σ = Standard deviation of the wind speed for the wind site

The original data series set, y_t , is used to create a wind speed time series referred to as an Auto-Regressive and Moving Average Model, ARMA (n, m), series model, as illustrated in Equation 2.74.

$$y_t = \phi_1 y_{t-1} + \phi_2 y_{t-2} + \dots + \phi_n y_{t-n} + \alpha_t - \theta_1 \alpha_{t-1} - \theta_2 \alpha_{t-2} - \dots - \theta_m \alpha_{t-m} \quad (2.74)$$

where:

- $\phi_i (i = 1, 2, \dots, n)$ = the auto-regressive parameters of the model
- $\theta_j (j = 1, 2, \dots, m)$ = the moving average parameters of the model
- $\alpha_t \in NID(0, \sigma_a^2)$ = a normal white noise process with zero mean and a variance of σ_a^2 .

A white noise process is a random process of random variables that are uncorrelated, have mean zero, and finite variance, σ_t . NID denotes Normally Independent Distributed. From Equation 2.74, new values of y_t can be calculated from α_t and previous values of y_{t-i} . The hourly wind speeds incorporating the wind speed time series can then be generated as illustrated in Equation 2.73. Each wind site has a unique ARMA time series model.

2.3.2 Wind Turbine Generator Modelling

The power output characteristics of a wind turbine generator (WTG) are quite different from those of conventional generating units as there is a non-linear relationship between the power output of the WTG and the wind speed. The power curve illustrates this non-linear relationship, and the relationship is usually described using the operational parameters of the WTG. The three commonly used parameters are the cut-in, rated and cut-out wind speeds. A general power curve is shown in Figure 2.13. The lowest wind speed that the WTG can produce power at is the cut-in wind speed, $V_{c,in}$. The rated wind speed, V_r , is the lowest wind speed that the WTG produce rated power at. The cut-off wind speed, $V_{c,out}$, is the designed wind speed at which the wind turbines stop producing power to prevent excessive stress and damage to the components of the WTG. The values of these parameters depend on the respective WTG model.

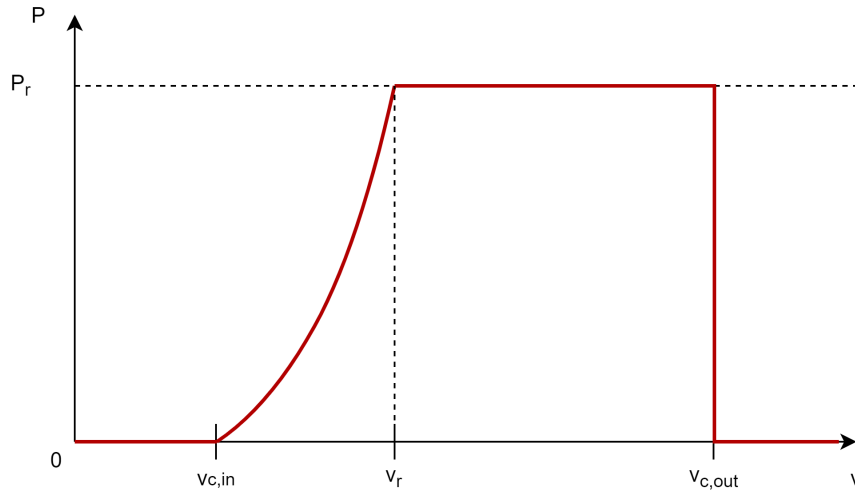


Figure 2.13: The general shape of a power curve for a WTG.

The WTG output, which reflects the power curve seen in Figure 2.13, is given by Equation 2.75.

$$P(W S_t) = \begin{cases} 0 & 0 \leq W S_t < V_{ci} \\ (A + B \cdot W S_t + C \cdot W S_t^2) \cdot P_r & V_{ci} \leq W S_t < V_r \\ P_r & V_r \leq W S_t < V_{co} \\ 0 & W S_t \geq V_{co} \end{cases} \quad (2.75)$$

where:

- $P(W S_t)$ = WTG output with the wind speed in time interval t [MW]
- $W S_t$ = Wind speed in time interval t [m/s]
- P_r = Rated output power from the WTG [MW]
- V_{ci} = Cut-in wind speed [m/s]
- V_r = Rated wind speed [m/s]
- V_{co} = Cut-out wind speed [m/s]

The constants A, B and C are found as functions of V_{ci} and V_r as shown in Equation 2.76.

$$\begin{aligned}
 A &= \frac{1}{(V_{ci} - V_r)^2} \left\{ V_{ci}(V_{ci} + V_r) - 4V_{ci}V_r \left[\frac{V_{ci} + V_r}{2V_r} \right]^3 \right\} \\
 B &= \frac{1}{(V_{ci} - V_r)^2} \left\{ 4(V_{ci} + V_r) \left[\frac{V_{ci} + V_r}{2V_r} \right]^3 - (3V_{ci} + V_r) \right\} \\
 C &= \frac{1}{(V_{ci} - V_r)^2} \left\{ 2 - 4 \left[\frac{V_{ci} + V_r}{2V_r} \right]^3 \right\}
 \end{aligned} \tag{2.76}$$

With the power curves and simulated wind speed, the available capacity, $C_{WTGs,i}(v)$, can be found for a WTG, as illustrated in Equation 2.77, by combining the WTG power output with a simulation of which units are on an outage.

$$C_{WTGs,j,i}(v) = P(v)x_{j,i} \tag{2.77}$$

Where:

- $C_{WTGs,j,i}(v)$ is the individual available capacity for WTG j at time i .
- v is the wind speed at time i .
- $P(v)$ is the function for the power curve.
- $x_{j,i}$ is the state of wind turbine j , either 0 or 1, at time instant i .

An example of the variation in output power from a WTG is provided in Figure 2.14, which illustrates the relation between wind speed and output power from a WTG. The illustration includes 500 consecutive hours of historical wind speed data from the ØrlandIII weather station(25.03.2015-15.04.2015) [61], and the corresponding output power from a WTG, obtained from Equation 2.75. The calculation utilised a cut-in wind speed, $V_{c,in}$, of $4m/s$, cut-out wind speed, $V_{c,out}$, of $22.22m/s$ and rated wind speed, V_r , of $10m/s$.

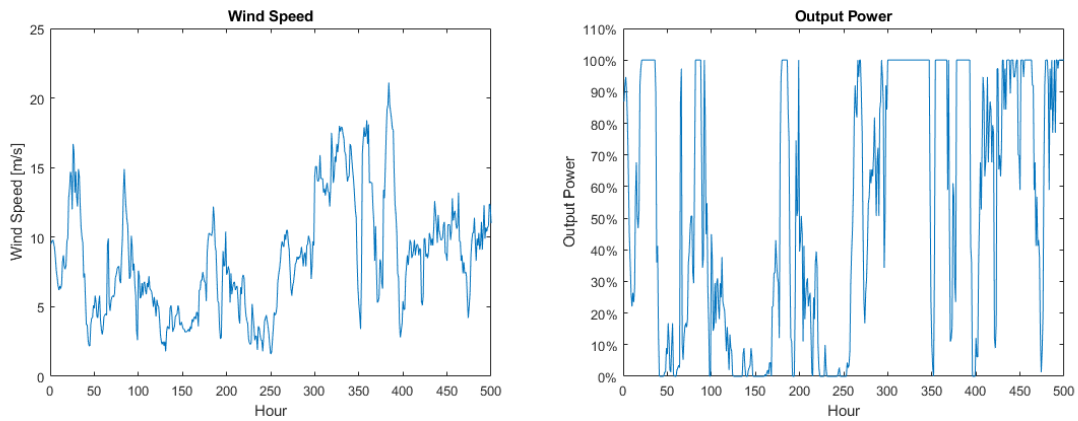


Figure 2.14: Illustration of the intermittent nature of the wind speed and the corresponding output power from a wind turbine generator.

2.3.3 Wind Speed Correlation

In HL-II assessment with wind power penetration, one is often interested in examining the impact of adding multiple WECS at different locations in a power system. In an HL-I assessment, where only the generation facilities are included, the locations of multiple WECS are not considered as load flows are not executed and individual bus indices are not considered. For the more complex HL-II assessment, however, the locations and distributions of wind power capacity can make a significant impact on the end results. An important consideration when adding multiple WECS to a power system is the degree of correlation between the wind speeds at the different sites. If the distances between wind farms are not very large, they are neither completely dependent nor independent, but are correlated to some degree. When the distance between two wind sites is very large, the wind speeds are approximately independent, while the wind speed within the same wind farm is approximately completely dependent [57]. The degree of correlation between wind sites is also dependent on factors such as geographic dispersion and the uniqueness of the individual wind regimes [53].

Wind speed correlation can be induced by generating correlated random numbers during the hourly simulation [59]. The correlation between sets of simulated wind speed data will then be close to the correlation between the random numbers. A challenge with this approach is to assure that the elements of the generated random variates are distributed uniformly over a given interval, e.g [0,1], while exhibiting a prespecified linear correlation.

A multivariate random variable X can be defined as illustrated in Equation 2.78, where F is some distribution function and $U \sim U[0, 1]$.

$$X = F^{-1}(U) \quad (2.78)$$

X will then be a random variable with distribution F . If this expression is reversed, one can create uniformly distributed variates from variates following other distributions by inserting the latter into their respective distribution function. However, such transformations typically affect the dependence between the original variates [62]. Linear correlation, known as Bravais-Pearson correlation, is not necessarily invariant to transformations, so there is no guaranty that a linear correlation between original non-uniform variates X will be preserved after a transformation. Rank correlation, known as Spearman correlation, is however invariant to any strictly increasing transformation. As long as F is strictly monotonically increasing, Spearman correlation will therefore be preserved. Further, the linear correlation (Bravais-Pearson) between uniforms obtained from transforming the original variates equals the rank correlation (Spearman) between the original variates. It is therefore possible to create linearly correlated normal variates from an adjusted linear correlation matrix, \sum^{adj} , and transform the normals into uniforms [62]. The adjusted correlation matrix, \sum^{adj} , is given by the relationship between Spearman correlation and Bravais-Pearson correlation, as illustrated in Equation 2.79.

$$\rho^B = 2\sin\left(\frac{\pi}{6}\rho^S\right) \quad (2.79)$$

- ρ^B = Bravais-Pearson correlation
- ρ^S = Spearman correlation

To generate the correlated normal variates, the concept of Cholesky Decomposition can be utilised. The Cholesky Decomposition is commonly used in the Monte Carlo method for simulating systems

with multiple correlated variables. The Cholesky decomposition is the process of decomposing any symmetric and positive definite matrix into the product of two triangular matrices, as illustrated in Equation 2.80, an upper-triangular matrix which when multiplied by its transpose produces the original symmetric matrix [63].

$$A = G^T \cdot G \quad (2.80)$$

- A = Symmetric positive definite matrix
- G = Upper triangular matrix with positive diagonal entries
- G^T = Transpose of matrix G

A set of r uncorrelated random number series with q members may be represented by a matrix X , as illustrated in Equation 2.81.

$$X = \begin{bmatrix} x_1^1 & \cdots & x_1^r \\ \vdots & \ddots & \vdots \\ x_q^1 & \cdots & x_q^r \end{bmatrix} \quad (2.81)$$

The desired correlation between any two sets of number series is represented by Equation 2.82

$$\Sigma = \begin{bmatrix} a_{11} & \cdots & a_{1r} \\ \vdots & \ddots & \vdots \\ a_{r1} & \cdots & a_{rr} \end{bmatrix} \quad (2.82)$$

- a_{ij} is the desired correlation between i^{th} and j^{th} column of matrix X .

The upper triangular matrix G can then be calculated using Cholesky decomposition [63]. A matrix X_C which contains p correlated random number series as defined in Equation 2.82 can be deduced as in Equation 2.83.

$$X_C = X \cdot G \quad (2.83)$$

If only two random number series are present, the method can be simplified as illustrated in Equation 2.84 [64].

$$X_C = X_1 \cdot r + X_2 \cdot \sqrt{1 - r^2} \quad (2.84)$$

- X_1 and X_2 are series of uncorrelated random numbers.
- r is the desired correlation coefficient from 0 to 1.
- Series X_C has a correlation of r with series X_1

While the Weibull wind speed model utilises uniformly generated numbers, the ARMA wind speed model utilises the random white function which follows a normal distribution with a set variance

and a mean of zero. The approach to induce correlated wind speed is therefore different for the ARMA wind speed model compared to the Weibull wind speed model.

In the ARMA wind speed model, the random numbers that input into the ARMA model need to be white noise. This means that they follow a normal distribution with a mean of 0. This white noise can therefore be generated by drawing random variables from the multivariate normal distribution. The two-dimensional multivariate normal distribution can be represented by a matrix $\boldsymbol{\mu}$, a vector of the mean values, and $\boldsymbol{\Sigma}$, the covariance matrix, as illustrated in Equation 2.85 and Equation 2.86. The relation between covariance and correlation is illustrated in Equation 2.87.

$$\boldsymbol{\mu} = \begin{bmatrix} \mu_1 \\ \mu_2 \end{bmatrix} \quad (2.85)$$

$$\boldsymbol{\Sigma} = \begin{bmatrix} \sigma_1 & \sigma_{1,2} \\ \sigma_{1,2} & \sigma_2 \end{bmatrix} \quad (2.86)$$

$$\text{Correlation} = \frac{\text{Covariance}}{\sigma_1 \sigma_2} \quad (2.87)$$

When both $\sigma_1 = \sigma_2 = 1$, a special case arises where the covariance and correlation are equal. Therefore, two random variables following a normal distribution with mean, $\mu = 0$, variance, $\sigma = 1$, and prespecified correlation $corr_{1,2}$ can be found by use of the two-dimensional multivariate normal distribution with parameters $\boldsymbol{\mu} = \begin{bmatrix} 0 \\ 0 \end{bmatrix}$ and $\boldsymbol{\Sigma} = \begin{bmatrix} 1 & corr_{1,2} \\ corr_{1,2} & 1 \end{bmatrix}$.

While the random variables used in the ARMA model have a mean, μ , of 0, the variance, σ , is not necessarily 1. The normal white noise processes, $\boldsymbol{\alpha}$, must therefore be scaled, as illustrated in Equation 2.88.

$$\alpha_{\mu=0, \sigma=\sigma_1} = \alpha_{\mu=0, \sigma=1} \cdot \sigma_1^2 \quad (2.88)$$

The scaled $\boldsymbol{\alpha}$ can now be utilised in Equation 2.74 which in turn can be used in Equation 2.73 to determine the correlated wind speeds.

3 Methodological Approach

The objective of this thesis was to create a comprehensive framework for assessing the reliability of a composite power system that contains significant wind penetration, through MCS. A suitable methodology for the PSR assessment, which enables the quantification of the system reliability with the help of appropriate indices is presented in this chapter. The developed software tools, based on the presented methodological approach, are applied to test systems, the RBTS, the MRBTS and the IEEE-RTS. A Sequential approach and a Non-sequential MCS approach have been developed for different wind speed models. It was determined that an accuracy of 2.5 % or better was sufficient for the obtained results. As such, the chosen amount of simulation years were based upon meeting this criterion.

3.1 Load Model

All of the simulations in the thesis utilise the hourly peak load model, which has 8736 load levels per year. More details about the load model is presented in section 2.1.4.

For a HL-II analysis, a load requirement for each bus is required. To determine the load at a given bus at a given hour, Equation 3.1 is utilised.

$$P_{load,i} = HPL \cdot c_i \quad (3.1)$$

where:

- $P_{load,i}$ = The loading at bus i at a given hour [MW]
- HPL = The hourly peak load at a given hour [MW]
- c_i = The percentage of the systems load that is located at bus i

In this thesis the following assumptions are made for the load models:

- Each bus will always take the same percentage of the load, no matter the total load level. As a result, c_i is constant for a given bus i .
- The hourly peak load follows a specified distribution, and is equal for every simulation year.

The formula to calculate the hourly peak load for each hour is presented in Equation 3.2. The values for l_w , l_d and l_h are presented in Appendix C, and are used for both the RBTS and the RTS. Yearly Peak Load for the RBTS and the RTS is presented in Appendix A and Appendix B, respectively.

$$HPL_{h,d,w} = YPL \cdot l_w \cdot l_d \cdot l_h \quad (3.2)$$

where:

- $HPL_{h,d,w}$ = Hourly Peak Load calculated by hourly, daily and weekly percentages [MW]
- YPL = Yearly peak load [MW]
- l_w = Weekly peak load as a percentage of yearly peak load
- l_d = Daily peak load as a percentage of weekly peak load
- l_h = Hourly peak load as a percentage of daily peak load

3.2 Non-sequential State Sampling Approach

The following step-for-step guide describes the algorithmic approaches for the Non-sequential State Sampling approach.

1. Initialising the script:
 - Loading in all the parameters.
 - Converting the values to the per unit system.
 - Calculating the power curve parameters.
 - Creating a vector to store the results of the OPF solver.
2. Running the simulation:
 - (a) For each hour in a year the following is computed:
 - i. Generate a random uniformly distributed number U in the range $[0,1]$ for each component in the system, and compare it against the FOR of that component to determine if it is in the up-or down-state.
 - ii. if the system is in a contingency state (at least one component in the down state):
 - Determine the wind speeds at each bus, by use of the Weibull distribution or ARMA-model.
 - Use the states of the generators and WTGs as well as the wind speeds to determine the available capacity at each bus.
 - Use the found capacity, line states and load curve to update the parameters for the OPF problem.
 - Run the OPF solver
 - If a solution with no curtailment was found, move to the next step
 - If a solution with curtailment was found, denote a failure and how much energy was curtailed and at which bus(es). Then move to the next step.
 - (b) Return to step 2(a) until the wanted number of years has been simulated.
3. Use the results from the simulation to calculate indices.

In Figure 3.1. a flowchart representation of the above instructions is presented. The green boxes symbolise the initialisation part of the algorithm, the black box symbolises the state determination part of the algorithm. The blue boxes symbolise the main loop of the algorithm, which keeps track of the current hour and year. The red boxes symbolise the OPF related part of the algorithm. Finally, the magenta box symbolises the calculation and exporting of the indices. In the flow chart, contingency case means a system state where at least one component is in the down state.

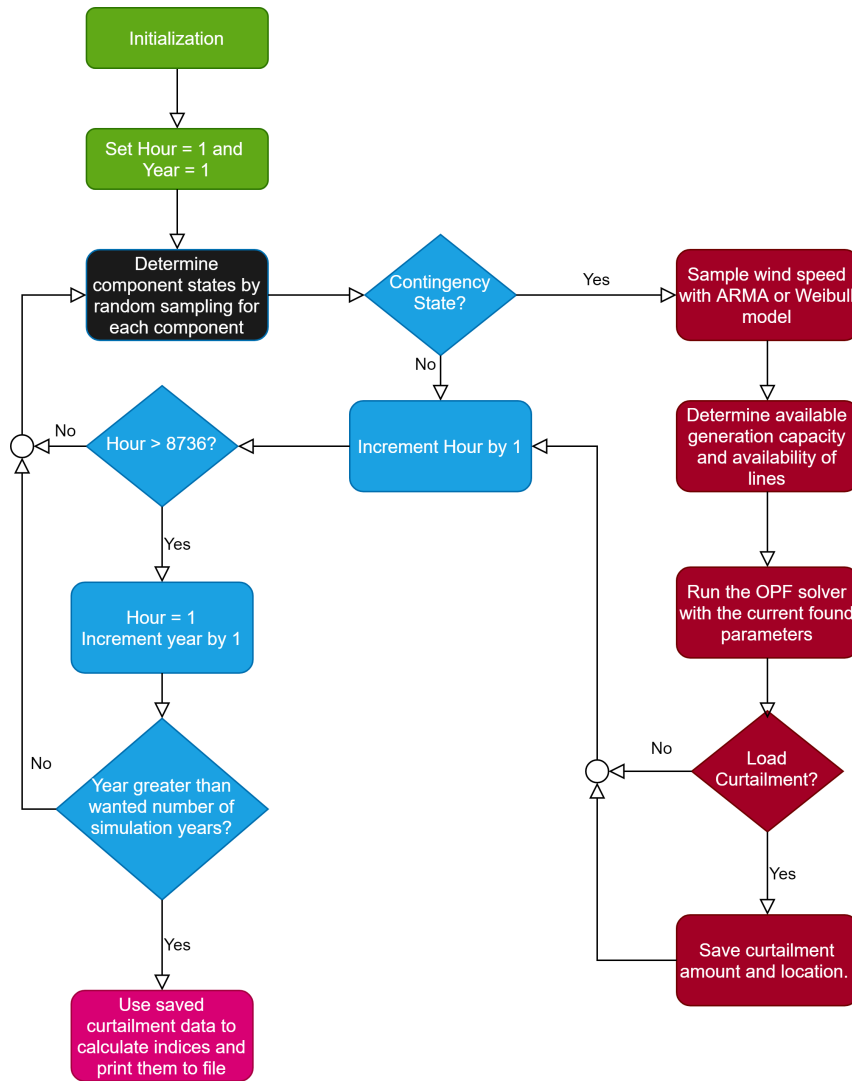


Figure 3.1: A flowchart detailing how the State Sampling algorithm works.

3.3 Sequential State Transition Approach

With the State Transition approach, it is entirely possible for components to change state multiple times between each hour. To account for this a time counting variable t is introduced. Every time a new component state is changed, t is incremented with the time to the next component transition. The counting variable for the hour (called “current hour”) is only incremented when t is larger than or equal to the current hour.

The step by step guide for the script now follows:

1. Initialising the script:

- Loading in all the parameters.
- Converting the values to the per unit system.
- Calculating the power curve parameters.
- Creating a vector to store the results of the OPF solver.
- Initialising the component state vector, assuming every component to be in the up-state.

- Calculate the time to the first state transition using Equation 2.16, and increment t with that amount.
2. Running the simulation:
 - (a) Check to see if the time counting variable t is larger than or equal to the next hour
 - i. If not; determine which component next transitions using Equation 2.17 and how long it is until it transitions using Equation 2.16.
 - ii. Update the vector of component states and increase t with the calculated time to next transition.
 - iii. Return to step 2(a).
 - (b) If t is larger than or equal to the current hour, compute the OPF at the given hour.
 - i. Determine which component is in the up and down state by using the current component state vector.
 - ii. if the system is in a contingency state (at least one component in the down state):
 - Determine the wind speeds at each bus, by use of the Weibull distribution or ARMA-model.
 - Use the states of the generators and WTGs as well as the wind speeds to determine the available capacity at each bus.
 - Use the found capacity, line states and load curve to update the parameters for the OPF problem.
 - Run the OPF solver
 - If a solution with no curtailment was found, move to the next step
 - If a solution with curtailment was found, denote a failure and how much energy was curtailed and at which bus(es). Then move to the next step.
 - iii. Increment the hour counter to the next hour
 - If this was the last hour in the year, reduce t with 8736 and go to step 2(c).
 - Otherwise, return to step 2(a).
 - (c) Repeat from step 2(a) until the wanted number of years have been simulated.
 3. Use the results from the simulation to calculate indices.

In Figure 3.2, a flowchart representation of the above instructions is presented. The green boxes symbolise the initialisation part of the algorithm, the black boxes symbolise the state determination part of the algorithm. The blue boxes symbolise the main loop of the algorithm, which keeps track of the current hour and year. The red boxes symbolise the OPF related part of the algorithm. Finally, the magenta box symbolises the calculation and exporting of the indices. In the flow chart, contingency case means a system state where at least one component is in the down state. Compared to the State Sampling approach as seen in Figure 3.1, only the black boxes and the addition of variable t in the initialisation are different.

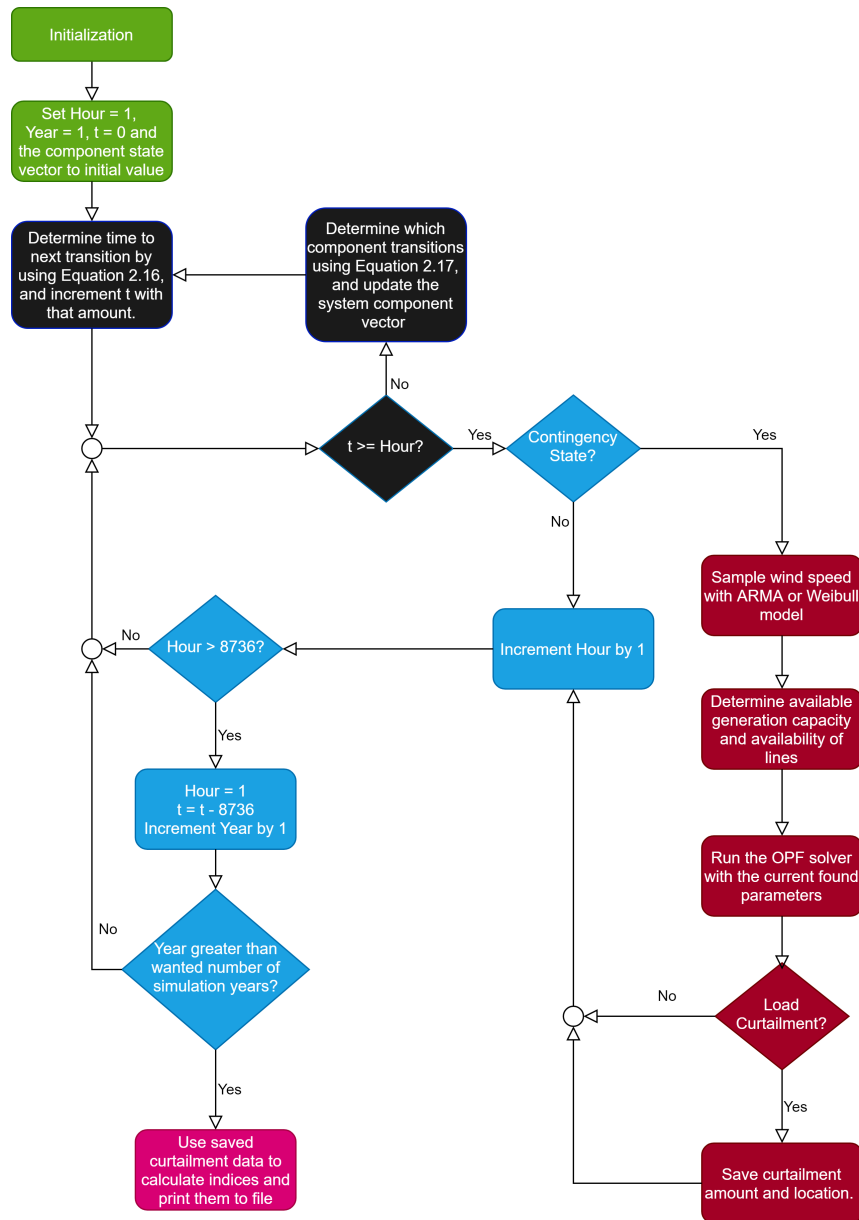


Figure 3.2: A flowchart detailing how the State Transition algorithm works.

3.4 Wind Speed Correlation

To include wind speed correlation between multiple WECS, the following methods were developed for the Weibull- and ARMA wind speed models.

3.4.1 Weibull Model

The Weibull wind speed model utilises randomly generated uniformly distributed variables in the range $[0,1]$. To achieve correlated wind speed data, uniformly distributed random variates need to remain bounded in the interval $[0,1]$ while exhibiting a given correlation coefficient between 0 and 1, where 0 implies no correlation and 1 implies completely correlation. The following method generates a set of correlated wind speeds in the Weibull wind speed model:

- Set up the desired correlation matrix, Σ , which specifies the desired linear correlation between wind sites.
- Find the linear correlation matrix, Σ^{adj} corresponding to the Spearman matrix Σ , as illustrated in Equation 3.3:

$$\Sigma^{adj} = 2 \cdot \sin\left(\frac{\pi}{6}\Sigma\right) \quad (3.3)$$

- Create normal variates with the adjusted correlations: $Z \sim \mathcal{N}(0, \Sigma^{adj})$ by using Cholesky factorisation [63].
- Transform the normal variates into uniform variates: $U = F(Z)$
- Generate wind speeds from the correlated numbers, $U = [U_i \cdots U_n]$, and the Weibull scale and shape parameters (α, β) , as illustrated in Equation 3.4:

$$v_i = \alpha_i (-\ln(U_i))^{\frac{1}{\beta_i}} \quad (3.4)$$

$$v_n = \alpha_n (-\ln(U_n))^{\frac{1}{\beta_n}}$$

Figure 3.3 shows a flowchart of the approach explained above. The developed code implementation of this approach is presented in appendix D.5 and appendix D.6.

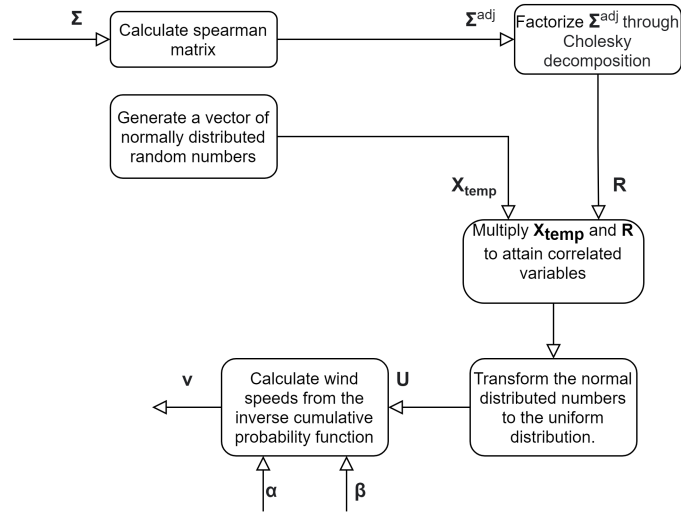


Figure 3.3: Flowchart showing the algorithmic process of attaining correlated wind speeds with the Weibull model.

The scatter plots of 2000 pairs of correlated random numbers, using different correlation coefficients, using the presented method are illustrated in Figure 3.4. For a correlation coefficient of 0.2, the actual correlation between the pairs was measured to be 0.1954. For a correlation coefficient of 0.5, the actual correlation between the pairs was measured to be 0.5053, while for a correlation coefficient of 0.8, the actual correlation was measured to be 0.8023.

To investigate the effect of correlation between wind speeds, the generated random numbers were applied to the Weibull wind speed equation, Equation 3.4. The scale parameter was set to 7 m/s,

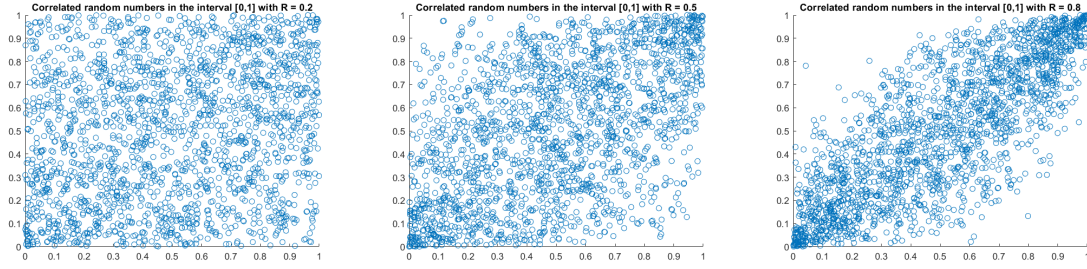


Figure 3.4: Scatter plots of correlated random numbers. Left: $R=0.2$. Middle: $R=0.5$. Right: $R=0.8$.

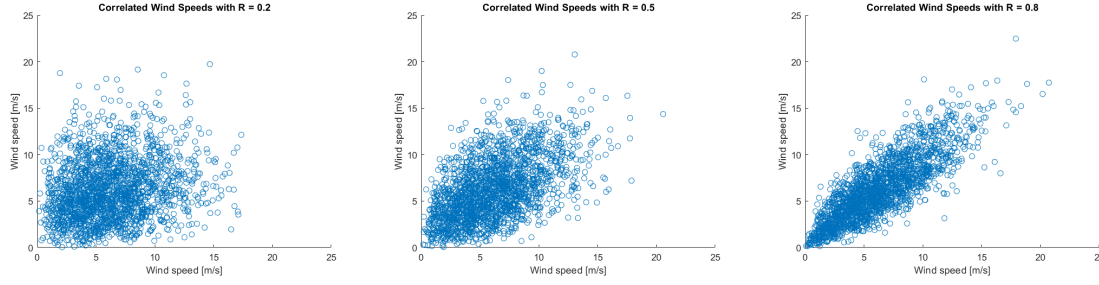


Figure 3.5: Scatter plots of correlated pairs of wind speed obtained from the Weibull wind speed model. Left: $R=0.2$. Middle: $R=0.5$. Right: $R=0.8$.

and the shape parameter was set to 2 m/s. The pairs of correlated numbers from Figure 3.4 were utilised, and the scatter plots of the pairs of the simulated wind speeds are presented in Figure 3.5.

It can be seen from Figure 3.4 and Figure 3.5 that the pairs of simulated wind speed series have a correlation close to the correlation of the random numbers. For a correlation coefficient of 0.2, the actual correlation between the wind speed pairs was measured to be 0.2145. For a correlation coefficient of 0.5, the actual correlation between the pairs was measured to be 0.5188, while for a correlation coefficient of 0.8, the actual correlation was measured to be 0.8238.

3.4.2 ARMA Model

The ARMA wind speed model utilises randomly generated normally distributed variables with mean $\mu = 0$ and variance σ^2 (white noise). To achieve correlated wind speed data, random numbers need to be drawn from this distribution with a given correlation coefficient between 0 and 1, where 0 implies no correlation and 1 implies completely correlation. The following method generates a set of correlated wind speeds in the ARMA wind speed modelling:

- Set up the desired correlation matrix, Σ , which specifies the desired linear correlation between wind sites. Σ is a $n \times n$ matrix, where n is the number of correlated variables wanted.
- Generate the correlated random numbers by drawing from the n -dimensional multivariate normal distribution with parameters $\mu = \begin{bmatrix} 0 & \dots & 0 \end{bmatrix}^T$ and Σ .
- The drawn variables have a variance of 1. Therefore, scale the variables to the correct variance by using Equation 3.5.

$$\alpha_{\mu=0, \sigma=\sigma_1} = \alpha_{\mu=0, \sigma=1} \cdot \sigma_1^2 \quad (3.5)$$

- Calculate y_t from the found correlated numbers and some of their previous values, $\alpha = [\alpha_t \cdots \alpha_{t-n}]$, the previous values of y_t : $[y_{t-1} \cdots y_{t-n}]$ and the corresponding ARMA model parameter for each variable, as illustrated in Equation 2.74. Note that different wind sites have different parameters for the ARMA models.
- Determine the wind speed by using Equation 2.73 with y_t , the mean and standard deviation of the wind regime.

Figure 3.6 shows a flowchart of the approach explained above. The developed code implementation of this approach is presented in appendix D.2, appendix D.3 and appendix D.4.

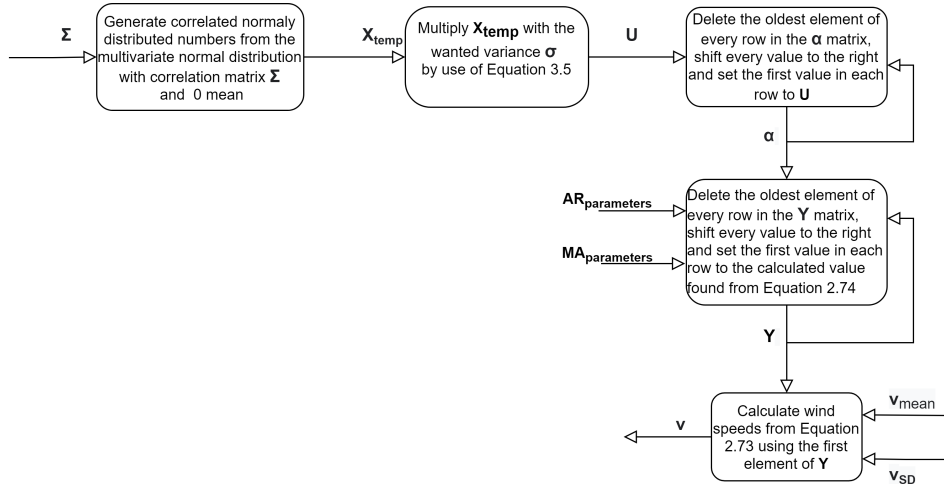


Figure 3.6: Flowchart showing the algorithmic process of attaining correlated wind speeds with the ARMA model.

200 000 pairs of correlated numbers were generated for different correlation coefficients, with the presented method. A scatter plot of the first 2000 pairs of correlated numbers is illustrated in Figure 3.7. For a correlation coefficient of 0.2, the actual correlation between the pairs was measured to be 0.1974. For a correlation coefficient of 0.5, the actual correlation between the pairs was measured to be 0.4993, while for a correlation coefficient of 0.8, the actual correlation was measured to be 0.8011.

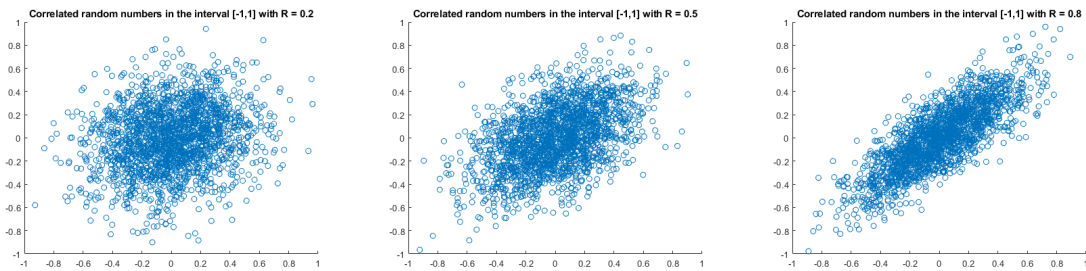


Figure 3.7: Scatter plots of normally distributed correlated random numbers with mean $\mu = 0$ and variance $\sigma^2 = 0.52476^2$. Left: $R=0.2$. Middle: $R=0.5$. Right: $R=0.8$.

To investigate the effect of correlation between wind speeds, the generated random numbers were applied to the Swift Current ARMA wind speed model, see Equation 4.1. The pairs of correlated numbers from Figure 3.7 were utilised, and the scatter plots of the first 2000 pairs of the simulated wind speeds are presented in Figure 3.8.

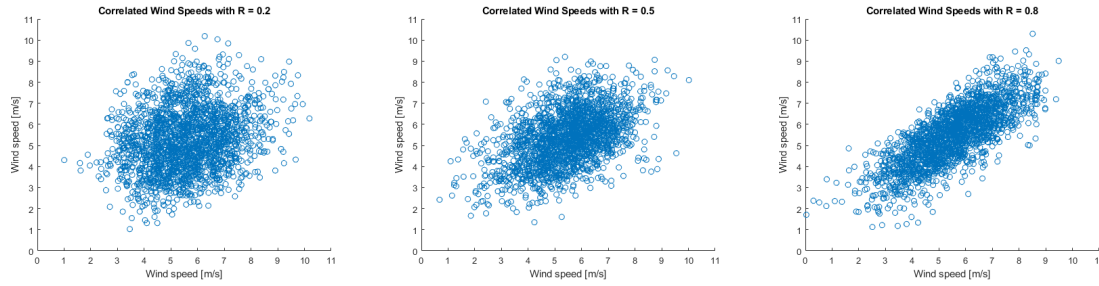


Figure 3.8: Scatter plots of correlated pairs of wind speed obtained from the Swift Current wind speed model. Left: $R=0.2$. Middle: $R=0.5$. Right: $R=0.8$.

It can be seen from Figure 3.7 and Figure 3.8 that the pairs of simulated wind speed series have a correlation close to the correlation of the random numbers. Calculating the correlation coefficient based on the 200 000 pairs for correlation 0.2, the actual correlation between the wind speed pairs was measured to be 0.1990. For a correlation coefficient of 0.5, the actual correlation between the pairs was measured to be 0.5013, while for a correlation coefficient of 0.8, the actual correlation was measured to be 0.8000.

3.5 Illustrative Example

In this section, a simple illustration of the principles for the algorithms is presented. The goal is to demonstrate step-by-step how the whole algorithm works, with calculations included. Calculations will be done from the initialisation of the script, until after one OPF problem has been solved, to demonstrate all parts of the algorithms, with the exception of the calculation of the indices.

3.5.1 The System Specifications

In this example, a three-bus configuration is considered. For simplicity, the DC-case will be considered, and the State Transition approach will be utilised. Figure 3.9 shows the three-bus system, while Table 3.1, Table 3.2 and Table 3.3 contain the parameters for the example system. Table 3.4 contains the parameters for the WTG specifications and the wind distribution, which in this example is given by a Weibull distribution. It is assumed that the two WTGs connected to bus 1 have a correlation of 0.8. Also, generator 6 is assumed to always be available. It is also assumed that the load model will be a yearly peak load model and 1 year will be investigated. The power base for the system is 50 MVA.

Table 3.1: The generator parameters for the illustration example.

Gen	Bus	Type	Capacity [MW]	Failure Rate [# /hour]	Repair Rate [# /hour]
1	1	Hydro	50	0.0004	0.02
2	1	Hydro	10	0.0006	0.02
3	1	Hydro	10	0.0006	0.02
4	1	Hydro	10	0.0006	0.02
5	1	Wind	5	0.001	0.1
6	1	Wind	5	0	-

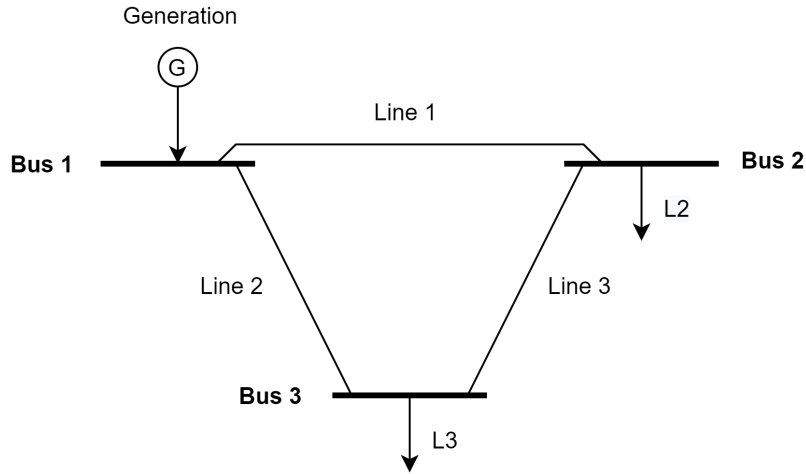


Figure 3.9: The system configuration used in the illustration example.

Table 3.2: The bus parameters for the illustration example.

Bus	Load [MW]	Curtailement cost [\$/KWh]
1	0	
2	25	1
3	35	2

Table 3.3: The line parameters for the illustration example.

Line	From Bus	To Bus	Failure Rate [# /hour]	Repair Rate [# /hour]	R [p.u]	Power limit [MW]
1	1	2	0.0002	0.1	0.1	50
2	1	3	0.0002	0.1	0.1	50
3	2	3	0.0002	0.1	0.05	50

Table 3.4: The WTG and wind speed parameters for the illustration example.

v_{ci}	v_r	v_{co}	A	B	C	α	β	corr
4	10	22.22	0.0311	-0.0776	0.0174	6	4	0.8

3.5.2 Initialisation and Pre-Calculation Work

With all the parameters as given in Table 3.1, Table 3.2, Table 3.2 and Table 3.4, the simulation can be started. Due to using the State Transition approach, the component state vector (also called system vector) is initialised first, with all components in the up-state. Since generator 6 in this example is assumed to always be available, it is not included in the component state vector. The form of the component vector is given in Equation 3.6, giving the component vector $S_0 = [0 \ 0 \ 0 \ 0 \ 0 \ 0 \ 0 \ 0]$. T , a variable keeping track of when the next transition of states occurs is initialised as $T = 0$.

$$S = [gen_1, \dots, gen_5, line_1, line_2, line_3] \quad (3.6)$$

Table 3.5: The intervals corresponding to component transfer for the illustration example.

Component	Lower Limit	Upper Limit
Gen_1	0.0000	0.1053
Gen_2	0.1053	0.2632
Gen_3	0.2632	0.4211
Gen_4	0.4211	0.5789
Gen_5	0.5789	0.8421
$Line_1$	0.8421	0.8947
$Line_2$	0.8947	0.9474
$Line_3$	0.9474	1.0000

3.5.3 Main Loop Calculations

Now, the main loop is entered, where the program iterates from hour 1 to hour 8736.

First, the time to the next transition needs to be calculated. Therefore, Equation 2.16 needs to be utilised. A uniformly distributed random number is therefore generated, yielding $U_1 = 0.7470$. Equation 2.16 uses the λ of each component. This value is either the Failure Rate of the component if it is in the up-state, or the Repair Rate if it is in the down-state. As each component is in the up-state, the following is obtained, illustrated in Equation 3.7.

$$t_1 = -\frac{1}{\sum_{i=1}^m \lambda_i} \ln U = -\frac{1}{0.0038} \ln 0.7470 = 76.76 \quad (3.7)$$

It is now known that the first transition of states happens after 76.76 hours, $t_1 = 76.76$. The time counting variable T is next incremented by one, then the algorithm checks if the system is in a contingent state (meaning any component in the down-state). As all components are in the up-state, T is incremented until $T = 77$. As a result, for the 76 first hours, there is no Loss of Load events.

3.5.4 First State Transition in Main Loop

Next, it is found that $t = 76.76 < T = 77$, and therefore the system switches state. Now, which component switches state needs to be determined. The interval $[0,1]$ can be divided up so that each number on the interval correspond to one of the components. For each generator and line, the probability that it is the component to transition is calculated by use of Equation 2.17. The calculation of this for the first generator is shown in Equation 3.8.

$$P_{gen_1} = \frac{\lambda_{gen_1}}{\sum_{i=1}^m \lambda_i} = \frac{0.0004}{0.0038} = 0.1053 \quad (3.8)$$

To determine the interval, the probabilities for each component are added cumulatively. The interval $[0, P_{gen_1} = 0.1053]$ will correspond to a transition of states for generator 1. Likewise, the interval from $[P_{gen_1}, P_{gen_1} + P_{gen_2}]$ will correspond to a transition of states for generator 2 etc. The calculated interval for this case is given in Table 3.5.

A new, uniformly distributed random number is then generated: $U_2 = 0.2589$. It is observed from Table 3.5 that U_2 falls within the limits of Gen_2 ($0.2589 \in (0.1053, 0.2632]$), meaning it is the component to transition at time $T = 76.76$. This gives $S_1 = [0 \ 1 \ 0 \ 0 \ 0 \ 0 \ 0 \ 0]$.

The time to transition now needs to be determined again. This time, the uniform random number

generator yields $U_1 = 0.3912$. Again, Equation 2.16 is utilised. Based on S_1 it is found that λ consists of the repair rate of generator 2 and the failure rate of all the other components. The calculation of t is shown in Equation 3.9.

$$t_2 = -\frac{1}{\sum_{i=1}^m \lambda_i} \ln U = -\frac{1}{0.0232} \ln 0.3912 = 40.45 \quad (3.9)$$

The system will now stay in state S_1 until $t = t_1 + t_2 = 117.21$.

Now $T = 77 \leq t = 117.21$, and the system is in a contingent state (S_1), and therefore the algorithm will now need to calculate if there is a loss of load incident by use of the OPF solver.

3.5.5 Determining Available Generating Capacity

Firstly, the maximum capacity that can be generated at each bus needs to be calculated. As there are WTGs in the system, the wind speeds needs to be determined.

3.5.5.1 Determining Correlated Wind Speeds

In this illustrative example, a Weibull distribution is used to sample the wind speed, and there are two correlated WTGs. Therefore, two correlated random uniformly distributed numbers need to be calculated from the desired correlation coefficient. Firstly, the 2x2 correlation matrix is constructed from Equation 2.82, as seen in Equation 3.10.

$$\Sigma = \begin{bmatrix} 1 & corr \\ corr & 1 \end{bmatrix} = \begin{bmatrix} 1 & 0.8 \\ 0.8 & 1 \end{bmatrix} \quad (3.10)$$

The linear correlation matrix, corresponding to the Spearman matrix, Σ^{adj} , is obtained by using Equation 3.3 as illustrated in Equation 3.11.

$$\Sigma^{adj} = 2 \cdot \sin\left(\frac{\pi}{6}\Sigma\right) = \begin{bmatrix} 2 \cdot \sin\left(\frac{\pi}{6} \cdot 1\right) & 2 \cdot \sin\left(\frac{\pi}{6} \cdot 0.8\right) \\ 2 \cdot \sin\left(\frac{\pi}{6} \cdot 0.8\right) & 2 \cdot \sin\left(\frac{\pi}{6} \cdot 1\right) \end{bmatrix} = \begin{bmatrix} 1 & 0.8135 \\ 0.8135 & 1 \end{bmatrix} \quad (3.11)$$

Now, Σ^{adj} need to be factorised using Cholesky decomposition. The resulting triangular matrix that fulfils Equation 2.80 is given in Equation 3.12.

$$\mathbf{G} = \begin{bmatrix} 1 & 0.8135 \\ 0 & 0.5816 \end{bmatrix} \quad (3.12)$$

Now, two normally distributed uncorrelated variables are created: $\mathbf{U} = \begin{bmatrix} -1.0524 & -0.5030 \end{bmatrix}^\top$. Next, correlation is induced between these variables by multiplying \mathbf{U} by \mathbf{G} , as seen in Equation 3.13.

$$\mathbf{U}_N = \mathbf{GU} = \begin{bmatrix} 1 & 0.8135 \\ 0 & 0.5816 \end{bmatrix} \begin{bmatrix} -1.0524 \\ -0.5030 \end{bmatrix} = \begin{bmatrix} -1.4616 \\ -0.2925 \end{bmatrix} \quad (3.13)$$

The final step is to transfer the normally distributed variables \mathbf{U}_N into a uniform distribution. By using the cumulative distribution function for a standard normal distribution the final random

variables U_W is found, as seen in Equation 3.14.

$$U_W = \begin{bmatrix} 0.0719 \\ 0.3849 \end{bmatrix} \quad (3.14)$$

Calculating the wind speed can now be done by using Equation 2.72. The WTGs have the same α and β giving the calculation as illustrated in Equation 3.15.

$$\mathbf{v} = \begin{bmatrix} \alpha(-\ln(U_{W1}))^{\frac{1}{\beta}} = 6(-\ln(0.0719))^{\frac{1}{4}} \\ \alpha(-\ln(U_{W2}))^{\frac{1}{\beta}} = 6(-\ln(0.3849))^{\frac{1}{4}} \end{bmatrix} = \begin{bmatrix} 7.6423[m/s] \\ 5.9308[m/s] \end{bmatrix} \quad (3.15)$$

Now, the generation capacity for the WTG needs to be determined from Equation 2.75. $v \in \langle v_{ci}, v_r \rangle$ for both wind speeds, therefore the calculation is as illustrated in Equation 3.16 and Equation 3.17.

$$\begin{aligned} P_{gen_5}(v_1, t = 77) &= (A + B \cdot v_1 + C \cdot v_1^2) \cdot P_{gen_5, rated} \\ &= (0.0311 - 0.0776 \cdot 7.6423 + 0.0174 \cdot 7.6423^2) \cdot 5 \\ &= 2.2715[MW] \end{aligned} \quad (3.16)$$

$$\begin{aligned} P_{gen_6}(v_2, t = 77) &= (A + B \cdot v_2 + C \cdot v_2^2) \cdot P_{gen_6, rated} \\ &= (0.0311 - 0.0776 \cdot 5.9308 + 0.0174 \cdot 5.9308^2) \cdot 5 \\ &= 0.9145[MW] \end{aligned} \quad (3.17)$$

The available capacity at each bus is further summed to determine the generating capacity, shown in Equation 3.18.

$$\begin{bmatrix} P_{Bus1,g} \\ P_{Bus2,g} \\ P_{Bus3,g} \end{bmatrix} = \begin{bmatrix} 1 \cdot P_{gen_1} + 0 \cdot P_{gen_2} + 1 \cdot P_{gen_3} + 1 \cdot P_{gen_4} + 1 \cdot P_{gen_5} + P_{gen_6} \\ 0 \\ 0 \end{bmatrix} = \begin{bmatrix} 73.1860 \\ 0 \\ 0 \end{bmatrix} [MW] = \begin{bmatrix} 1.4637 \\ 0 \\ 0 \end{bmatrix} [pu] \quad (3.18)$$

3.5.6 Calculating the Reactance Matrix and the Distribution Factors

The reactance matrix, \mathbf{X} , needs to be found for the line configuration of the system, as the elements of the matrix are used in Equation 2.45 to calculate line flows. The line susceptance is found first, as seen in Equation 3.19.

$$\begin{aligned} b_{12} = b_{21} &= -\frac{1}{X_{12}} = -\frac{1}{0.1} = -10 \\ b_{13} = b_{31} &= -\frac{1}{X_{13}} = -\frac{1}{0.1} = -10 \\ b_{23} = b_{32} &= -\frac{1}{X_{23}} = -\frac{1}{0.05} = -20 \end{aligned} \quad (3.19)$$

This gives the susceptance matrix B as shown in Equation 3.20.

$$\begin{aligned}
 \mathbf{B} &= \begin{bmatrix} B_{11} & B_{12} & B_{13} \\ B_{21} & B_{22} & B_{23} \\ B_{31} & B_{32} & B_{33} \end{bmatrix} \\
 &= \begin{bmatrix} -(b_{12} + b_{13}) & b_{12} & b_{13} \\ b_{21} & -(b_{21} + b_{23}) & b_{23} \\ b_{31} & b_{32} & -(b_{31} + b_{32}) \end{bmatrix} \\
 &= \begin{bmatrix} 20 & -10 & -10 \\ -10 & 30 & -20 \\ -10 & -20 & 30 \end{bmatrix}
 \end{aligned} \tag{3.20}$$

Bus 1 is the chosen slack bus in this system, resulting in the reduced matrix \mathbf{B}' , given in Equation 3.21.

$$\mathbf{B}' = \begin{bmatrix} B_{22} & B_{23} \\ B_{32} & B_{33} \end{bmatrix} = \begin{bmatrix} 30 & -20 \\ -20 & 30 \end{bmatrix} \tag{3.21}$$

The inverse of \mathbf{B}' is found in Equation 3.22.

$$(\mathbf{B}')^{-1} = \begin{bmatrix} 0.06 & 0.04 \\ 0.04 & 0.06 \end{bmatrix} \tag{3.22}$$

Using $(\mathbf{B}')^{-1}$ the \mathbf{X} matrix is found as illustrated in Equation 3.23.

$$\mathbf{X} = \begin{bmatrix} 0 & 0 & 0 \\ 0 & 0.06 & 0.04 \\ 0 & 0.4 & 0.06 \end{bmatrix} \tag{3.23}$$

The distribution factor matrix is now to be calculated. By using Equation 2.46 and Equation 2.45 these elements can be found, which is done in the proceeding equations.

The distribution factors for line 1-2 is found in Equation 3.24.

$$\begin{aligned}
 P_{12} &= a_{12,1}P_1 + a_{12,2}P_2 + a_{12,3}P_3 \\
 &= \frac{x_{11} - x_{21}}{X_{12}}P_1 + \frac{x_{12} - x_{22}}{X_{12}}P_2 + \frac{x_{13} - x_{23}}{X_{12}}P_3 \\
 &= \frac{0 - 0}{0.1}P_1 + \frac{0 - 0.06}{0.1}P_2 + \frac{0 - 0.04}{0.1}P_3 \\
 &= 0P_1 - 0.6P_2 - 0.4P_3
 \end{aligned} \tag{3.24}$$

The distribution factors for line 1-3 is found in Equation 3.25.

$$\begin{aligned}
P_{13} &= a_{13,1}P_1 + a_{13,2}P_2 + a_{13,3}P_3 \\
&= \frac{x_{11} - x_{31}}{X_{13}}P_1 + \frac{x_{12} - x_{32}}{X_{13}}P_2 + \frac{x_{13} - x_{33}}{X_{13}}P_3 \\
&= \frac{0 - 0}{0.1}P_1 + \frac{0 - 0.04}{0.1}P_2 + \frac{0 - 0.06}{0.1}P_3 \\
&= 0P_1 - 0.4P_2 - 0.6P_3
\end{aligned} \tag{3.25}$$

The distribution factors for line 2-3 is found in Equation 3.26.

$$\begin{aligned}
P_{23} &= a_{23,1}P_1 + a_{23,2}P_2 + a_{23,3}P_3 \\
&= \frac{x_{21} - x_{31}}{X_{23}}P_1 + \frac{x_{22} - x_{32}}{X_{23}}P_2 + \frac{x_{23} - x_{33}}{X_{23}}P_3 \\
&= \frac{0 - 0}{0.05}P_1 + \frac{0.06 - 0.04}{0.05}P_2 + \frac{0.04 - 0.06}{0.05}P_3 \\
&= 0P_1 + 0.4P_2 - 0.4P_3
\end{aligned} \tag{3.26}$$

In Equation 3.27 all the distribution factors are grouped into one matrix.

$$\mathbf{A}_{DF} = \begin{bmatrix} a_{12,1} & a_{12,2} & a_{12,3} \\ a_{13,1} & a_{13,2} & a_{13,3} \\ a_{23,1} & a_{23,2} & a_{23,3} \end{bmatrix} = \begin{bmatrix} 0 & -0.6 & -0.4 \\ 0 & -0.4 & -0.6 \\ 0 & 0.4 & -0.4 \end{bmatrix} \tag{3.27}$$

3.5.7 Calculating OPF Constraints

Now, all required parameters for calculating the constraints on the OPF problem have been found, and as such the constraints are to be calculated. The following is needed: the cost function, the equality constraint, the limits on the decision variables and the inequality constraints.

This system would usually have 6 decision variables, the active power generation $P_{Bus1,g}$, $P_{Bus2,g}$ and $P_{Bus3,g}$ as well as the power curtailment at each bus C_1 , C_2 and C_3 . For this system there is only generation at bus 1, and there is only load at bus 2 and 3. Therefore the decision variables $P_{Bus2,g}$, $P_{Bus3,g}$ and C_1 can be removed.

3.5.7.1 Cost Function

As can be observed from Equation 2.49, the cost function is found from the cost of rescheduling for the generation decision variables, while it is the cost of curtailment for the power curtailment decision variables. The cost function for this system is shown in Equation 3.28.

$$f = 0P_{Bus1,g} + 1C_2 + 2C_3 \tag{3.28}$$

3.5.7.2 Equality Constraint

The equality constraint follows from the power balance in the system, $\sum P_{gen} + C_P - P_{load} = 0$. The resulting equality constraint is shown in Equation 3.29.

$$\begin{aligned} P_{Bus1,g} + C_2 + C_3 &= P_{Bus2,l} + P_{Bus3,l} \\ P_{Bus1,g} + C_2 + C_3 &= 1.2 \end{aligned} \quad (3.29)$$

3.5.7.3 Decision Variable Bounds

The bounds on the decision variables follow from the generation and load, and is presented in Equation 3.30, scaled to the per-unit system.

$$\begin{aligned} 0 &\leq P_{Bus1,g} \leq 1.4637 \\ 0 &\leq C_2 \leq 0.5 \\ 0 &\leq C_3 \leq 0.7 \end{aligned} \quad (3.30)$$

3.5.7.4 Inequality Constraints

Solvers used to calculate the OPF problem take the inequalities input as matrix A and vector b , shown in Equation 3.31 and Equation 3.32.

$$\mathbf{A} = \begin{bmatrix} \mathbf{A}_1 & \cdots & \mathbf{A}_k \end{bmatrix}^T \quad (3.31)$$

$$\mathbf{b} = \begin{bmatrix} b_1 & \cdots & b_k \end{bmatrix}^T \quad (3.32)$$

Each inequality constraint needs to be specified in the form of Equation 3.33.

$$\mathbf{A}_i \begin{bmatrix} P_{Bus1,g} \\ C_2 \\ C_3 \end{bmatrix} \leq b_i \quad (3.33)$$

The inequality constraints in this OPF come only from the line transfer limits. The line limits are shown in Equation 3.34. \mathbf{T} is the matrix of transferred power across the lines.

$$-\mathbf{T}_{max} \leq \mathbf{T} \leq \mathbf{T}_{max} \quad (3.34)$$

To get the correct form of the inequality constraints, Equation 3.34 is divided up as shown in Equation 3.35. Then, Equation 2.47 and Equation 2.48 are used to calculate the limits in terms of the decision variables as seen in Equation 3.36 and Equation 3.37.

$$\begin{aligned} -\mathbf{T} &\leq \mathbf{T}_{max} \\ \mathbf{T} &\leq \mathbf{T}_{max} \end{aligned} \quad (3.35)$$

$$\begin{aligned}
& -\mathbf{T} \leq \mathbf{T}_{max} \\
& - \begin{bmatrix} 0P_{Bus1,g} - 0.6(C_2 - P_2) - 0.4(C_3 - P_3) \\ 0P_{Bus1,g} - 0.4(C_2 - P_2) - 0.6(C_3 - P_3) \\ 0P_{Bus1,g} + 0.4(C_2 - P_2) - 0.4(C_3 - P_3) \end{bmatrix} = \begin{bmatrix} 1 \\ 1 \\ 1 \end{bmatrix} \\
& \begin{bmatrix} 0P_{Bus1,g} + 0.6C_2 + 0.4C_3 \\ 0P_{Bus1,g} + 0.4C_2 + 0.6C_3 \\ 0P_{Bus1,g} - 0.4C_2 + 0.4C_3 \end{bmatrix} = \begin{bmatrix} 1 + 0.6P_2 + 0.4P_3 \\ 1 + 0.4P_2 + 0.6P_3 \\ 1 - 0.4P_2 + 0.4P_3 \end{bmatrix} \\
& \begin{bmatrix} 0P_{Bus1,g} + 0.6C_2 + 0.4C_3 \\ 0P_{Bus1,g} + 0.4C_2 + 0.6C_3 \\ 0P_{Bus1,g} - 0.4C_2 + 0.4C_3 \end{bmatrix} = \begin{bmatrix} 1.58 \\ 1.62 \\ 1.08 \end{bmatrix}
\end{aligned} \tag{3.36}$$

$$\begin{aligned}
& \mathbf{T} \leq \mathbf{T}_{max} \\
& \begin{bmatrix} 0P_{Bus1,g} - 0.6(C_2 - P_2) - 0.4(C_3 - P_3) \\ 0P_{Bus1,g} - 0.4(C_2 - P_2) - 0.6(C_3 - P_3) \\ 0P_{Bus1,g} + 0.4(C_2 - P_2) - 0.4(C_3 - P_3) \end{bmatrix} = \begin{bmatrix} 1 \\ 1 \\ 1 \end{bmatrix} \\
& \begin{bmatrix} 0P_{Bus1,g} - 0.6C_2 - 0.4C_3 \\ 0P_{Bus1,g} - 0.4C_2 - 0.6C_3 \\ 0P_{Bus1,g} + 0.4C_2 - 0.4C_3 \end{bmatrix} = \begin{bmatrix} 1 - 0.6P_2 - 0.4P_3 \\ 1 - 0.4P_2 - 0.6P_3 \\ 1 + 0.4P_2 - 0.4P_3 \end{bmatrix} \\
& \begin{bmatrix} 0P_{Bus1,g} - 0.6C_2 - 0.4C_3 \\ 0P_{Bus1,g} - 0.4C_2 - 0.6C_3 \\ 0P_{Bus1,g} + 0.4C_2 - 0.4C_3 \end{bmatrix} = \begin{bmatrix} 0.42 \\ 0.38 \\ 0.92 \end{bmatrix}
\end{aligned} \tag{3.37}$$

3.5.8 OPF Problem Formulation

The total OPF problem can be summarised as shown in Equation 3.38.

$$\min \quad f = 0 \cdot P_{Bus1,g} + 1 \cdot C_2 + 2 \cdot C_3; \tag{3.38}$$

$$\text{subject to} \quad \mathbf{A}_{eq} \cdot \mathbf{x} = b_{eq} \tag{3.39}$$

$$\mathbf{A} \cdot \mathbf{x} \leq \mathbf{b} \tag{3.40}$$

$$\mathbf{lb} \leq \mathbf{x} \leq \mathbf{ub} \tag{3.41}$$

Where:

$$\begin{aligned}
 \mathbf{x} &= \begin{bmatrix} P_{Bus1,g} \\ C_2 \\ C_3 \end{bmatrix} && = \text{The decision variables.} \\
 \mathbf{A}_{eq} &= \begin{bmatrix} 1 & 1 & 1 \end{bmatrix} && = \text{The equality constraint matrix.} \\
 b_{eq} &= 1.2 && = \text{The equality constraint value.} \\
 \mathbf{A} &= \begin{bmatrix} 0 & 0.6 & 0.4 \\ 0 & 0.4 & 0.6 \\ 0 & -0.4 & 0.4 \\ 0 & -0.6 & -0.4 \\ 0 & -0.4 & -0.6 \\ 0 & 0.4 & -0.4 \end{bmatrix} && = \text{The inequality constraint matrix.} \\
 \mathbf{b} &= \begin{bmatrix} 1.58 \\ 1.62 \\ 1.08 \\ 0.42 \\ 0.38 \\ 0.92 \end{bmatrix} && = \text{The inequality values} \\
 \mathbf{lb} &= \begin{bmatrix} 0 \\ 0 \\ 0 \end{bmatrix} && = \text{The lower bounds of } \mathbf{x}. \\
 \mathbf{ub} &= \begin{bmatrix} 1.4637 \\ 0.5 \\ 0.7 \end{bmatrix} && = \text{The upper bounds of } \mathbf{x}.
 \end{aligned}$$

3.5.9 OPF Results

Solving the OPF problem yields the results presented in Equation 3.42.

$$\begin{aligned}
 \begin{bmatrix} P_{Bus1,g} \\ C_2 \\ C_3 \end{bmatrix} &= \begin{bmatrix} 1.2 \\ 0 \\ 0 \end{bmatrix} \\
 f &= 0
 \end{aligned} \tag{3.42}$$

The power flows for this system is illustrated in Figure 3.10, which were calculated from Equation 2.46 and the obtained generation, load curtailment and system distribution factors.

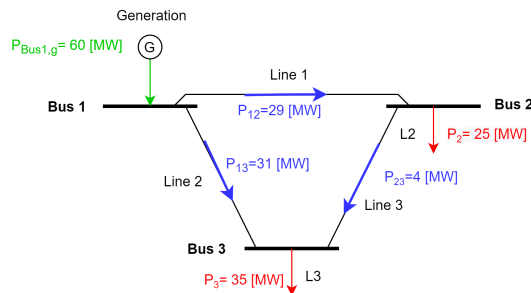


Figure 3.10: The system with calculated line flows.

3.5.10 Further Calculations

Due to the OPF-solver yielding no curtailment ($f = 0$ and $C_2 = C_3 = 0$), there was no loss of load event, and nothing will be recorded. The time will be incremented to $T = 78$. Again $T < t$ and the system is in a contingent case, which means the OPF solver will be run again. The wind speed will be sampled for this hour, and then the OPF-solver is run again with the updated parameters. No further calculations will be illustrated in this example, but the general further procedure for the algorithm will be explained:

The algorithm will continue to sample wind speeds and solving the OPF at each hour, until $T = 118$. At that point, the next component to transition will be found. The component state vector will be updated and the next time to transition will be determined until $T < t$. Then the OPF solver will run at $T = 118$ with the updated system vector and new sampled wind speed. This will continue until the wanted number of hours have been simulated.

At that point, the LOLE and EENS will be calculated, as illustrated in section 2.1.7.7.

4 Case Studies and Results

To examine the adopted methodological approaches of the thesis, the developed scripts are executed on selected standardised test systems. Obtained results are compared to corresponding benchmark results. Various cases and methods are examined, and sensitivity analyses are conducted.

4.1 Test Systems

The thesis utilises test systems with specified standard parameters (e.g. generation capacity, load capacity, line capacity, failure rates and repair times of the components) to perform power system reliability assessment. There exist two well-established test systems for HL-I and HL-II PSR assessment: the Roy Billinton Test System (RBTS) and the Institute of Electrical and Electronics Engineers-Reliability Test System (IEEE-RTS or simply RTS). The RBTS is a 6-bus system with 11 generators, 9 lines and a peak load of 185 MW. The relatively larger RTS consists of 32 generators, 38 lines and a peak load of 2850 MW. The RBTS and the RTS utilise the same chronological load curve specified in percent of system peak load for 8736 load points per year, as illustrated in Appendix C. The two systems are detailed in Appendix A and Appendix B. The priority order load curtailment philosophy controls the load curtailment in the test systems based on the reliability worth index IEAR-values expressed in \$/kWh. The composite system delivery point with the highest IEAR has the highest priority, and the delivery point with the lowest IEAR has the lowest priority.

4.2 Verifying the Developed Script: Swift Current Case Study

The previously presented concepts in the thesis were used to develop HL-II MCS MATLAB scripts that include wind power penetration. The developed scripts were tested on a modified version of the RBTS (MRBTS) and the RTS, and verified against the results presented in [53], which is considered as the benchmark. The benchmark, [53], is the work of Billinton, Gao, Huang and Karki, who are considered to be important contributors to research within the field of power system reliability. The utilised wind speed data is from the Swift Current site located in the Province of Saskatchewan, Canada, presented in Table 4.1. The hourly wind speed data is from a 20-year database (1 Jan. 1984 to 31 Dec. 2003) obtained from Environment Canada [53].

Table 4.1: The wind speed data for Swift Current [53]

Swift Current	
Mean wind speed, μ (km/h)	19.46
Standard deviation, σ (km/h)	9.70

The optimal ARMA time series model based on the data presented in Table 4.1, is an ARMA (4, 3) model with parameters as presented in Equation 4.1. The Swift Current ARMA wind model was developed by using the ARMASA Toolbox and was published in [59].

$$y_t = 1.1772y_{t-1} + 0.1001y_{t-2} - 0.3572y_{t-3} + 0.0379y_{t-4} + \alpha_t - 0.5030\alpha_{t-1} - 0.2924\alpha_{t-2} + 0.1317\alpha_{t-3} \quad (4.1)$$

where $\alpha_t \in NID(0, 0.524760^2)$ is a normal white noise process with zero mean and variance 0.524760^2 [59]. The simulated time-dependent wind speed is then given by Equation 2.73.

The wind speed data were also used to estimate the Weibull scale and shape parameters. These are presented in Table 4.2.

Table 4.2: Estimated Weibull scale and shape parameters for the Swift Current wind-regime

Swift Current	
α	5.9334
β	4.2913

The WTG modelling utilised the generator power curve with a cut-in wind speed of 4 m/s, rated wind speed of 10 m/s and cut-out wind speed of 22.222 m/s. The WTG units are considered to have a capacity of 2MW.

4.2.1 20MW WECS Added to the MRBTS

The RBTS is a 6-bus system presented in Appendix A. The RBTS has some designed-in weaknesses, one of which is the radial supply to Bus 6 [53]. The RBTS can therefore be modified by adding a transmission line designated as line 10 between bus 5 and bus 6. Line 10 has the same parameters as the existing line 9 between bus 5 and 6. By utilising the MRBTS, the effects of adding wind penetration to the overall system reliability can be better illustrated. The single line diagram of the modified-RBTS, MRBTS, is illustrated in Figure 4.1

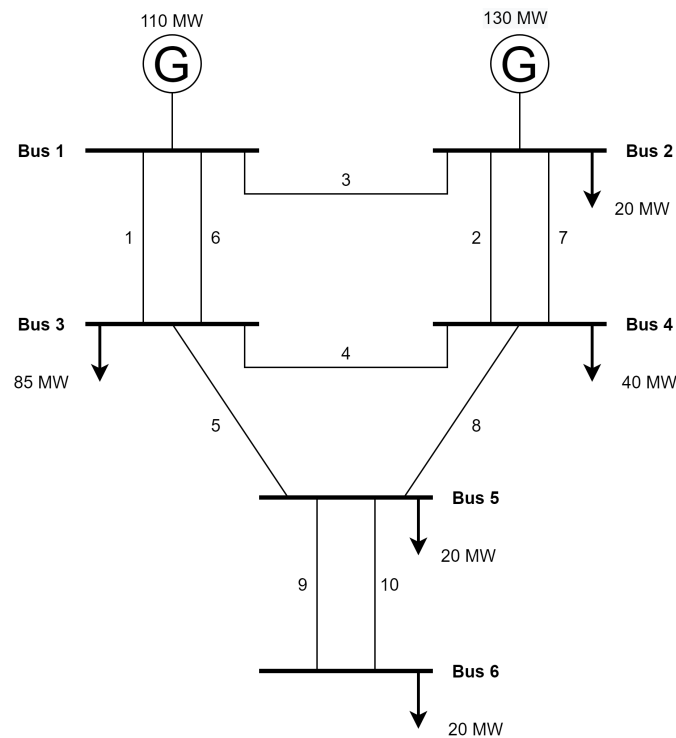


Figure 4.1: Single line diagram of the MRBTS.

The system with added wind power penetration is designated as MRBTWS, and consists of 10 2MW WTGs added at Bus 4. The WTGs have a FOR equal to zero. 20 MW WECS added to the MRBTS yields a wind penetration level of approximately 8%. The WECS was connected through a single transmission line with an unavailability and average repair time of 0.00058 and 10 h, which is equivalent to a FOR of 0.0548. The priority order philosophy is utilised to control the load shedding.

4.2.1.1 DC-based Load Flow Approach

This section presents the obtained bus and system EENS-estimates for the DC-based load flow approach using the State Sampling and State Transition approach. The LOLE estimates and standard deviations of the estimates are provided in Appendix E, Appendix F and Appendix G.

4.2.1.1.1 State Sampling

The estimates of the EENS-index were obtained by simulations of 1000 years and are presented in Table 4.3.

Table 4.3: Obtained estimates for the MRBTSW-4 State Sampling DC-case study

Bus nr.	Priority order	EENS [MWh/year]		
		MRBTS	MRBTSW-ARMA	MRBTSW-WB
2	1	0.0351	0.0169	0.0190
3	5	10.4255	7.9755	7.8365
4	3	0.0183	0.0000	0.0000
5	2	0.1248	0.1331	0.1698
6	4	0.2138	0.2548	0.2717
System	-	10.8174	8.3803	8.2972

4.2.1.1.2 State Transition

The estimates of the EENS-index were obtained by simulations of 7500 years and are presented in Table 4.4.

Table 4.4: Obtained estimates for the MRBTSW-4 State Transition DC-case study

Bus nr.	Priority order	EENS [MWh/year]		
		MRBTS	MRBTSW-ARMA	MRBTSW-WB
2	1	0.0000	0.0173	0.0535
3	5	9.6398	7.1730	8.0018
4	3	0.0000	0.0066	0.0534
5	2	0.0761	0.1262	0.2064
6	4	0.3115	0.2648	0.4105
System	-	10.0274	7.5880	8.7256

The obtained estimates from the State Sampling and State Transition techniques with the DC-based contingency solver are summarised in Figure 4.2.

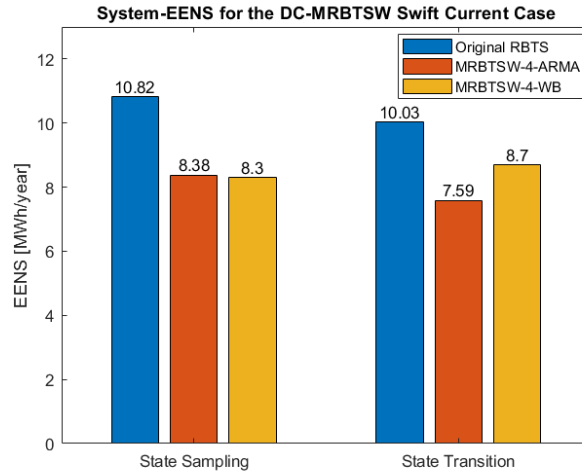


Figure 4.2: Comparison of the system-EENS in the MRBTS before and after the wind penetration, obtained by the State Sampling and State Transition techniques

4.2.1.2 AC-based Load Flow Approach

This section presents the obtained bus and system EENS-estimates for the AC-based load flow approach using the State Sampling and State Transition approach. The LOLE estimates and standard deviations of the estimates are provided in Appendix E, Appendix F and Appendix G.

4.2.1.2.1 State Sampling

The estimates of the EENS-index were obtained by simulations of 1000 years and are presented in Table 4.5.

Table 4.5: Obtained estimates for the MRBTSW-4 State Sampling AC-case study

Bus nr.	Priority order	EENS [MWh/year]		
		MRBTS	MRBTSW-ARMA	MRBTSW-WB
2	1	0.0090	0.0421	0.0265
3	5	15.6779	12.7562	12.7424
4	3	0.0000	0.0415	0.0000
5	2	0.1584	0.1289	0.1461
6	4	1.3189	1.1124	1.1821
System	-	17.1642	14.0811	14.0970

4.2.1.2.2 State Transition

The estimates of the EENS-index were obtained by simulations of 7500 years and are presented in Table 4.6.

Table 4.6: Obtained estimates for the MRBTSW-4 State Transition AC-case study

Bus nr.	Priority order	EENS [MWh/year]		
		MRBTS	MRBTSW-ARMA	MRBTSW-WB
2	1	0.0194	0.0063	0.0139
3	5	16.5168	12.7359	12.2706
4	3	0.0000	0.0000	0.0000
5	2	0.1408	0.1902	0.1347
6	4	1.1900	1.0844	1.1390
System	-	17.8670	14.0169	13.5582

The obtained estimates from the State Sampling and State Transition techniques with the AC-based contingency solver are summarised in Figure 4.3.

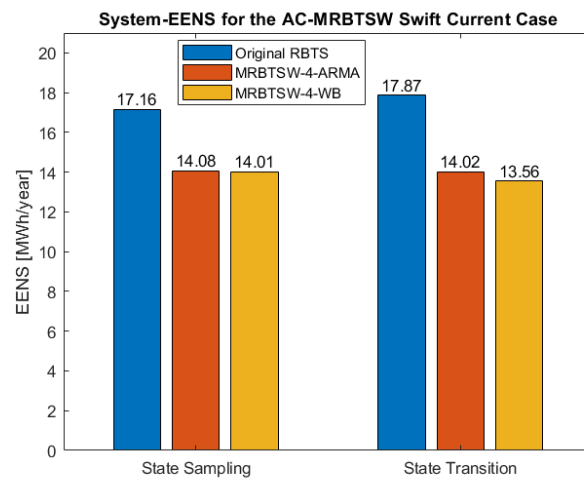


Figure 4.3: Comparison of the system-EENS in the MRBTS before and after the wind penetration, obtained by the State Sampling and State Transition techniques

4.2.1.3 Benchmark comparison: DC-based State Sampling MCS

The benchmark paper presents two different results for the MRBTS-Swift Current assessment. One result was obtained by utilising the MECORE program, which utilises a combination of the State Sampling MCS and enumeration techniques. This program uses the DC-based load flow approach and the priority order philosophy is based on ranking the composite system delivery points using the reliability worth index IEAR expressed in \$/kWh. The program utilises a five-state COPT to model the WECS, and the ARMA-wind speed model. The WTG units are assigned a FOR of 0%. The MECORE results [53] are presented and compared to the obtained DC-based State Sampling estimates in Table 4.7.

Table 4.7: MRBTS-Swift Current case comparison against the State Sampling MECORE program benchmark results

Bus	Benchmark EENS [MWh/year]			Obtained EENS[MWh/year]		
	Priority	MRBTS	MRBTSW	Priority	MRBTS	MRBTSW-ARMA
2	1	0.000	0.000	1	0.0351	0.0169
3	5	12.566	8.644	5	10.4255	7.9755
4	2	0.029	0.009	3	0.0183	0.0000
5	3	0.293	0.200	2	0.1248	0.1331
6	4	0.674	0.545	4	0.2138	0.2548
System	-	13.562	9.399	-	10.8174	8.3803

The differences between the bus estimates of the EENS-index are illustrated in Figure 4.4, and the differences between the system-EENS estimates are illustrated in Figure 4.5.

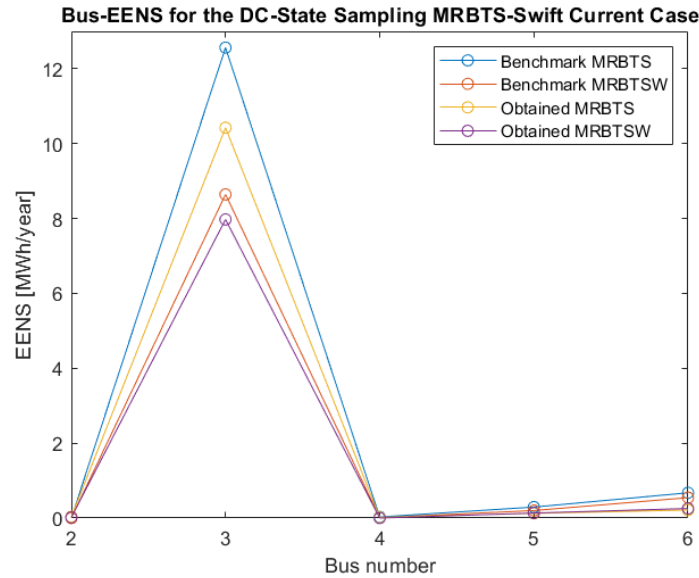


Figure 4.4: Benchmark comparison of the EENS at the buses in the MRBTS before and after wind penetration

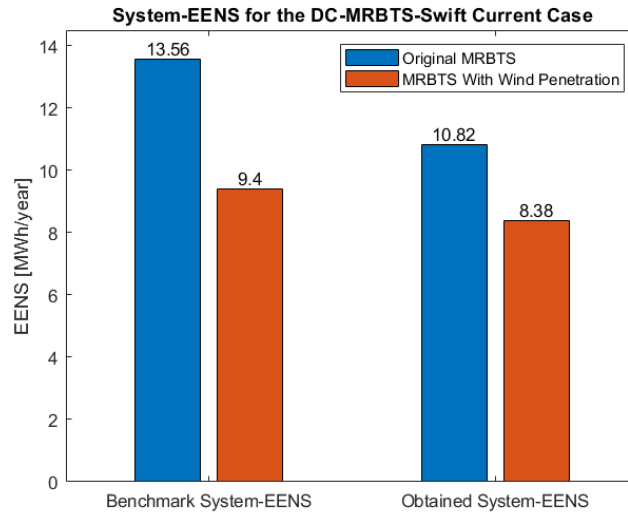


Figure 4.5: Benchmark comparison of the system-EENS for the DC-State Sampling approach in the MRBTS before and after the wind penetration

4.2.1.4 Benchmark Comparison: AC-based Sequential MCS

The benchmark paper also utilised the RapHL-II program, which uses the Fast-Decoupled AC load flow technique to calculate load flows and line loadings and to check the system operating constraints. An OPF approach is used to conduct corrective actions to alleviate operating constraints, and the load shedding philosophy employed is known as the Pass-I policy, where loads are curtailed at the delivery points that are closest (or one line away from) the element(s) on outage [53]. The simulation sample size utilised was 10,000 years. The program utilises the ARMA-wind speed model. The RapHL-II results [53] are presented and compared to the AC-based State Transition estimates in Table 4.8.

Table 4.8: MRBTS-Swift Current case comparison against the Sequential RapHL-II program benchmark results

Bus	Benchmark EENS [MWh/year]			Obtained EENS [MWh/year]		
	Priority	MRBTS	MRBTWS	Priority	MRBTS	MRBTWS-ARMA
2	-	0.4762	0.2568	1	0.0194	0.0063
3	-	7.3563	4.2447	5	16.5168	12.7359
4	-	5.347	3.3721	3	0.0000	0.0000
5	-	0.1098	0.0786	2	0.1408	0.1902
6	-	0.0588	0.0453	4	1.1900	1.0844
System	-	13.3464	7.9974	-	17.8670	14.0169

The differences between the system-EENS estimates are illustrated in Figure 4.6. It should be noted that the benchmark paper used the Pass-I load shedding philosophy, instead of the priority order philosophy, which has a large impact on the end results, as elaborated in section 4.2.4.

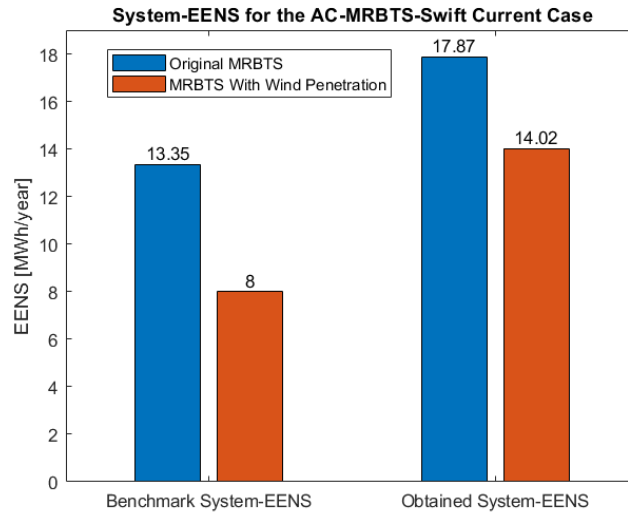


Figure 4.6: Benchmark comparison of the system-EENS for the AC-State Transition approach in the MRBTS before and after the wind penetration

4.2.2 600 MW WECS Added to the RTS

The RTS is a 24-bus system with 10 generator buses, 17 load buses, 38 transmission lines and 32 generating units. The system peak load is 2850 MW and the total generation is 3405MW. The RTS is considered to have a strong transmission network and a relatively weak generation system [53]. The system is detailed and illustrated in Appendix B. The subsequent study involves the addition of 300 2MW WTGs for a total of 600 MW WECS at Bus 19 in the northern part of the RTS. This system is designated as RTSW-19. 600 MW wind power added to the RTS yields a wind penetration level of approximately 15%. The WECS was connected through a single transmission line with an unavailability and average repair time of 0.00058 and 10 h, which is equivalent to a FOR of 0.0548.

This section presents the obtained bus and system EENS-estimates for the DC-based load flow approach using the State Sampling and State Transition approaches. The LOLE estimates and standard deviations of the estimates are provided in Appendix E, Appendix F and Appendix G.

4.2.2.1 State Sampling

The estimates of the EENS-index were obtained by simulations of 1000 years and are presented in Table 4.9. The buses that are not included have zero EENS.

Table 4.9: Obtained estimates for the RTSW-19 State Sampling case study

Bus nr.	EENS [MWh/year]		
	RTS	RTSW-19-ARMA	RTSW-19-WB
4	0.0599	0.0000	0.0484
5	0.1278	0.0928	0.0000
6	0.4285	0.4256	0.5242
7	231.0165	235.2007	236.1584
8	0.1702	0.2319	0.4097
9	853.0728	517.3422	517.7288
10	9.3407	4.8211	3.8000
14	262.3221	145.0649	153.8644
18	0.8933	0.2207	0.3652
19	53.3067	28.8700	29.2246
System	1410.7383	932.2700	942.1236

4.2.2.2 State Transition

The estimates of the EENS-index were obtained by simulations of 7500 years and are presented in Table 4.10. The buses that are not included have zero EENS.

Table 4.10: Obtained estimates for the RTSW-19 State Transition case study

Bus nr.	EENS [MWh/year]		
	RTS	RTSW-19-ARMA	RTSW-19-WB
3	0.0000	0.0000	0.0262
4	0.0000	0.0577	0.1670
5	0.0000	0.0695	0.0143
6	1.3700	0.2176	0.5626
7	226.9890	229.7046	241.4480
8	0.0572	0.0420	0.0984
9	861.1061	503.4852	498.0605
10	8.6326	4.9881	3.1274
14	260.0709	140.4356	137.6013
18	0.7255	0.5509	0.4093
19	53.7246	26.2229	23.2630
20	0.0000	0.0000	0.0638
System	1412.6758	905.7741	904.8418

The obtained estimates from the State Sampling and State Transition techniques are summarised in Figure 4.7.

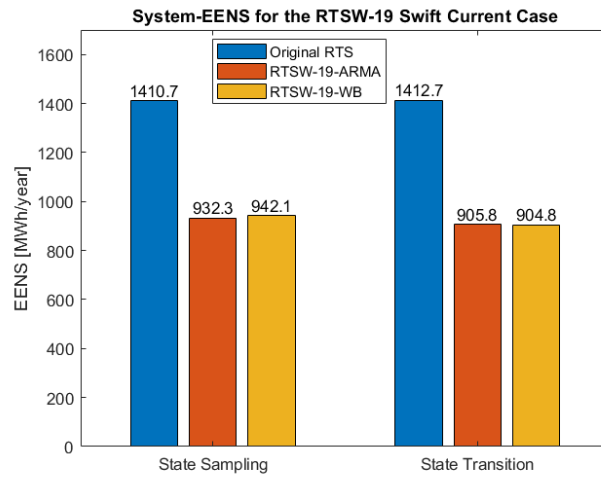


Figure 4.7: Comparison of the system-EENS in the RTS before and after the wind penetration, obtained by the State Sampling and State Transition techniques

4.2.2.3 Benchmark Comparison: DC-based State Sampling MCS

For the RTS-Swift Current case, the benchmark utilised the MECORE program, which uses the Non-sequential State Sampling approach and enumeration techniques, DC-load flow and economic priority order as the load curtailment policy [53]. This program utilises the ARMA wind speed model. The benchmark results [53] are presented and compared to the obtained RTS DC-State Sampling estimates in Table 4.11.

Table 4.11: RTS-Swift Current case comparison against the State Sampling MECORE program benchmark results

Bus nr.	Benchmark EENS [MWh/year]		Obtained EENS [MWh/year]	
	RTS	RTSW-19	RTS	RTSW-19-ARMA
2	0.399	0.204	0.0000	0.0000
3	0.345	0.169	0.0000	0.0000
4	0.000	0.000	0.0599	0.0000
5	0.000	0.000	0.1278	0.0928
6	0.394	0.392	0.4285	0.4256
7	0.008	0.004	231.0165	235.2007
8	0.020	0.008	0.1702	0.2319
9	407.226	240.042	853.0728	517.3422
10	1.857	0.994	9.3407	4.8211
13	0.146	0.060	0.0000	0.0000
14	68.057	38.827	262.3221	145.0649
15	310.220	180.886	0.0000	0.0000
16	18.572	10.485	0.0000	0.0000
18	13.670	7.458	0.8933	0.2207
19	757.805	451.468	53.3067	28.8700
20	14.454	8.051	0.0000	0.0000
System	1593.130	939.004	1410.7383	932.2700

The differences between the bus estimates of the EENS-index are illustrated in Figure 4.8, and the

differences between the system-EENS estimates are illustrated in Figure 4.9.

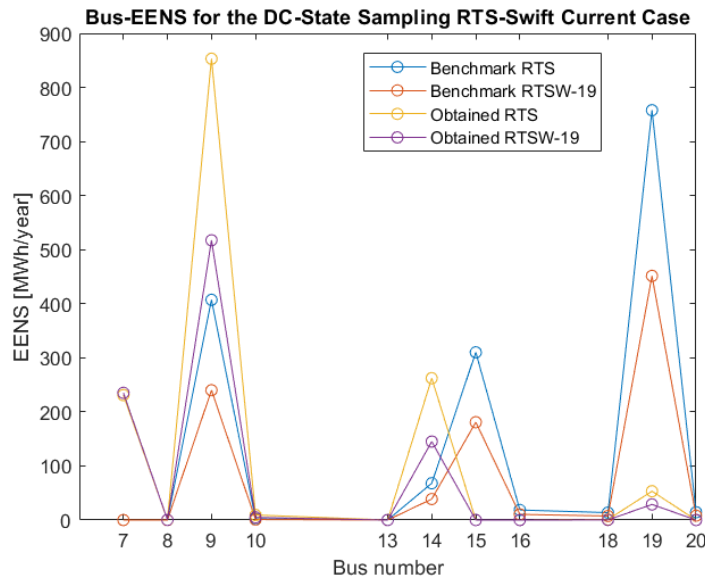


Figure 4.8: Benchmark comparison of the EENS at the buses in the RTS before and after the wind penetration

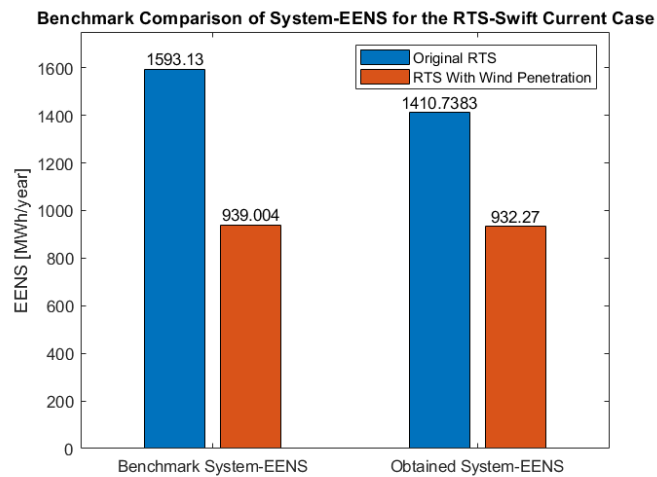


Figure 4.9: Benchmark comparison of the system-EENS in the RTS before and after the wind penetration

4.2.3 Multiple WECS at RTS by Incorporating Wind Speed Correlation

Multiple WECS at different locations can be integrated into power systems. The locations can have different wind speed characteristics, and have different impacts on the reliability of a power system. An important factor for the contribution that multiple WECS can have to the adequacy of a power system is the degree of wind speed correlation between the locations. Two WECS were added to the RTS, one having the wind speed characteristics of Swift Current, and the other having the wind speed characteristics of Regina, also located in the Province of Saskatchewan, Canada. The mean wind speed and standard deviation of the two sites are illustrated in Table 4.12.

The optimal ARMA time series model, based on the data presented in Table 4.12, for Swift Current

Table 4.12: The wind speed data for Regina and Swift Current, Canada [53]

	Regina	Swift Current
Mean wind speed, μ (km/h)	19.52	19.46
Standard deviation, σ (km/h)	10.99	9.70

was presented in Equation 4.1. A similar model for the Regina wind site [53], is illustrated in Equation 4.2.

$$y_t = 0.9336y_{t-1} + 0.4506y_{t-2} - 0.5545y_{t-3} + 0.1110y_{t-4} + \alpha_t - 0.2033\alpha_{t-1} - 0.4684\alpha_{t-2} + 0.2301\alpha_{t-3} \quad (4.2)$$

where $\alpha_t \in NID(0, 0.409423^2)$ is a normal white noise process with zero mean and variance 0.409423^2 . The simulated time-dependent wind speed is then given by Equation 2.73.

The wind speed data was also used to estimate the Weibull scale and shape parameters for the Regina wind site. These are presented in Table 4.13.

Table 4.13: Estimated Weibull scale and shape parameters for the Regina wind site

Regina Wind Site	
α	5.8602
β	5.5308

4.2.3.1 300 MW WECS Added at Buses 1 and 3

The subsequent assessment involves the connection of 300 MW WECS to two buses in the southern portion of the RTS. 300 MW WECS was connected to bus 1 and to bus 3, to include a total of 600 MW WECS. The WECS connected to bus 1 has the wind regime of the Swift Current wind site, while the WECS connected to bus 3 has the wind regime of the Regina wind site. 600 MW wind power connected to the RTS yields a wind penetration level of approximately 15%. The system EENS is compared with various degrees of wind speed correlation. The unavailability and average repair time of the WECS connection lines are 0.00058 and 10 h, respectively. This is equivalent to a FOR of 0.0548. The State Sampling approach with DC-LF was utilised for the assessment and the estimates were obtained by simulations of 1000 years. The results of the system-EENS with various degrees of wind speed correlation is presented in Table 4.14. A comparison of the estimates obtained by the ARMA- and Weibull wind speed model is provided in Figure 4.10.

Table 4.14: The system EENS for the RTS with different degrees of wind speed correlation

R	EENS [MWh/year]		
	RTS	RTSW-1&3-ARMA	RTSW-1&3-WB
0.0	1410.7383	861.1635	861.6070
0.2		880.8309	862.6898
0.5		892.1401	869.4094
0.8		911.4227	906.9571

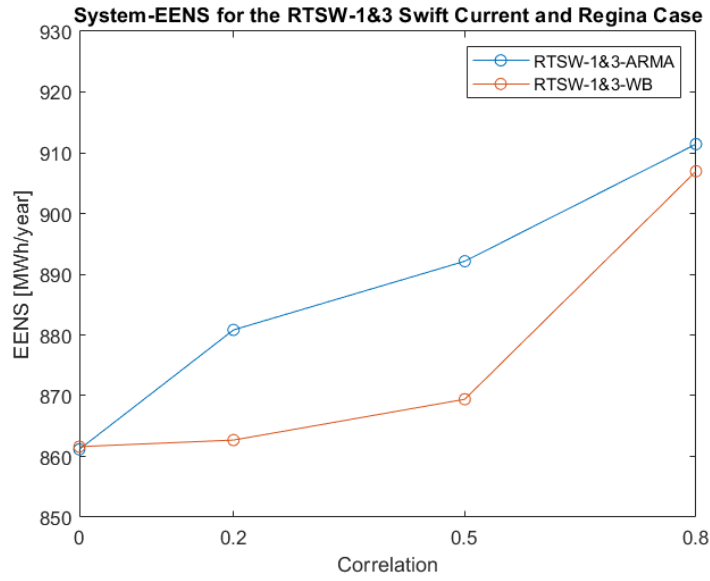


Figure 4.10: The system-EENS of the RTSW-1&3-Swift Current and Regina Case with the ARMA and Weibull models

4.2.3.2 Benchmark Comparison: DC-based State Sampling MCS with Correlation

The benchmark utilised the MECORE software, which uses the Non-sequential State Sampling approach and enumeration techniques, DC-load flow and economic priority order as the load curtailment policy [53]. This program utilises the ARMA wind speed model. It was not specified which bus that experienced the Swift Current and Regina wind regime. The benchmark results for the RTSW-1&3 are presented and compared to the obtained RTSW-1&3 estimates in Table 4.15. A comparison of the system-EENS with the benchmark results is provided in Figure 4.11.

Table 4.15: RTSW-1&3-Swift Current and Regina Case comparison against the State Sampling MECORE program benchmark results

R	Benchmark EENS [MWh/year]		Obtained EENS [MWh/year]	
	RTS	RTSW-1&3	RTS	RTSW-1&3-ARMA
0.0	1593.130	751.189	1410.7383	861.1635
0.2		784.810		880.8309
0.5		840.307		892.1401
0.8		893.648		911.4227

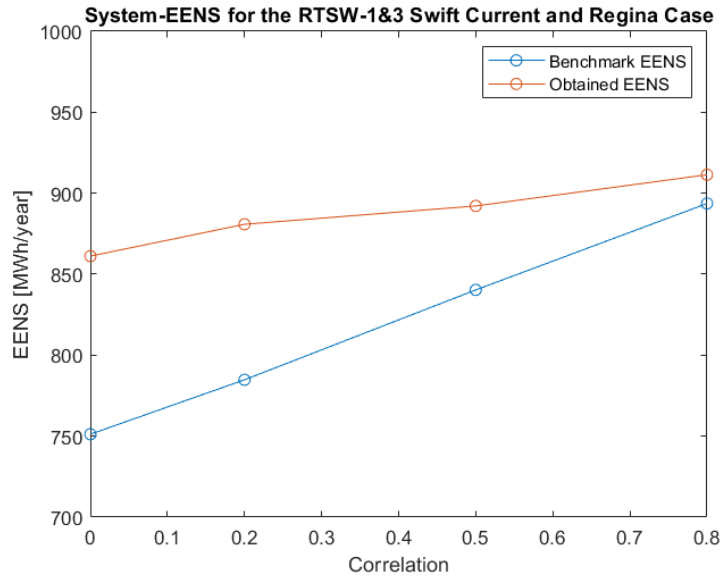


Figure 4.11: Benchmark comparison of the system-EENS of the RTSW-1&3-Swift Current and Regina Case

4.2.4 Observations and Discussion

The presented, obtained estimates deviate somewhat from the benchmark estimates. Due to the complexity of HL-II assessment, there could be multiple reasons for this. The obtained estimates for the AC-based load flow approach are the most pessimistic. This is expected since the AC-based load flow approach includes more considerations than the simplified DC-based approach. In the AC-based approach, transmission losses are included, so there is a higher generation requirement in the system to meet the load demands. Naturally, this leads to an increase in insufficient generation capacity to meet the load demands. Also, voltage limits are considered in the AC-based approach, which means that the buses with the lowest priority orders often will experience load curtailment when there is a voltage limit violation in the system. The significant drawback with the AC-based approach is the large increase in computation time, compared to the DC-based approach. Also, as the systems increase in size, the computation time increases further for the AC-based approach. As an example, it was observed that a State Sampling simulation in the MRBTS that utilised the AC-based approach required a computation time of 19 270 seconds, while the same simulation with the DC-approach required a computation time of 1 885 seconds. Because of this relationship, the AC-based approach was limited to the assessment in the MRBTS.

The benchmark estimates from the RapHL-II program utilised an AC-based load flow approach. However, the program utilised a different load shedding philosophy, where loads are curtailed at the delivery points that are closest to the elements on an outage, without any ranking of the delivery points. This is expected to have a large impact on the end results, and as illustrated in Figure 4.6, the system-EENS, before and after wind penetration, is much lower compared to the obtained estimates which utilised the priority order philosophy. Therefore, the RapHL-II estimates cannot be directly compared to the obtained AC-based estimates in this thesis.

As opposed to the RapHL-II program, the MECORE program utilised the same load shedding philosophy as this thesis. However, the MECORE program utilised a five-state COPT to model the WECS, which can decrease the accuracy of the results. In general, the MECORE estimates are slightly more pessimistic, both with and without wind penetration. An exception is observed for the estimates considering wind speed correlation, where the obtained estimates were slightly

more pessimistic. This could be because MECORE utilises a different priority order, as explained in the subsequent paragraph. In general, the approach utilised by MECORE, combining the State Sampling MCS and enumeration techniques is expected to be less accurate than the MCS methods in this thesis.

The priority order of the system delivery points can have a large impact on the final results. It was observed that the benchmark results from the MECORE program most likely utilised different IEAR-values than this thesis. This thesis utilised IEAR-values for the buses in the (M)RBTS and RTS as presented in [3]. The benchmark paper does not present its bus IEAR-values, however, one of the co-authors presents MECORE IEAR-values in [55]. The bus IEAR-values for the (M)RBTS presented in [55] is illustrated in Table 4.16. The bus IEAR-values for the (M)RBTS presented in [3], and utilised in this thesis, is illustrated in Table 4.17. This is also presented in Appendix A.

Table 4.16: Bus IEAR-values and priority order in the RBTS utilised in the MECORE Software [55].

Bus nr.	IEAR (\$/kWh)	Priority Order
2	7.41	1
3	2.69	5
4	6.78	2
5	4.82	3
6	3.63	4

Table 4.17: Bus IEAR-values and priority order in the RBTS utilised in this thesis.

Bus nr.	IEAR (\$/kWh)	Priority Order
2	9.6325	1
3	4.3769	5
4	8.0267	3
5	8.6323	2
6	5.5132	4

As seen in Table 4.16 and Table 4.17, the priority order is not the same, as the IEAR-value of bus 4 is higher than bus 5 in the MECORE software, while this thesis utilises a higher IEAR-value for bus 5 than bus 4. Except for this swap, however, the priority order is the same. Bus number 3 has the lowest priority in the RBTS for both the MECORE program and this thesis. Therefore, the load curtailment is the largest at this delivery point. The MECORE bus IEAR-values for the RTS presented in [55] is illustrated in Table 4.18. The bus IEAR-values for the RTS presented in [3], and utilised in this thesis, is illustrated in Table 4.19. IEAR-values for the RTS is also presented in Appendix B.

Table 4.18: Bus IEAR-values and priority order in the RTS utilised in the MECORE Software [55].

Bus nr.	IEAR (\$/kWh)	Priority Order
1	6.20	1
2	4.89	9
3	5.30	8
4	5.62	3
5	6.11	2
6	5.50	4
7	5.41	5
8	5.40	6
9	2.30	16
10	4.14	10
13	5.39	7
14	3.41	14
15	3.01	15
16	3.54	13
18	3.75	11
19	2.29	17
20	3.63	12

Table 4.19: Bus IEAR-values and priority order in the RTS utilised in this thesis.

Bus nr.	IEAR (\$/kWh)	Priority Order
1	8.9815	3
2	7.3606	5
3	5.8990	11
4	9.5992	1
5	9.2323	2
6	6.5238	9
7	7.0291	8
8	7.7742	4
9	3.6623	17
10	5.1940	14
13	7.2813	6
14	4.3717	16
15	5.9744	10
16	7.2305	7
18	5.6149	13
19	4.5430	15
20	5.6836	12

As seen in Table 4.18 and Table 4.19, the priority order for the buses in the RTS is quite different in the MECORE software. In general, the buses in the MECORE software with a high priority order also tend to have a high priority order in the utilised data, but the order is quite different. In the RTSW-19 assessment, the benchmark MECORE EENS estimates were dominated by the load curtailment at bus 19, bus 9 and bus 15. The EENS estimates obtained by the developed methods were dominated by the load curtailment at bus 9, bus 7 and bus 14. Bus 19, which has the highest EENS estimate in the benchmark, has the lowest RTS-priority order in the MECORE Software (17

of 17). Bus 9 has the highest EENS estimates in this thesis' RTSW-19 estimates. Table 4.19 shows that bus 9 has the lowest priority order in the RTS in this thesis (17 of 17). The same pattern can be seen for other buses with high EENS-estimates from the MECORE software and this thesis. It is therefore clear that the priority order was different in the benchmark MECORE estimates, compared to this thesis, and that the priority order has a significant impact on the end results.

For the AC approach in the MRBTS, the inclusion of 20MW WECS reduces the system-EENS by approximately 18% (Table 4.5). For the DC-approach in the MRBTS, the inclusion of 20MW WECS reduces the system-EENS by approximately 13-25% (Table 4.3 and Table 4.4). The benefit of adding WECS to the system-EENS in the MRBTS is mostly affected by the reduction of the EENS at bus 3, which has the lowest priority order.

For the inclusion of 600MW WECS at bus 19 in the RTS, the system-EENS decreases by approximately 33-36% (Table 4.9 and Table 4.10). The percentage reduction of the system-EENS is larger in the RTS than in the MRBTS. This is expected, since 600MW WECS in the RTS is equivalent to approximately 15% wind power penetration, while 20MW WECS is equivalent to approximately 8% wind power penetration in the MRBTS. Nevertheless, both systems achieve a significant improvement for the system-EENS. These results could indicate that the systems have a strong transmission network, as the generated power is easily transported to the buses in the systems.

In the RTS, the two buses with the highest EENS without wind power penetration, bus 9 and bus 14, also have the lowest priority in the system. These buses achieve a reduction in EENS of approximately 39-47% when the wind is integrated. Bus 7, however, which is the bus with the third-highest EENS-value without wind in the system, has a higher priority order (8 of 17). Despite adding wind power to the system, the EENS at bus 7 barely changes. From Figure B.1, it is observed that bus 7 is located in the south-east of the RTS, and is connected to the rest of the system through a single transmission line (line 11) to bus 8. If this transmission line experiences a failure, there will always be load curtailment at bus 7. Because of this, the added WECS have no impact on the EENS at bus 7.

It is also observed that the MECORE benchmark estimates of the EENS at bus 7 is approximately equal to zero, both before and after the wind penetration. This might suggest that some of the tools to evaluate system states are different for the thesis' and the MECORE program contingency solvers. The choices that are made for e.g how system states with isolated buses are handled, can have a significant impact on the results of composite studies. As a result, the estimates of various studies can deviate significantly [3].

The deviation between the obtained estimates from the State Sampling and State Transition approaches, and ARMA- and Weibull-models, could likely be reduced by increasing the number of simulation years. No pattern was observed for the deviation between the estimates obtained by the ARMA- and Weibull models. For the State Sampling and State Transition approaches, however, most estimates obtained by the State Sampling technique provided slightly more pessimistic estimates, compared to the State Transition technique. For the RTS, the obtained system-EENS was approximately 3-4% lower for the State Transition technique (Figure 4.7). The same pattern could be observed for the AC-MRTBS case (Figure 4.3), however, this was not the case for the DC-MRBTS case (Figure 4.2).

4.3 Ørland Case Study

The effect of integrating wind power having the wind regime of Ørland in Trøndelag county, Norway is investigated in this section. The analysis utilised the DC-based OPF-approach.

4.3.1 The Wind Speed Data

Historical wind speed data for Ørland was extracted from the Norwegian Meteorological Institute [61]. The data was collected from the ØrlandIII observation station, and the maximum median wind per hour was retrieved for the period from 01/01/2015 to 01/01/2021. The wind speed regime for the first 2000 hours is plotted in Figure 4.12. The mean wind speed and the corresponding standard deviation is given in Table 4.20.

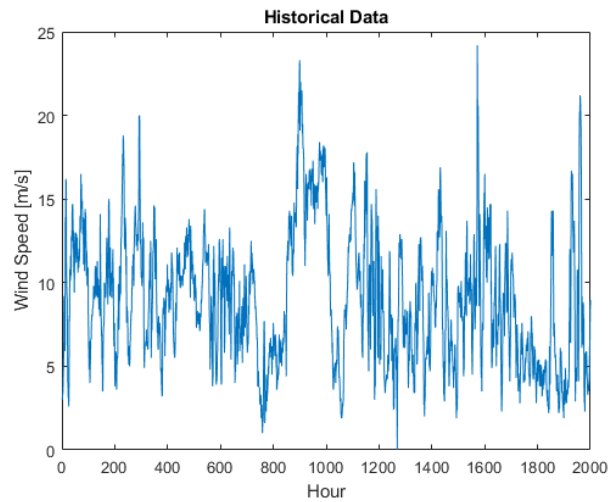


Figure 4.12: A plot of 2000 consecutive data points for the Ørland historical data.

Table 4.20: The wind speed data for Ørland [53]

	Ørland [m/s]	Ørland [km/h]
Mean wind speed, μ	7.2274	26.0186
Standard deviation, σ	3.7366	13.4518

4.3.1.1 The Weibull Model

To determine the Weibull parameters from the historical data, the MATLAB function *wblfit* [65] was used on the wind data collected from ØrlandIII. Due to *wblfit* only accepting positive numbers, all missing measurements (denoted with not a number in the data), as well as all measurements that were equal to 0, were removed from the data before the *wblfit* function was run. The Weibull parameters are given in Table 4.21. A plot of the wind speed using this model is given in Figure 4.13.

Table 4.21: Estimated Weibull parameters for the Ørland wind-regime

Ørland, Trøndelag	
α	8.1906
β	2.0604

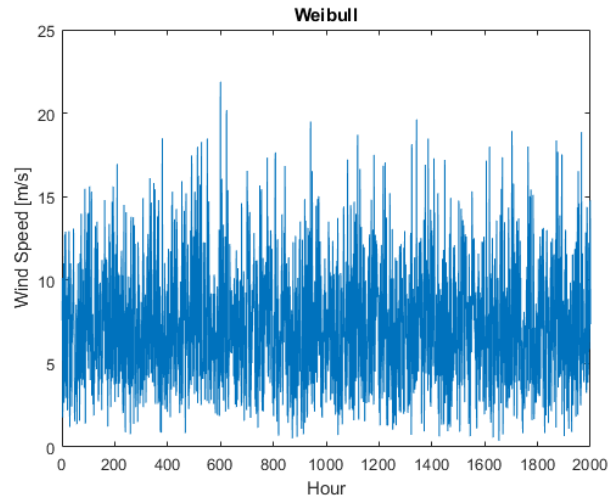


Figure 4.13: A plot of 2000 consecutive data points for the Ørland Weibull model.

4.3.1.2 The ARMA Model

The ARMA model for Ørland was developed using the ARMASA Toolbox in MATLAB [66]. The MATLAB function *sig2arma* was used to determine an ARMA(4,3) model, based on the historical wind speed data from the ØrlandIII observation station [61]. Missing measurements (denoted with Not a Number in the data), as well as measurements that were equal to 0, were removed from the data. The obtained model is given in Equation 4.3. A plot of the wind speed using this model is given in Figure 4.14.

$$y_t = 1.2244y_{t-1} - 0.0124y_{t-2} - 0.0180y_{t-3} - 0.2052y_{t-4} + \alpha_t - 0.2772\alpha_{t-1} - 0.2868\alpha_{t-2} - 0.2199\alpha_{t-3} \quad (4.3)$$

where $\alpha_t \in NID(0, 0.575103^2)$ is a normal white noise process with zero mean and variance 0.575103^2

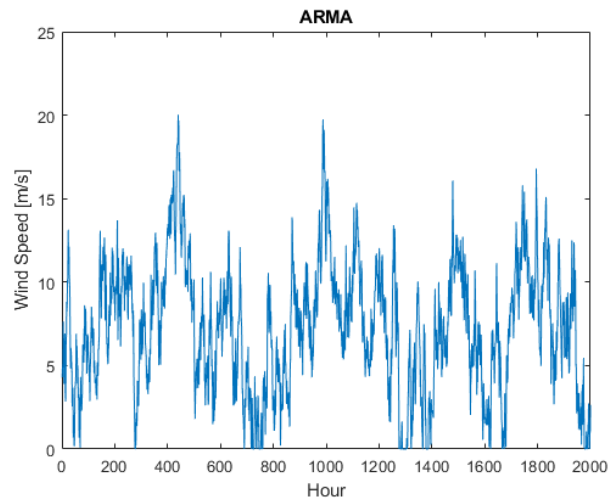


Figure 4.14: A plot of 2000 consecutive data points for the Ørland ARMA model.

The above-presented wind speed regimes are compared in the cumulative wind speed-plot, as illustrated in Figure 4.15.

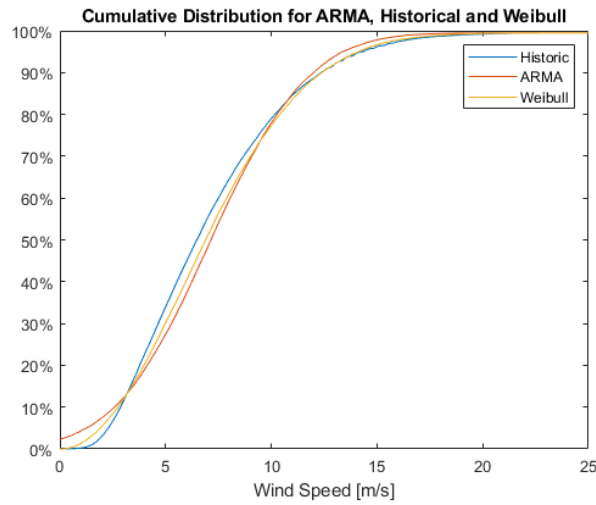


Figure 4.15: A plot of the different wind models for Ørland against each other. Data is sampled for a 5 year period.

To examine the difference between the wind speed models, the average yearly output power was calculated. The calculation used a cut-in wind speed of 4 m/s, rated wind speed of 10 m/s and cut-out wind speed of 22.222 m/s. The average output power was based on a simulation of 1000 years of hourly wind speeds from both the ARMA- and Weibull model. The result is presented in Table 4.22.

Table 4.22: Average output power from the WTGs using the different models for Ørland.

ARMA	Weibull	Historical
18.33 %	18.54%	17.85 %

4.3.2 RBTS

20 MW WECS was added to the RBTS, at bus 4, with WTG FOR set equal to zero. The WTG modelling utilised the generator power curve with a cut-in wind speed of 4 m/s, rated wind speed of 10 m/s and cut-out wind speed of 22.222 m/s. Each WTG unit is considered to have a capacity of 2MW. The WECS is connected to bus 4 through a single transmission line with an unavailability and average repair time of 0.00058 and 10h, which is equivalent to a FOR of 0.0548.

This section presents the obtained bus and system EENS-estimates for the DC-based load flow approach using the State Sampling and State Transition approach. The LOLE estimates and standard deviations of the estimates are provided in Appendix E, Appendix F and Appendix G.

4.3.2.1 State Sampling

The estimates of the EENS-index for the State Sampling technique were obtained by 1000 simulation years, and are presented in Table 4.23.

Table 4.23: Obtained estimates for the Ørland RBTSW-4 State Sampling case study

Bus nr.	EENS [MWh/year]		
	RBTS	RBTSW-4-ARMA	RBTSW-4-WB
2	0.0171	0.0297	0.0000
3	9.9993	5.1086	5.7674
4	0.0000	0.0332	0.0000
5	0.0780	0.1392	0.1743
6	122.4004	122.1977	122.5959
System	132.4949	127.5084	128.5377

4.3.2.2 State Transition

The estimates of the EENS-index for the State Transition technique were obtained by 7500 simulation years, and are presented in Table 4.24.

Table 4.24: Obtained estimates for the Ørland RBTSW-4 State Transition case study

Bus nr.	EENS [MWh/year]		
	RBTS	RBTSW-4-ARMA	RBTSW-4-WB
2	0.0214	0.0182	0.0066
3	9.1255	4.8198	5.4927
4	0.0099	0.0000	0.0000
5	0.1858	0.1130	0.1487
6	122.6094	120.6649	118.0777
System	131.9520	125.6160	123.7257

The obtained estimates from the State Sampling and State Transition techniques are summarised in Figure 4.16.

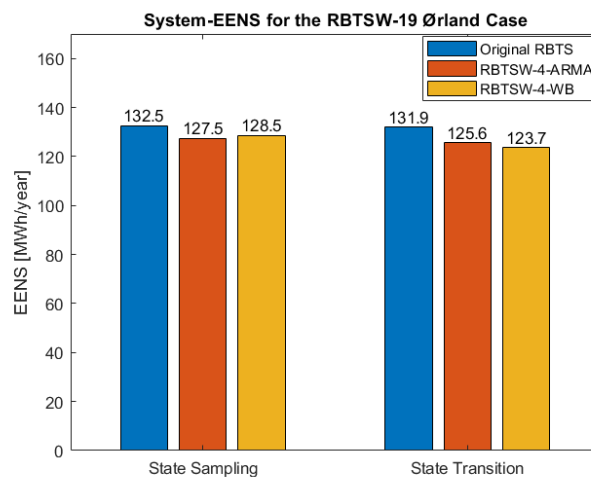


Figure 4.16: Comparison of the system-EENS in the RBTS before and after the wind penetration, obtained by the State Sampling and State Transition techniques

4.3.3 RTS

600MW WECS was added to the northern part of the RTS, at bus 19. The FOR of the WTGs were set equal to 0. The WTG modelling utilised the generator power curve with a cut-in wind speed of 4 m/s, rated wind speed of 10 m/s and cut-out wind speed of 22.222 m/s. The WTG units are considered to have a capacity of 2MW. The WECS was connected through a single transmission line with an unavailability and average repair time of 0.00058 and 10h, which is equivalent to a FOR of 0.0548.

This section presents the obtained bus and system EENS-estimates for the DC-based load flow approach using the State Sampling and State Transition approach. The LOLE estimates and standard deviations of the estimates are provided in Appendix E, Appendix F and Appendix G.

4.3.3.1 State Sampling

The State Sampling MCS was performed for 1000 simulation years. Table 4.25 presents the bus and system estimates of the EENS obtained with the State Sampling approach utilising the ARMA and the Weibull wind speed models. The buses that are excluded have zero EENS.

Table 4.25: Obtained estimates for the Ørland RTSW-19 State Sampling case study.

Bus nr.	EENS [MWh/year]		
	RTS	RTSW-19-ARMA	RTSW-19-WB
4	0.0599	0.0325	0.0595
5	0.1278	0.0000	0.0000
6	0.4285	0.2384	0.3659
7	231.0165	232.0092	234.8121
8	0.1702	0.6663	0.0000
9	853.0728	333.2722	361.4564
10	9.3407	3.0513	3.3821
14	262.3221	98.7885	102.9933
18	0.8933	0.6108	0.3232
19	53.3067	17.6784	20.7840
System	1410.7383	686.3476	724.1766

4.3.3.2 State Transition

The State Transition MCS was performed for 7500 simulation years. Table 4.26 presents the bus and system estimates of the EENS obtained with the State Transition approach utilising the ARMA and the Weibull wind speed models. The buses that are excluded have zero EENS.

The obtained estimates from the State Sampling and State Transition techniques are summarised in Figure 4.17.

Table 4.26: Obtained estimates for the Ørland RTSW-19 State Transition case study.

Bus nr.	EENS [MWh/year]		
	RTS	RTSW-19-ARMA	RTSW-19-WB
4	0.000	0.0544	0.6402
5	0.000	0.0463	0.0000
6	1.3700	0.5590	0.0000
7	226.9890	227.7337	252.1489
8	0.0572	0.2438	0.5874
9	861.1061	326.2495	338.8379
10	8.6326	3.0710	0.1848
14	260.0709	98.9796	88.8600
18	0.7255	0.2551	0.0000
19	53.7246	18.9523	11.8725
System	1412.6758	676.1447	693.1318

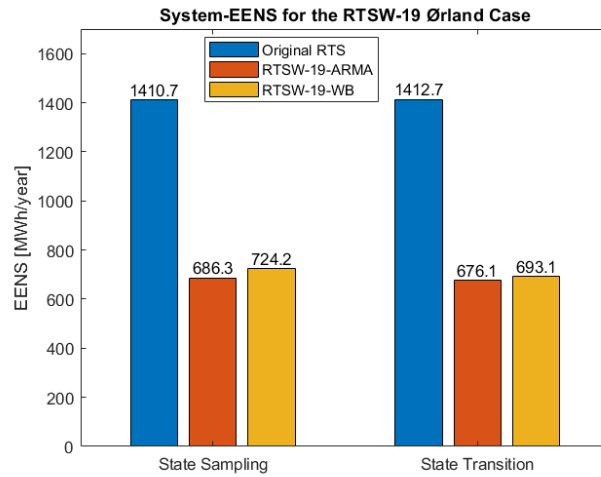


Figure 4.17: Comparison of the system-EENS in the RTS before and after the wind penetration, obtained by the State Sampling and State Transition techniques

4.3.4 Observations and Discussion

The obtained estimates for the Ørland Case Study were conducted in the RBTS and the RTS. For the RBTS, the system-EENS prior to adding the wind power is heavily dominated by the EENS at bus 6, even though bus 3 has the lowest priority order in the system. This is due to the weak single transmission line between bus 5 and bus 6. The conventional generators in this system are located north in the system, at bus 1 or bus 2. The WECS is added to bus 4, in the central part of the system. If the single transmission line in the south, from bus 5 to bus 6, experiences a failure, this will always lead to load curtailment at bus 6. Therefore, the EENS at bus 6 remains unchanged after the wind energy is included at bus 4, as illustrated in Table 4.23 and Table 4.24. The EENS at bus 3 is, however, decreased by approximately 50%. However, since the system-EENS is so heavily dominated by the EENS at bus 6, the system-EENS is only decreased by approximately 3-5% after the wind penetration.

For the RTS, it is observed that the Ørland wind speed regime has a larger impact on reducing the EENS than the Swift Current wind regime, when WECS is included at bus 19. For the Swift

Current wind regime, and inclusion of 600MW WECS, the system-EENS decreases by approximately 33-36% (Table 4.9 and Table 4.10). For the Ørland wind-regime the system-EENS decreases by approximately 49-52% (Table 4.25 and Table 4.26). A comparison of the two wind speed regimes is illustrated in Figure 4.18.

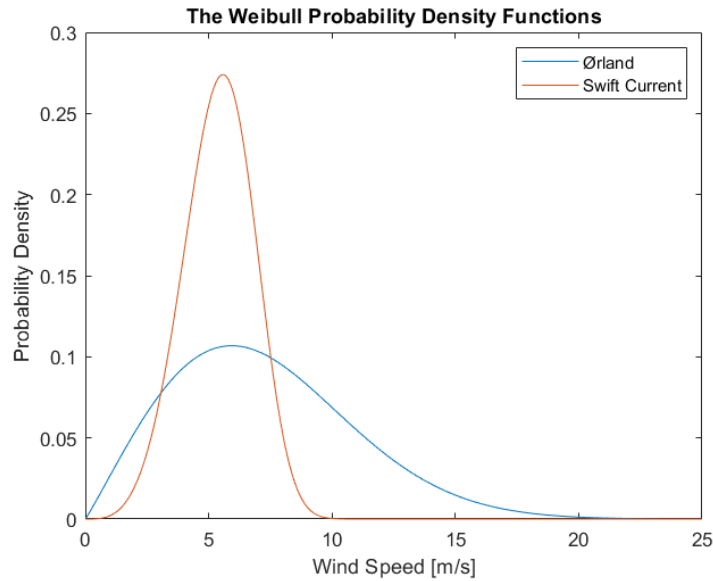


Figure 4.18: The Weibull probability density functions for Ørland and Swift Current.

Figure 4.18 illustrates that the Ørland wind speed regime is better suited for the WECS integration with the cut-in, rated and cut-out wind speeds that were utilised in the WTG modelling of this thesis. This is because a higher proportion of the wind speeds are above, or close to, the rated wind speed of 10 m/s. Subsequently, this results in a higher WTG output power delivered to the system. If the mean wind speed and standard deviation of the Ørland wind speed data (Table 4.20) are compared to the mean wind speed and standard deviation of the Swift Current wind speed data (Table 4.1), it is also observed that the Ørland wind speed data has a much higher mean wind speed. The mean wind speed at the Ørland wind site was measured to be approximately 26 km/h (7.2 m/s), while the mean wind speed at the Swift Current wind site was measured to be approximately 19.5 km/h (5.4 m/s).

The differences between the ARMA- and Weibull wind speed models are illustrated in Figure 4.13 and Figure 4.14. The ARMA model follows a more realistic regime, as the wind speed at a particular hour is autocorrelated with the previous wind speeds. With this model, there can be long periods of low/high wind speeds, until a period of high/low wind speeds begins. The wind speed regime from the Weibull model, however, fluctuates randomly, as the wind speed at a particular hour has no autocorrelation with the previous hours. If the wind speed data obtained from the two methods are compared to the historical data, Figure 4.12, it is clear that only the wind speed regime from the ARMA model reflects the fluctuation of the historical data in a realistic way. However, when the wind speed data is sampled for a long period, e.g 5 years, like in this thesis, both the Weibull and ARMA models are able to represent the historical wind data adequately, as illustrated in Figure 4.15. In certain studies, like assessment incorporating the correlation between wind speed and load demand, only the ARMA model is suitable. This is because only the ARMA model can illustrate the impact of wind speed variation within a year. However, for the assessment conducted in this thesis, the Weibull model also represents the wind speed adequately. As illustrated in Table 4.22, the obtained average output power from the WTGs are very similar for the wind speed models and the Ørland wind speed regime. The output power when the Weibull model was utilised

was measured to be 1.1% higher than the ARMA model.

4.3.5 Sensitivity Analyses

The sensitivity associated with selected considerations when integrating wind power to composite power systems is analysed in this section. The assessment utilises the DC-based load flow approach and the Weibull- and ARMA wind speed models.

4.3.5.1 Degree of Wind Power Capacity

The impact of integrating wind power with different degrees of installed wind power capacity in the RTS is analysed in this section. The analysis utilised the Weibull wind speed model. The different degrees of installed wind power penetrations examined are 15%, 30%, 45% and 60% of the total capacity in the RTS. Without any wind penetration, the installed capacity of the RTS is 3405 MW. With 15% wind power in the system, 600 MW WECS is added. 30% wind power is equivalent to 1460 MW WECS added to the system, 45% wind power is equivalent to 2786 MW WECS added to the system, and 60% wind power is equivalent to 5108 MW WECS added to the system. The WECS was added to bus 19 in the RTS, having both the wind speed regime of the Ørland wind site and the Swift Current wind site. The system EENS with the different degrees of installed wind power capacity compared to the total capacity in the RTS is illustrated in Figure 4.19.

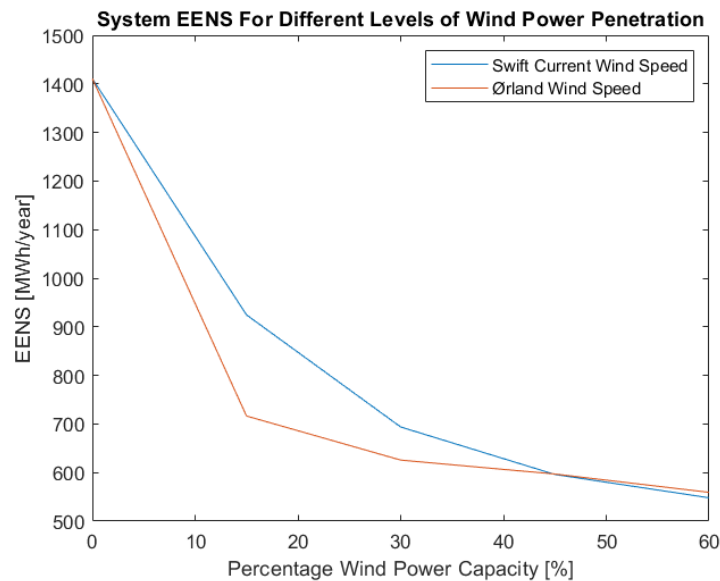


Figure 4.19: The system EENS for different levels of installed wind power capacity at bus 19 in the RTS.

Figure 4.19 illustrates the degree of adequacy reliability benefit of adding WECS with different wind speed regimes to the RTS. For the Ørland wind regime, if added WECS capacity at bus 19 composed of 15% of the total capacity in the system, the system EENS is reduced by almost 50%. For the Swift Current wind regime, the system EENS is reduced by approximately 35%. For an increase in added wind power capacity to 30% of the total installed capacity, the system EENS is reduced by approximately 56% for the Ørland wind regime. For the Swift Current wind regime, the system EENS is decreased by approximately 50%. As the installed WECS capacity is increased further, the system EENS decreases at a much lower rate. At a certain point, increasing the installed WECS capacity does not contribute to lowering the system EENS. This point, where

increasing the WECS capacity barely contributes to decreasing the system EENS, is very dependent on the system characteristics. The RTS is considered to have a strong transmission network, and therefore the power is relatively easily transported to the buses. The RBTS, however, has a weak transmission network, due to the radial supply to bus 6. Increasing the installed WECS capacity in such a system could therefore lead to a much smaller decrease in the system EENS-metric.

The impact of the wind speed regime on the reliability benefit of adding WECS to the system is clearly illustrated in Figure 4.19. For the Ørland wind regime, the system-EENS is reduced by approximately 50% when the installed wind power capacity represents 15% of the total capacity in the RTS (600MW WECS). To achieve the same reduction in system-EENS for the Swift Current wind regime, the installed wind power capacity must be increased to approximately 1460MW. In this case, the installed wind power capacity compose of approximately 30% of the total capacity in the RTS. When the percentage wind power capacity in the system is increased to approximately 45% (2786MW WECS), the decrease in system-EENS is approximately equal for both wind speed regimes.

4.3.5.2 Single Site Location Analysis

The impact of integrating wind power at different locations in the RTS is analysed in this section. 600MW WECS was individually added at selected buses in the RTS with the Ørland wind speed regime. The system-EENS with the addition of WECS at the selected locations is illustrated in Figure 4.20.

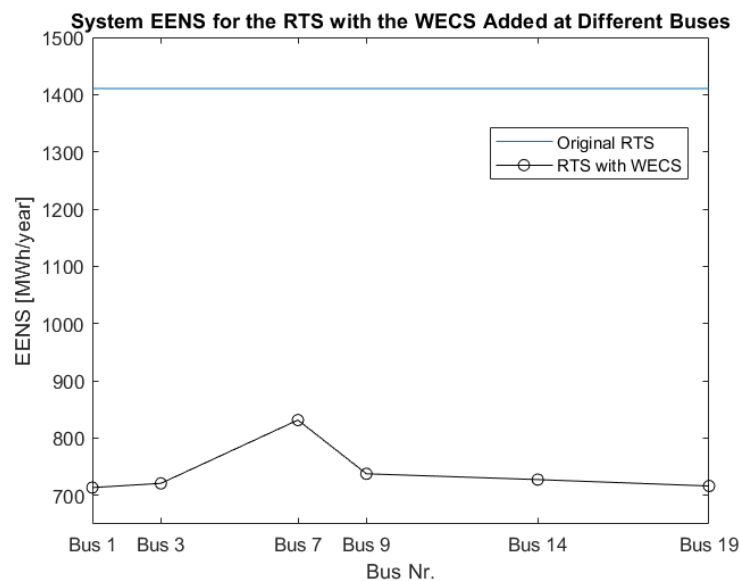


Figure 4.20: The system EENS for addition of WECS at different single sites.

It is observed that the system-EENS is relatively constant when WECS is added at most of the buses in the RTS. The exception is the addition of WECS at bus 7, which yields a significantly higher system-EENS compared to the addition at the other buses. This is likely to be because bus 7 is connected to the rest of the system by a single radial line in the southeast of the RTS (Figure B.1). If this transmission line experiences a failure, the generated power at bus 7 cannot be transported to the rest of the system. Subsequently, the system and load point reliabilities are not improved as much as for the addition of WECS at buses with a strong connection to the rest of the system.

4.3.5.3 Wind Speed Correlation Between Two Sites

The impact of integrating multiple WECS in the RTS with different degrees of wind speed correlation is analysed in this section. Two WECS having a capacity of 300MW were added to bus 1 and bus 3 in the RTS. 600 MW is equivalent to 15% installed wind power capacity in the RTS. Both WECS had the wind-regime of Ørland, as presented in section 4.3.1.2. The different degrees of wind speed correlation examined is 0, 0.2, 0.5, 0.8 and 1. The system-EENS with the different degrees of wind speed correlation is illustrated in Table 4.27. The ARMA model was utilised to model the wind speeds.

Table 4.27: System-EENS for wind speed correlation at RTS with the Ørland wind regime.

R	EENS [MWh/year]	
	RTS	RTSW-1&3-Ørland
0.0	1410.738	532.375
0.2		549.340
0.5		581.333
0.8		622.084
1.0		655.140

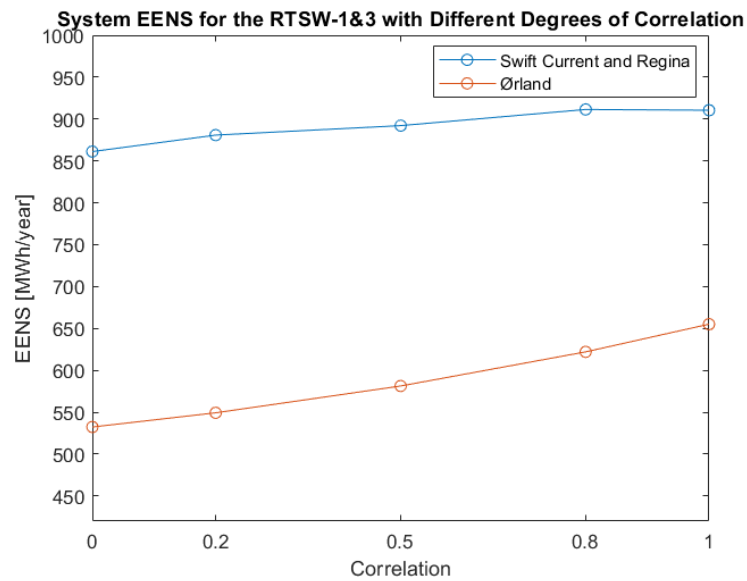


Figure 4.21: The system EENS for different levels of wind speed correlation between bus 1 and bus 3.

The results presented in Table 4.27 are plotted in Figure 4.21, and compares the results to the corresponding Swift Current/Regina results presented in Table 4.14. The results presented in Table 4.14 used the Swift Current wind speed regime at bus 1, and the Regina wind speed regime at bus 3, instead of using the Ørland wind speed regime at bus 1 and bus 3. It is observed that the system-EENS is significantly lower for the Ørland wind speed regime for all levels of wind speed correlation between the sites. The reason for this is likely to be that the Ørland site has higher mean wind speed values, as presented in the preceding sections.

It is further observed that the system-EENS for the Ørland-case is more sensitive to the degree of wind speed correlation between the two sites, compared to the Swift Current/Regina case. The

reason for this can be how the wind speeds for the different sites are distributed. Figure 4.22 illustrates the probability density distributions of the wind speeds from the three sites. It can be seen that the Ørland wind speed values are spread over a longer interval, and in general deviate more compared to the Swift Current and Regina wind speed regimes. The Swift Current and Regina wind speed regimes, however, have a more peaked distribution, since the wind speeds tend to be close to a certain value. In addition, the distributions of the Swift Current and Regina wind speeds are very similar, as the distributions peak at very similar wind speeds. These characteristics are related to the shape parameter, β , of the Weibull probability density function. Since the distribution of the Ørland wind speed regime is less peaked, and the wind speed model subsequently can take a larger set of values, the cases with a low degree of correlated wind speeds can have a higher deviation between the wind speeds at the two sites, compared to the Swift Current- and Regina wind speed regimes. A higher difference between the hourly wind speeds at multiple sites will subsequently lead to a larger benefit(decrease) in the system-EENS.

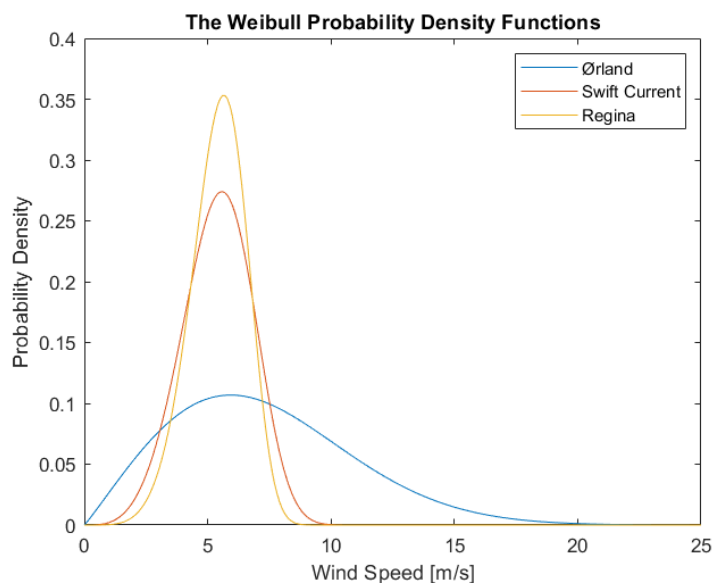


Figure 4.22: The Weibull probability density functions for Swift Current, Regina and Ørland.

4.3.5.4 Wind Turbine Generators Replacing Conventional Generators

This section analyses the impact of adding wind turbine generators while also removing some of the existing conventional generators in the RTS. A list of the existing conventional generators in the RTS is shown in Table B.1. The analysis includes 600MW WECS added to bus 19 in the RTS for all cases. The wind speed sampling used the Ørland Weibull wind speed model. All simulations used the DC-based approach and the State Sampling technique. The following three cases are examined:

- RTSW-13-197: A 197 MW (oil) generator is removed from bus 13. 600MW WECS is added at bus 19.
- RTSW-18-400: A 400MW (nuclear) generator is removed from bus 18. 600MW WECS is added at bus 19.
- RTSW-18-21-400: A 400MW (nuclear) generator is removed from bus 18, and a 400MW (nuclear) generator is removed from bus 21. 600MW WECS is added at bus 19.

The results of the three cases are presented and compared to the corresponding cases for the RTS without wind penetration in Figure 4.23 and Table 4.28.

Table 4.28: System-EENS while removing conventional generation from the RTS.

Cases	EENS [MWh/year]	
	Without wind penetration	With wind penetration
RTS	1410.7383	724.1766
RTSW-13-197	4797.0245	2216.9316
RTSW-18-400	8279.3988	3696.0748
RTSW-18-21-400	54180.6326	23636.0992

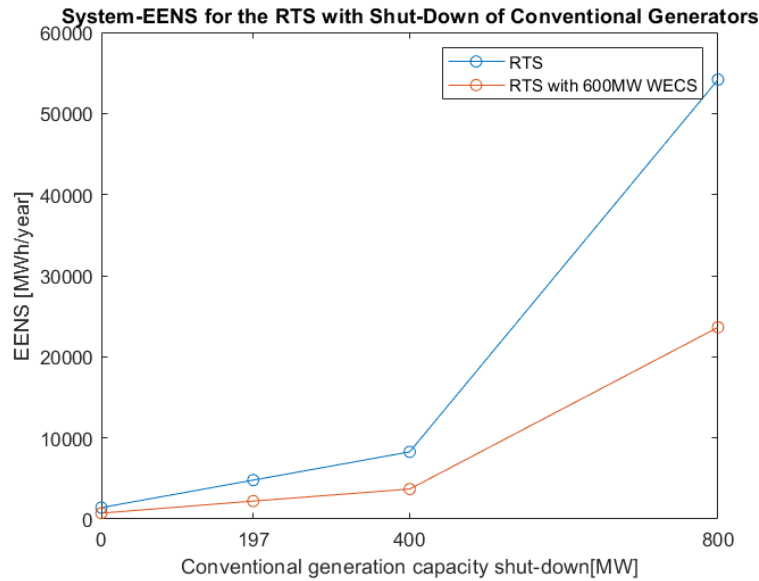


Figure 4.23: The system EENS with removed existing conventional generators in the RTS.

It is observed that the system-EENS increases significantly for all the examined cases. For the RTSW-13-197-case, where the installed wind capacity is approximately three times the capacity of the removed conventional generator, there is an increase of approximately 57% for the system-EENS from the RTS-base case without wind penetration. For the RTSW-18-400-case there is an increase of approximately 162%, while there is an increase of approximately 1573% in the system-EENS for the RTSW-18-21-400-case. Extensive large-scale WECS installations are required if wind power is going to replace existing conventional generation, while maintaining the same level of system-EENS, for a system like the RTS. The analysis illustrates that the RTS has a weak generation system, as the system-EENS is very sensitive to the removal of the existing conventional generators. This is confirmed in [53].

4.3.5.5 Increasing the System Peak Load

This section analyses the impact of increasing the system peak load in the RTS while adding WECS to the system. The peak load in the original RTS is 2850MW. The percentage hourly peak load is illustrated in Appendix C. The analysis includes 600MW WECS to bus 19 and uses the State Sampling technique and the Weibull wind speed model with the Ørland wind speed regime. The following cases are investigated:

- System peak load is increased by 5%. This is equivalent to increasing the peak load to 2992.5MW.
- System peak load is increased by 10 %. This is equivalent to increasing the peak load to 3143MW.
- System peak load is increased by 15 %. This is equivalent to increasing the peak load to 3277.5MW
- System peak load is increased by 20 %. This is equivalent to increasing the peak load to 3420MW

The results are presented in Table 4.29, and illustrated in Figure 4.24.

Table 4.29: System-EENS for system load increases in RTS with the Ørland wind regime.

Peak Load Increase	EENS [MWh/year]	
	RTS	RTSW-19-Ørland
0 %	1410.7383	724.1766
5 %	3308.2508	1547.8594
10 %	8000.7691	3494.6482
15 %	16382.0783	7628.6637
20 %	33397.9598	15811.7726

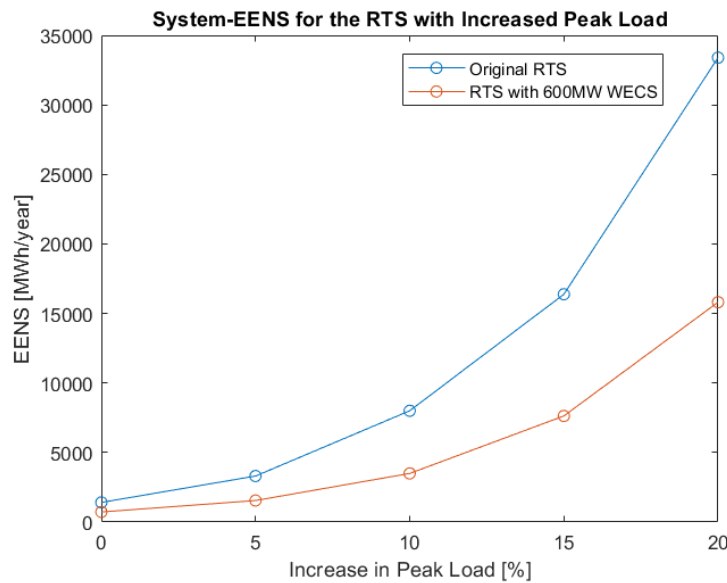


Figure 4.24: The system EENS for different levels of increased peak load.

It is observed that the system-EENS increases exponentially as the peak load increases. This coincides with the results in section 4.3.5.4, where generation was removed from the system. With wind penetration in the system, the system-EENS decreases approximately equivalently to decreasing the peak load of the system by 5%. Without wind in the system, the system-EENS is doubled compared to the RTSW-case, for all levels of increased peak load in the system. It should be noted that this thesis utilises the same load curves at all the buses of the test systems, instead of using individual load curves at the different buses. As in the preceding chapter, it is observed that the RTS has a relatively weak generation system, that is sensitive to an increase in the load demand.

4.3.5.6 Number of Wind Farms

The impact of spreading the WECS generation across multiple wind farms/sites in the RTS is analysed in this section. The total WECS capacity is 600MW for all simulations. Four different scenarios are considered: 600MW WECS connected to one bus, 600MW WECS spread over two buses(300MW at each bus), 600MW WECS spread over 3 buses(200MW at each bus) and 600MW spread over 4 buses(150MW at each bus). The analysis utilised the State Sampling approach with the Weibull wind speed model and the Ørland wind speed regime. The simulations were capped at 1000 simulation years. To provide realistic scenarios, the following wind penetration(s) and wind speed correlation(s) was considered in the analysis:

- 1 Wind Site: WECS added to bus 19.
- 2 Wind Sites: WECS added to bus 1 and 3. $R = 0.8$.
- 3 Wind Sites: WECS added to bus 1, 3 and 19. Wind speed correlation between bus 1 and 3: $R_{1,3} = 0.8$. Wind speed correlation between bus 1 and 19, and bus 3 and 19: $R_{1,19} = R_{3,19} = 0.2$. The correlation matrix, Σ , is illustrated in Equation 4.4.

$$\Sigma = \begin{bmatrix} 1 & 0.8 & 0.2 \\ 0.8 & 1 & 0.2 \\ 0.2 & 0.2 & 1 \end{bmatrix} \quad (4.4)$$

- 4 Wind Sites: WECS added to bus 1, 3, 19 and 21. Wind speed correlation between bus 1 and 3, 19 and 21: $R_{1,3} = R_{19,21} = 0.8$. Wind speed correlation between bus 1 and 19, and bus 3 and 19: $R_{1,19} = R_{3,19} = 0.2$. The correlation matrix, Σ , is illustrated in Equation 4.5.

$$\Sigma = \begin{bmatrix} 1 & 0.8 & 0.2 & 0.2 \\ 0.8 & 1 & 0.2 & 0.2 \\ 0.2 & 0.2 & 1 & 0.8 \\ 0.2 & 0.2 & 0.8 & 1 \end{bmatrix} \quad (4.5)$$

The estimated system-EENS for the presented scenarios are illustrated, and compared to the original RTS, in Table 4.30 and Figure 4.25.

Table 4.30: System-EENS for the RTS with multiple, correlated wind sites with the Ørland wind speed regime

Nr. of Wind Sites	System-EENS [MWh/year]
0	1410.738
1	693.1318
2	622.084
3	537.3723
4	520.7887

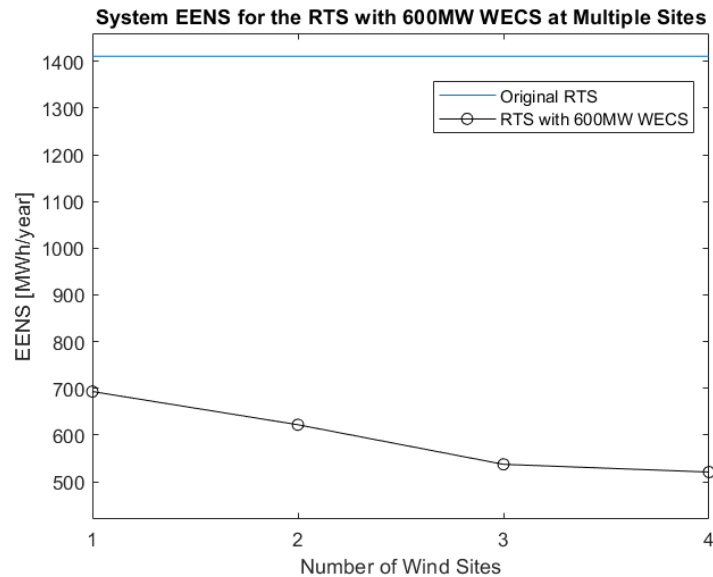


Figure 4.25: The system EENS for different numbers of wind sites.

The effect of connecting different numbers of multiple WECS in the RTS is clearly illustrated in Table 4.30 and Figure 4.25. The system-EENS decreases as the number of wind farms increase. There can be multiple reasons for this. If the generation is spread over a larger area, the added generation is closer to the delivery points, and the transmission lines would in general less often experience a failure. Also, when the WECS is spread over a larger area, the wind speed correlation between the wind farms decrease, which is beneficial for the reliability benefit. As illustrated in Figure B.1, bus 1 and bus 3 is located in the southwest of the RTS, while bus 19 and bus 21 is located in the north of the RTS. The buses that are located in close proximity in the RTS were assigned a high degree of wind speed correlation. The wind speed correlation between the buses with a large distance, however, was assigned a low degree of correlation.

It is observed that the system-EENS decreases by approximately 10% when the number of wind sites is increased from 1 to 2, and there is a relatively high degree of wind speed correlation between the sites (0.8). When the number of wind sites is increased to 3, there is a further approximately 14% decrease in the system-EENS compared to having 2 wind sites. The reason for the larger decline in the system-EENS, compared to going from 1 to 2 wind farms, is likely because there is a much lower degree of wind speed correlation between the third bus added (19) and the first two buses (1 and 3). The addition of bus 19, therefore, contributes more to the overall system reliability. From having 3 wind sites to 4 wind sites in the RTS, the system-EENS decreases further by approximately 3%. The last wind site addition (bus 21) has a high degree of correlation with bus 19 and is not able to decrease the system-EENS to the same degree as the addition of bus 19. It should be noted that the WECS in this case is connected to relatively strong points in the transmission system.

5 Conclusions and Future Work

5.1 Conclusions

The thesis examined methods of assessing the impact of integrating wind power on the reliability (adequacy aspect) of composite power systems. A framework for assessing the reliability of a composite power system that contains significant wind penetration was created through the State Sampling and State Transition MCS methods. A suitable methodology for the PSR assessment was identified through a literature review, and in-house software tools were developed to obtain appropriate HL-II indices. The developed scripts were tested on three test systems: the RBTS, MRBTS and RTS.

One of the challenges with including wind power in reliability assessment, is to provide an accurate representation of the variability and intermittent nature of the wind speed, and subsequently the output power of the WTGs. This thesis identified and developed two wind speed models, the Weibull wind speed model and the ARMA wind speed model, that were included in the framework. Further, wind speed correlation between wind sites was identified as an important factor to the accuracy of quantifying the potential impact of integrating wind power to the reliability of power systems. Methods that can incorporate wind speed correlation between multiple wind sites were identified and developed.

The examined concepts and methods were implemented in the existing composite adequacy MATLAB scripts at the Department of Electric Power Engineering at NTNU, using both a DC-based contingency solver and an AC-based contingency solver. It was observed that the results obtained from the AC-based contingency solver were more pessimistic, since this approach includes more considerations than the simplified DC-based contingency solver. Further, the AC-based approach required extensive computation time compared to the DC-based approach. Because of this, most of the assessment in this thesis utilised the DC-based contingency solver. The EENS-metric was identified as the preferred HL-II metric to examine the impact of integrating wind power in composite systems. In addition to the EENS-index, the developed scripts include LOLE-calculation. The LOLE-metric only considers the expected number of time units in which the system experiences a LOL situation, while the EENS quantifies the severity of LOL events.

Computational efficiency, accuracy and precision of the MCS approach have not been examined in the thesis. The focus has been to develop scripts that provide a good, basic job of obtaining reliability indices. The number of simulation years was capped at 1000 years for the State Sampling approach, and 7500 years for the State Transition approach, as this was in general considered to yield a sufficient precision for the purposes of the thesis. The standard deviations of the results are included in the appendix.

The developed scripts were implemented on standard test systems and their results compared with benchmark results; for validation, the Swift Current wind speed regime in Canada was used as input. It was observed that there are many considerations that can have a large impact on the results in HL-II studies. One important factor is the load shedding philosophy, which controls the load curtailment at the buses. This thesis utilised the priority order philosophy, which is based on ranking the composite system delivery points by setting different costs for load curtailment at the delivery points according to a reliability worth index.

Since the validation of the developed scripts was successfully tested for the Canadian case study, the proof was deemed sufficient enough for conducting a successful case study involving the wind speed regime of Ørland, Norway. (No benchmark comparison is available in the literature for this Norwegian case study.) An ARMA model was developed based on historical data, as well as the

Weibull scale and shape parameters used to sample the wind speed with the Weibull distribution. It was observed that the Ørland wind speed regime is well-suited for wind integration in power systems, compared to the Swift Current wind speed regime. For 15% installed wind power penetration, with the Ørland wind-regime in the RTS, the system-EENS decreased by approximately 49-52%. The impact of integrating wind power at a specific location can be very different for each delivery point. It was observed that if buses have a radial connection with the rest of the system, the reliability at such a delivery point can be strongly dependent on the reliability of the radial connection. Integrating wind power to a system with weak reliability of radial connections, might not affect the reliability at the vulnerable delivery points.

The ARMA model and the Weibull model provided similar estimates for the EENS-metric when power systems with wind penetration were examined. Neither of the two methods was preferred in this thesis, however, the ARMA model is able to illustrate the variability of a real wind speed regime, due to autocorrelation between wind speeds at a particular hour and the previous hours. Therefore, in certain types of assessment, e.g assessment considering the impact of load-wind correlation, only the ARMA-model is sufficient. The drawback with the ARMA model is that a large historical wind data set can be required for the model to be accurate.

The Non-sequential State Sampling and the Sequential State Transition approaches are compared in the thesis. Both methods provide similar results, and the small deviation could be decreased by increasing the number of simulation years. Relatively small modifications were required for the developed wind speed models to be included in the Sequential and Non-sequential approaches. It was observed that the State Sampling approach required fewer simulation years than the State Transition approach to obtain the same accuracy of the indices. Therefore, the computation time was shorter for the State Sampling approach, to obtain estimates with sufficient accuracy.

5.2 Future Work

The work conducted in this thesis could be extended to quantify the impact of wind and load correlation on the reliability of power systems. The different buses in the test systems could have individual load curves, instead of using the same load curves. It could also be interesting to examine real power systems, instead of standardised test systems. The scope could also be extended to an HL-III assessment, by including the distribution facilities.

The thesis developed software tools that are applicable to contingency solvers based on DC-load flow analysis and AC-load flow analysis. The AC-based approach required considerable more computation time, and was therefore limited to the most basic assessment, despite yielding higher estimates. The software tools could be developed to reduce the computational time of the AC-based approach, for example by using a decoupled OPF approach.

The software tools developed in this thesis could be extended to be used in a well-being analysis with significant wind penetration. The well-being analysis combines the deterministic and probabilistic methods, and can provide an extended viewpoint of the effects of integrating wind power to a system. The Sequential simulation technique is the only realistic option available to investigate the distributional aspects associated with the well-being analysis [26].

Battery energy storage systems may be an essential key in exploiting wind energy. The work of this thesis can be extended to include battery energy storage system considerations.

Solar power is another renewable energy source that is growing at a fast pace. It would be interesting to quantify the impact of significant solar power penetration on the reliability of the composite power system. The interaction and correlation between solar power- and wind power production

could be examined and included in a reliability assessment.

The decrease in output power due to the wake effect between multiple wind turbines in a wind farm is not included in this thesis. Methods to incorporate the effects of this phenomena could be developed. Also, the wind speeds were not adjusted for the hub heights of wind turbines.

The effect of seasonal wind speed variations could be examined. Seasonal variations could improve the wind speed model.

Increased penetration of wind power introduces uncertainties associated with the security aspect of power system reliability. The effects of significant wind power penetration on the dynamic conditions of the power system, such as transient or voltage instability associated with sudden disturbances of system components, could be examined.

References

- [1] United Nations. *Global Energy Interconnection Is Crucial for Paris Goals*. 2018. URL: <https://unfccc.int/news/global-energy-interconnection-is-crucial-for-paris-goals> (visited on 12/02/2021).
 - [2] International Energy Agency. *Onshore wind power generation in the Sustainable Development Scenario 2000-2030*. 2020. URL: <https://www.iea.org/data-and-statistics/charts/onshore-wind-power-generation-in-the-sustainable-development-scenario-2000-2030> (visited on 11/05/2021).
 - [3] Ø. Laengen. ‘Application of Monte Carlo Simulation to Power System Adequacy Assessment’. MA thesis. NTNU, 2018.
 - [4] H. Mediaas. ‘Contribution of Energy Storage to Generation Adequacy’. MA thesis. NTNU, 2020.
 - [5] P. Kundur et al. *Definition and classification of power system stability IEEE/CIGRE joint task force on stability terms and definitions*. Vol. 19. IEEE Transactions on Power Systems, 3. 2004, pp. 1387–1401.
 - [6] R. Billinton and W. Li. *Reliability Assessment of Electric Power Systems Using Monte Carlo Methods*. Boston: Springer Science, 1994.
 - [7] F. Mohamad, J. Teh, C.-M. Lai and L.-R. Chen. *Development of Energy Storage Systems for Power Network Reliability: A Review*. Vol. 11. Energies. Aug. 2018, p. 2278.
 - [8] A. Solheim. ‘Incorporating Demand Side Response in Power System Adequacy Studies’. MA thesis. NTNU, 2019.
 - [9] R. Billinton and R. N. Allan. *Power-system reliability in perspective*. Vol. 30. Electronics and Power 3. 1984, pp. 231–236.
 - [10] GARPUR Consortium. *D1.1: State of the Art on Reliability Assessment in Power Systems*. 2014. URL: <https://www.sintef.no/projectweb/garpur/> (visited on 02/05/2021).
 - [11] M. Bjørkeland. ‘Generation system adequacy studies in the presence of wind energy resources’. MA thesis. NTNU, 2018.
 - [12] K. Koldingsnes. ‘Reliability-based Derating Approach for Interconnectors’. MA thesis. NTNU, 2017.
 - [13] R. Billinton and R. Allan. *Reliability Evaluation of Engineering Systems: Concepts and Techniques*. Springer US, 1992. URL: <https://books.google.no/books?id=nqm9N6Yfk9sC>.
 - [14] R. Billinton and R. Allan. *Reliability Evaluation of Power Systems, 2nd edition*. Springer US, 1996. URL: <https://books.google.no/books?id=b6l4MdiVgn8C>.
 - [15] North American Electric Reliability Corporation. *Methods to Model and Calculate Capacity Contributions of Variable Generation for Resource Adequacy Planning*. 2011. URL: <https://www.nerc.com/files/ivgtf1-2.pdf> (visited on 11/02/2021).
 - [16] International Energy Agency. *Re-powering Markets*. 2016, p. 246. URL: <https://www.oecd-ilibrary.org/content/publication/9789264209596-en> (visited on 01/12/2020).
 - [17] Ø. Laengen and V. Vadlamudi. ‘DC and AC Contingency Solvers in Composite Power System Adequacy Assessment’. In: *Advances in RAMS Engineering: In Honor of Professor Ajit Kumar Verma on His 60th Birthday*. Jan. 2020, pp. 3–48.
 - [18] W. Li and P. Choudhury. *Probabilistic transmission planning*. Vol. 5. IEEE power and energy magazine 5. IEEE, 2007, pp. 46–53.
 - [19] M. Khan and R. Billinton. *A hybrid model for quantifying different operating states of composite power systems*. Vol. 7. IEEE Transactions on Power Systems 1. 1992, pp. 187–193.
-

-
- [20] V. Levi, J. Nahman and D. Nedic. *Security modeling for power system reliability evaluation*. Vol. 16. IEEE Transactions on Power Systems 1. 2001, pp. 29–37.
- [21] GARPUR Consortium. *The GARPUR Project Results*. 2017. URL: <https://www.sintef.no/globalassets/project/garpur/deliverables/garpur-brochure.pdf> (visited on 02/05/2021).
- [22] D. Huang and R. Billinton. *Effects of Wind Power on Bulk System Adequacy Evaluation Using the Well-Being Analysis Framework*. Vol. 24. IEEE Transactions on Power Systems 3. 2009, pp. 1232–1240.
- [23] W. Wangdee, R. Billinton and W. Li. ‘Adequacy and security measures in integrated intermittent renewable generation systems’. In: *Reliability and Risk Evaluation of Wind Integrated Power Systems*. Springer, 2013, pp. 75–89.
- [24] R. Billinton, R. Karki and A. Verma. *Reliability and Risk Evaluation of Wind Integrated Power Systems*. Reliable and Sustainable Electric Power and Energy Systems Management. Springer India, 2013. URL: <https://books.google.no/books?id=yfIHAAAAQBAJ>.
- [25] R. Billinton et al. *Adequacy Assessment Considerations in Wind Integrated Power Systems*. Vol. 27. IEEE Transactions on Power Systems 4. 2012, pp. 2297–2305.
- [26] W. Wangdee and R. Billinton. *Bulk electric system well-being analysis using sequential Monte Carlo simulation*. Vol. 21. IEEE Transactions on Power Systems 1. 2006, pp. 188–193.
- [27] R. Billinton, M. Fotuhi-Firuzabad and S. Aboreshaid. *Power system health analysis*. Vol. 55. Reliability Engineering System Safety 1. 1997, pp. 1–8. URL: <http://www.sciencedirect.com/science/article/pii/S0951832096001184>.
- [28] CIGRE Technical Brochure 434. *Review of the current status of tools and techniques for risk-based and probabilistic planning in power systems*. WG 601 of SC C4. 2010.
- [29] F. Chen et al. *Reliability assessment method of composite power system with wind farms and its application in capacity credit evaluation of wind farms*. Vol. 166. Electric Power Systems Research. 2019, pp. 73–82. URL: <http://www.sciencedirect.com/science/article/pii/S0378779618303171>.
- [30] A. Keane et al. *Capacity Value of Wind Power*. Vol. 26. IEEE Transactions on Power Systems 2. 2011, pp. 564–572.
- [31] I. Vetvik. ‘Hywind Powering Utsira’. MA thesis. NTNU, 2017.
- [32] C. L. T. Borges and J. P. Galvão. ‘Evaluation of Wind Energy Sources Influence on Composite Generation and Transmission Systems Reliability’. In: *Proceedings of the Power Systems Computation Conference*. 2005.
- [33] R. Billinton, H. Chen and R. Ghajar. *Time-series models for reliability evaluation of power systems including wind energy*. Vol. 36. Microelectronics Reliability 9. 1996, pp. 1253–1261. URL: <https://www.sciencedirect.com/science/article/pii/0026271495001549>.
- [34] P. Giorsetto and K. F. Utsurogi. *Development of a New Procedure for Reliability Modeling of Wind Turbine Generators*. Vol. PAS-102. IEEE Transactions on Power Apparatus and Systems 1. 1983, pp. 134–143.
- [35] R. Billinton and G. Bai. *Generating capacity adequacy associated with wind energy*. Vol. 19. IEEE Transactions on Energy Conversion 3. 2004, pp. 641–646.
- [36] R. Billinton, H. Chen and R. Ghajar. *A sequential simulation technique for adequacy evaluation of generating systems including wind energy*. Vol. 11. IEEE Transactions on Energy Conversion 4. 1996, pp. 728–734.
- [37] R. Zheng and J. Zhong. ‘Generation adequacy assessment for power systems with wind turbine and energy storage’. In: *2010 Innovative Smart Grid Technologies (ISGT)*. 2010, pp. 1–6.
-

-
- [38] S. I. Arman, R. Karki and R. Billinton. ‘Resource strength and location impact of wind power on bulk electric system reliability’. In: *2016 International Conference on Probabilistic Methods Applied to Power Systems (PMAPS)*. 2016, pp. 1–6.
- [39] M. Hosseinpour, H. Mashhadi and E. Hajiabadi. *A probabilistic model for assessing the reliability of wind farms in a power system*. Vol. 14. Journal of Zhejiang University SCIENCE C. June 2013.
- [40] J. Lin et al. *Reliability based power systems planning and operation with wind power integration: A review to models, algorithms and applications*. Vol. 31. Renewable and Sustainable Energy Reviews. 2014, pp. 921–934. URL: <https://www.sciencedirect.com/science/article/pii/S1364032113008484>.
- [41] R. Billinton and D. Huang. *Incorporating Wind Power in Generating Capacity Reliability Evaluation Using Different Models*. Vol. 26. IEEE Transactions on Power Systems 4. 2011, pp. 2509–2517.
- [42] R. Billinton et al. ‘Adequacy assessment considerations in wind integrated power systems’. In: vol. 27. IEEE Transactions on Power Systems 4. IEEE, 2012, pp. 2297–2305.
- [43] S. Shi and K. L. Lo. ‘Reliability assessment of power system considering the impact of wind energy’. In: *2012 47th International Universities Power Engineering Conference (UPEC)*. 2012, pp. 1–6.
- [44] L. Wu et al. ‘Reliability assessment of composite generation and transmission system containing wind farms’. In: *IEEE PES Innovative Smart Grid Technologies*. 2012, pp. 1–5.
- [45] J. Wen, Y. Zheng and F. Donghan. *A review on reliability assessment for wind power*. Vol. 13. Renewable and sustainable energy reviews 9. Elsevier, 2009, pp. 2485–2494.
- [46] R. A. Vergara and M. A. Ríos. ‘Probabilistic Model of Wind Power Parks for Reliability Assessment’. In: *2020 IEEE ANDESCON*. 2020, pp. 1–5.
- [47] M. Lei et al. *A review on the forecasting of wind speed and generated power*. Vol. 13. Renewable and Sustainable Energy Reviews 4. 2009, pp. 915–920. URL: <http://www.sciencedirect.com/science/article/pii/S1364032108000282>.
- [48] Y.P. Faniband and S.M. Shaahid. *Forecasting Wind Speed using Artificial Neural Networks - A Case Study of a Potential Location of Saudi Arabia*. Vol. 173. E3S Web Conf. 2020, p. 01004. URL: <https://doi.org/10.1051/e3sconf/202017301004>.
- [49] C. Lowery and M. O’Malley. ‘Wind Power Scenario Tree Tool: Development and Methodology’. In: *Reliability and Risk Evaluation of Wind Integrated Power Systems*. Ed. by R. Billinton, R. Karki and A. K. Verma. India: Springer India, 2013, pp. 13–27. URL: https://doi.org/10.1007/978-81-322-0987-4_2.
- [50] R. Billinton and Y. Gao. *Adequacy assessment of composite power generation and transmission systems with wind energy*. Vol. 2. International Journal of Reliability and Safety 1/2. 2008, pp. 79–98. URL: <https://EconPapers.repec.org/RePEc:ids:ijrsaf:v:2:y:2008:i:1/2:p:79-98>.
- [51] R. Billinton and Y. Gao. *Multistate wind energy conversion system models for adequacy assessment of generating systems incorporating wind energy*. Vol. 23. IEEE Transactions on Energy Conversion 1. IEEE, 2008, pp. 163–170.
- [52] R. Billinton, Y. Gao and R. Karki. *Composite System Adequacy Assessment Incorporating Large-Scale Wind Energy Conversion Systems Considering Wind Speed Correlation*. Vol. 24. IEEE Transactions on Power Systems 3. 2009, pp. 1375–1382.
- [53] R. Billinton, Y. Gao, D. Huang and R. Karki. *Adequacy assessment of wind-integrated composite generation and transmission systems*. Springer, 2011, pp. 141–167.
-

-
- [54] Y. Gao, R. Billinton and R. Karki. ‘Composite generation and transmission system adequacy assessment considering wind energy seasonal characteristics’. In: *2009 IEEE Power Energy Society General Meeting*. 2009, pp. 1–7.
- [55] Y. Gao. ‘Adequacy Assessment of Composite Generation and Transmission Systems Incorporating Wind Energy Conversion Systems’. PhD thesis. University of Saskatchewan, 2010.
- [56] W. Wangdee and R. Billinton. *Reliability assessment of bulk electric systems containing large wind farms*. Vol. 29. International Journal of Electrical Power Energy Systems 10. 2007, pp. 759–766. URL: <https://www.sciencedirect.com/science/article/pii/S0142061507000683>.
- [57] D. Huang. ‘Bulk electric system reliability evaluation incorporating wind power and demand side management’. PhD thesis. University of Saskatchewan, 2010.
- [58] R. Billinton and W. Wangdee. *Predicting bulk electricity system reliability performance indices using sequential Monte Carlo simulation*. Vol. 21. IEEE Transactions on Power Delivery 2. 2006, pp. 909–917.
- [59] W. Wangdee and R. Billinton. *Considering load-carrying capability and wind speed correlation of WECS in generation adequacy assessment*. Vol. 21. IEEE Transactions on Energy Conversion 3. 2006, pp. 734–741.
- [60] S. Karaki, B. Salim and R. Chedid. *Probabilistic model of a two-site wind energy conversion system*. Vol. 17. IEEE Transactions on Energy Conversion 4. 2002, pp. 530–536.
- [61] Meteorologisk Institutt. *Observations - Hourly Data*. 2021. URL: http://sharki.oslo.dnmi.no/portal/page?_pageid=73,39035,73_39049&_dad=portal&_schema=PORTAL (visited on 04/04/2021).
- [62] E. Schumann. *Generating Correlated Uniform Variates*. URL: <http://comisef.wikidot.com/tutorial:correlateduniformvariates> (visited on 06/04/2021).
- [63] MathWorks. *chol - Cholesky factorization*. URL: <https://se.mathworks.com/help/matlab/ref/chol.html> (visited on 11/05/2021).
- [64] R. Karki, D. Dhungana and R. Billinton. *An Appropriate Wind Model for Wind Integrated Power Systems Reliability Evaluation Considering Wind Speed Correlations*. Vol. 3. Applied Sciences. Mar. 2013, pp. 107–121.
- [65] MathWorks. *wblfit - Weibull parameter estimates*. URL: <https://se.mathworks.com/help/stats/wblfit.html> (visited on 02/05/2021).
- [66] P. M. T. Broersen. *ARMASA - MATLAB Central File Exchange*. 2021. URL: <https://www.mathworks.com/matlabcentral/fileexchange/1330-armasa> (visited on 23/05/2021).
- [67] R. Billinton and S. Jonnavithula. *A test system for teaching overall power system reliability assessment*. Vol. 11. IEEE Transactions on Power Systems 4. 1996, pp. 1670–1676.
- [68] C. Barrows et al. *The IEEE reliability test system: A proposed 2019 Update*. Vol. 35. IEEE Transactions on Power Systems 1. IEEE, 2019, pp. 119–127.
- [69] C. Ordoudis, P. Pinson, J. M. Morales and M. Zugno. *An updated version of the IEEE RTS 24-bus system for electricity market and power system operation studies*. Technical University of Denmark. 2016, pp. 0885–8950.
- [70] C. Grigg et al. *The IEEE reliability test system-1996. A report prepared by the reliability test system task force of the application of probability methods subcommittee*. Vol. 14. IEEE Transactions on power systems 3. IEEE, 1999, pp. 1010–1020.
-

Appendix

A RBTS

The RBTS is a PSR test system developed by the Power Systems Research Group at the University of Saskatchewan [67]. The system gives enough parameters to conduct both HL-I and HL-II PSR studies. The design intent of the system was to develop a system for educational purposes that is intricate enough to reflect nuances of PSR, while simultaneously being small enough to be able to be analyzed by hand or small computer programs [67].

The system is a 6-bus system with 11 generators, 9 transmission lines, an installed capacity of 240 MW and a peak load of 185 MW. The generators are divided on two buses, 1 and 2. The single line diagram of the generation and transmission system is illustrated in Figure A.1. The system data that is required to conduct HL-II assessment is provided in Table B.1, Table B.2, Table B.3 and Table B.4.

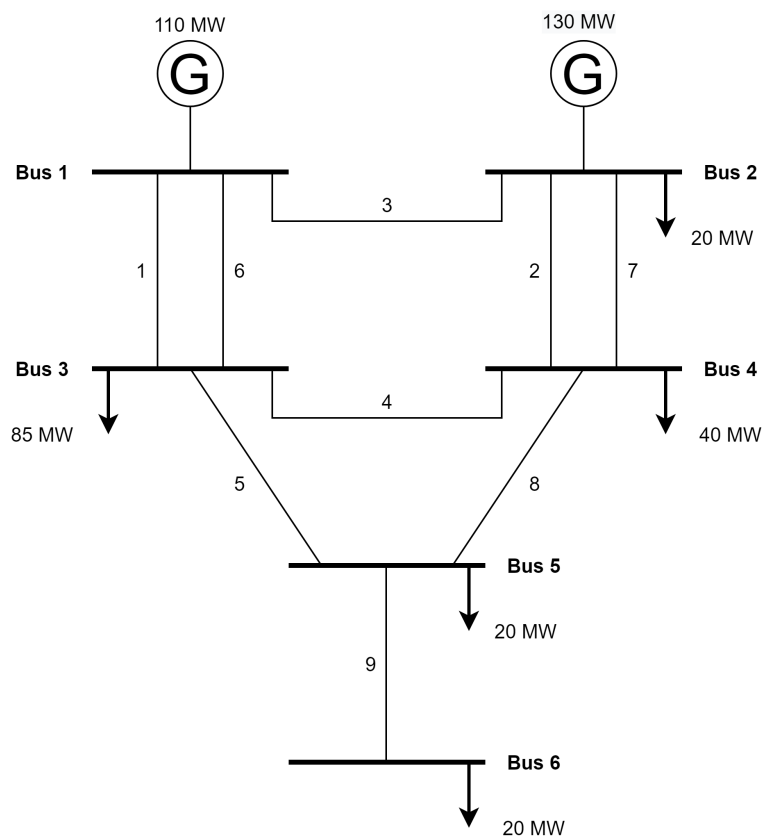


Figure A.1: Single line diagram of the RBTS

A.1 The RBTS Generator Data

Table A.1: The generator data of the RBTS test system

Generator	Capacity [MW]	Bus	Reactive min [MVar]	Reactive max [MVar]	FOR	Failure rate [1/year]	Repair rate [1/year]
1	10	1	0	7	0.020	4.0	196.0
2	20	1	-7	12	0.025	5.0	195.0
3	40	1	-15	17	0.030	6.0	194.0
4	40	1	-15	17	0.030	6.0	194.0
5	5	2	0	5	0.010	2.0	198.0
6	5	2	0	5	0.010	2.0	198.0
7	20	2	-7	12	0.015	2.4	157.6
8	20	2	-7	12	0.015	2.4	157.6
9	20	2	-7	12	0.015	2.4	157.6
10	20	2	-7	12	0.015	2.4	157.6
11	40	2	-15	17	0.020	3.0	147.0

A.2 The RBTS Network Data

Table A.2: The outage data of the RBTS network.

Line	From Bus	To Bus	Failure rate [1/year]	MTTR [hours]	FOR
1	1	3	1.5	10	0.00171
2	2	4	5.0	10	0.00568
3	1	2	4.0	10	0.00455
4	3	4	1.0	10	0.00114
5	3	5	1.0	10	0.00114
6	1	3	1.5	10	0.00171
7	2	4	5.0	10	0.00568
8	4	5	1.0	10	0.00114
9	5	6	1.0	10	0.00114

Table A.3: The RBTS network parameters.

Line	From Bus	To Bus	Resistance [pu]	Reactance [pu]	B/2 [pu]	Current Rating [pu]
1	1	3	0.0342	0.18	0.0106	0.85
2	2	4	0.1140	0.60	0.0352	0.71
3	1	2	0.0912	0.48	0.0282	0.71
4	3	4	0.0228	0.12	0.0071	0.71
5	3	5	0.0228	0.12	0.0071	0.71
6	1	3	0.0342	0.18	0.0106	0.85
7	2	4	0.1140	0.60	0.0352	0.71
8	4	5	0.0228	0.12	0.0071	0.71
9	5	6	0.0228	0.12	0.0071	0.71

A.3 The RBTS Bus Data

Table A.4: The Bus data of the RBTS

Bus	Share of load	V_{min} [p.u]	V_{max} [p.u]	Curtailement cost [\$/kWh]
1	0	0.97	1.05	0
2	0.1081	0.97	1.05	9.6325
3	0.4595	0.97	1.05	4.3769
4	0.2162	0.97	1.05	8.0267
5	0.1081	0.97	1.05	8.6323
6	0.1081	0.97	1.05	5.5132

B IEEE-RTS

The IEEE-RTS is a widely used test system, originally developed in 1979. The following presents the 1996 version (IEEE-RTS96). Several modified versions have since been developed [68, 69].

The model has 3 different configurations, a single-area 24-bus system, a two-area 48-bus system and a three-area 73-bus system [70]. The thesis utilizes the single area 24-bus system, as illustrated in Figure B.1.

As with the RBTS, the IEEE-RTS has sufficient data to conduct HL-II PSR studies, but the system is more complex. The single-area configuration has an installed capacity of 3405 MW and a peak load of 2850 MW. The system consists of 32 generators, ranging from a capacity of 12 MW to 400 MW. The system data that is required to conduct HL-II assessment is provided in Table B.1, Table B.2, Table B.3 and Table B.4.

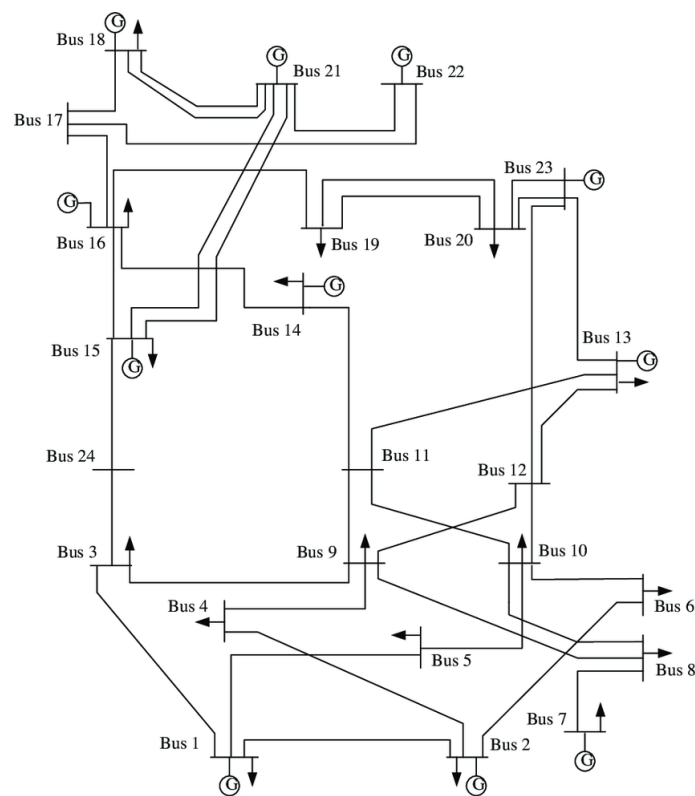


Figure B.1: Single line diagram of the RTS [70]

B.1 The RTS Generator Data

Table B.1: The generator data of the IEEE-RTS

Capacity [MW]	Bus	X_{min} [MVar]	X_{max} [MVar]	FOR	MTTF	MTTR
12	15	0	6	0.02	2940	60
12	15	0	6	0.02	2940	60
12	15	0	6	0.02	2940	60
12	15	0	6	0.02	2940	60
12	15	0	6	0.02	2940	60
20	1	0	10	0.1	450	50
20	1	0	10	0.1	450	50
20	2	0	10	0.1	450	50
20	2	0	10	0.1	450	50
50	22	-10	16	0.01	1980	20
50	22	-10	16	0.01	1980	20
50	22	-10	16	0.01	1980	20
50	22	-10	16	0.01	1980	20
50	22	-10	16	0.01	1980	20
50	22	-10	16	0.01	1980	20
76	1	-25	30	0.02	1960	40
76	1	-25	30	0.02	1960	40
76	2	-25	30	0.02	1960	40
76	2	-25	30	0.02	1960	40
100	7	0	60	0.04	1200	50
100	7	0	60	0.04	1200	50
100	7	0	60	0.04	1200	50
155	15	-50	80	0.04	960	40
155	16	-50	80	0.04	960	40
155	23	-50	80	0.04	960	40
155	23	-50	80	0.04	960	40
197	13	0	80	0.05	950	50
197	13	0	80	0.05	950	50
197	13	0	80	0.05	950	50
350	23	-25	150	0.08	1150	100
400	18	-50	200	0.12	1100	150
400	21	-50	200	0.12	1100	150
0	14	-50	200	0	-	-
0	6	-100	0	0	-	-

B.2 The RTS Network Data

Table B.2: The outage data of the RTS network.

Line	From Bus	To Bus	Failure rate [1/year]	MTTR [hours]	FOR
1	1	2	0.24	16	0.000438164
2	1	3	0.51	10	0.000581853
3	1	5	0.33	10	0.000376570
4	2	4	0.39	10	0.000445007
5	2	6	0.48	10	0.000547645
6	3	9	0.38	10	0.000433602
7	3	24	0.02	768	0.001750356
8	4	9	0.36	10	0.000410790
9	5	10	0.34	10	0.000387977
10	6	10	0.33	35	0.001316757
11	7	8	0.30	10	0.000342349
12	8	9	0.44	10	0.000502031
13	8	10	0.44	10	0.000502031
14	9	11	0.02	768	0.001750356
15	9	12	0.02	768	0.001750356
16	10	11	0.02	768	0.001750356
17	10	12	0.02	768	0.001750356
18	11	13	0.40	11	0.000502031
19	11	14	0.39	11	0.000489486
20	12	13	0.40	11	0.000502031
21	12	23	0.52	11	0.000652542
22	13	23	0.49	11	0.000614918
23	14	16	0.38	11	0.000476941
24	15	16	0.33	11	0.000414212
25	15	21	0.41	11	0.000514575
26	15	21	0.41	11	0.000514575
27	15	24	0.41	11	0.000514575
28	16	17	0.35	11	0.000439305
29	16	19	0.34	11	0.000426758
30	17	18	0.32	11	0.000401665
31	17	22	0.54	11	0.000677623
32	18	21	0.35	11	0.000439305
33	18	21	0.35	11	0.000439305
34	19	20	0.38	11	0.000476941
35	19	20	0.38	11	0.000476941
36	20	23	0.34	11	0.000426758
37	20	23	0.34	11	0.000426758
38	21	22	0.45	11	0.000564749

Table B.3: The RTS network parameters.

Line	From Bus	To Bus	Resistance [pu]	Reactance [pu]	B/2 [pu]	Current Rating [pu]
1	1	2	0.0026	0.0139	0.23055	1.93
2	1	3	0.0546	0.2112	0.0286	2.08
3	1	5	0.0218	0.0845	0.01145	2.08
4	2	4	0.0328	0.1267	0.01715	2.08
5	2	6	0.0497	0.192	0.026	2.08
6	3	9	0.0308	0.119	0.0161	2.08
7	3	24	0.0023	0.0839	0	5.1
8	4	9	0.0268	0.1037	0.01405	2.08
9	5	10	0.0228	0.0883	0.01195	2.08
10	6	10	0.0139	0.0605	1.2295	1.93
11	7	8	0.0159	0.0614	0.0083	2.08
12	8	9	0.0427	0.1651	0.02235	2.08
13	8	10	0.0427	0.1651	0.02235	2.08
14	9	11	0.0023	0.0839	0	5.1
15	9	12	0.0023	0.0839	0	5.1
16	10	11	0.0023	0.0839	0	5.1
17	10	12	0.0023	0.0839	0	5.1
18	11	13	0.0061	0.0476	0.04995	6
19	11	14	0.0054	0.0418	0.04395	6
20	12	13	0.0061	0.0476	0.04995	6
21	12	23	0.0124	0.0966	0.1015	6
22	13	23	0.0111	0.0865	0.0909	6
23	14	16	0.005	0.0389	0.0409	6
24	15	16	0.0022	0.0173	0.0182	6
25	15	21	0.0063	0.049	0.0515	6
26	15	21	0.0063	0.049	0.0515	6
27	15	24	0.0067	0.0519	0.05455	6
28	16	17	0.0033	0.0259	0.02725	6
29	16	19	0.003	0.0231	0.02425	6
30	17	18	0.0018	0.0144	0.01515	6
31	17	22	0.0135	0.1053	0.1106	6
32	18	21	0.0033	0.0259	0.02725	6
33	18	21	0.0033	0.0259	0.02725	6
34	19	20	0.0051	0.0396	0.04165	6
35	19	20	0.0051	0.0396	0.04165	6
36	20	23	0.0028	0.0216	0.02275	6
37	20	23	0.0028	0.0216	0.02275	6
38	21	22	0.0087	0.0678	0.0712	6

B.3 The RTS Bus Data

Table B.4: The Bus data of the RTS

Bus	Share of load	V_{min} [p.u]	V_{max} [p.u]	Curtailment cost [\$/kWh]
1	0.038	0.95	1.05	8.9815
2	0.034	0.95	1.05	7.3606
3	0.063	0.95	1.05	5.8990
4	0.026	0.95	1.05	9.5992
5	0.025	0.95	1.05	9.2323
6	0.048	0.95	1.05	6.5238
7	0.044	0.95	1.05	7.0291
8	0.06	0.95	1.05	7.7742
9	0.061	0.95	1.05	3.6623
10	0.068	0.95	1.05	5.1940
11	0	0.95	1.05	0.0000
12	0	0.95	1.05	0.0000
13	0.093	0.95	1.05	7.2813
14	0.068	0.95	1.05	4.3717
15	0.111	0.95	1.05	5.9744
16	0.035	0.95	1.05	7.2305
17	0	0.95	1.05	0.0000
18	0.117	0.95	1.05	5.6149
19	0.064	0.95	1.05	4.5430
20	0.045	0.95	1.05	5.6836
21	0	0.95	1.05	0.0000
22	0	0.95	1.05	0.0000
23	0	0.95	1.05	0.0000
24	0	0.95	1.05	0.0000

C Test System Load

Table C.1: The weekly peak load, used in the hourly peak load model for all simulations.

Week	Peak Load [%]	Week	Peak Load [%]	Week	Peak Load [%]	Week	Peak Load
1	86.2	14	75.0	27	75.5	40	72.4
2	90.7	15	72.1	28	81.6	41	74.3
3	87.8	16	80.0	29	80.1	42	74.4
4	83.4	17	75.4	30	88.0	43	80.0
5	88.0	18	83.7	31	72.2	44	88.1
6	84.1	19	87.0	32	77.6	45	88.5
7	83.2	20	88.0	33	80.0	46	90.9
8	80.6	21	85.6	34	72.9	47	94.0
9	74.0	22	81.1	35	72.6	48	89.0
10	73.7	23	90.0	36	70.5	49	94.2
11	71.5	24	88.7	37	78.0	50	97.0
12	72.7	25	89.6	38	69.5	51	100.0
13	70.4	26	86.1	39	72.4	52	95.2

Table C.2: The weekday peak load, used in the hourly peak load model for all simulations.

Day	Peak Load [%]
Monday	93
Tuesday	100
Wednesday	98
Thursday	96
Friday	94
Saturday	77
Sunday	75

Table C.3: The hourly peak load, used in the hourly peak load model for all simulations.

Hour	Winter weeks 1-8 & 44-52		Summer weeks 18-30		Spring/fall weeks 9-17 & 31-43	
	Weekday	Weekend	Weekday	Weekend	Weekday	Weekend
0-1	67	78	64	74	63	75
1-2	63	72	60	70	62	73
2-3	60	68	58	66	60	69
3-4	59	66	56	65	58	66
4-5	59	64	56	64	59	65
5-6	60	65	58	62	65	65
6-7	74	66	64	62	72	68
7-8	86	70	76	66	85	74
8-9	95	80	87	81	95	83
9-10	96	88	95	86	99	89
10-11	96	90	99	91	100	92
11-12	95	91	100	93	99	94
12-13	95	90	99	93	93	91
13-14	95	88	100	92	92	90
14-15	93	87	100	91	90	90
15-16	94	87	97	91	88	86
16-17	99	91	96	92	90	85
17-18	100	100	96	94	92	88
18-19	100	99	93	95	96	92
19-20	96	97	92	95	98	100
20-21	91	94	92	100	96	97
21-22	83	92	93	93	90	95
22-23	73	87	87	88	80	90
23-24	63	81	72	80	70	85

D MATLAB Codes

In this section, selected parts of the developed MATLAB code is presented. All of the proceeding code is related to the WTG power output.

D.1 wtg_poweroutput

```

1 function [powerfraction] = wtg_poweroutput(v,A,B,C,v_ci,v_r,v_co)
2 % Returns a number between 0 and 1 corresponding to the amount of rated
3 % power a WIG can produce under the given windspeed v.
4
5 if v < v_ci
6     powerfraction = 0;
7 elseif v < v_r
8     powerfraction = A+B*v+C*v^2;
9 elseif v < v_co
10    powerfraction = 1;
11 else
12    powerfraction = 0;
13 end
14 end

```

D.2 ARMAy

```

1 function [Yt,Alphat] = ARMAy(Yt,Alphat,AR,MA,sigma,u)
2 %Receives a 5 element vector YT and 4 element Alphat, position 1 is for
3 %time = t, position 2 is for time = t-1 and so on.
4 %Generates the next Y and Alpha, and shifts the vector
5 %AR,MA and sigma is the ARMA model parameters
6 %u is a random number normally distributed number (from the randn function).
7
8 Yt = circshift(Yt,1); %moves each element one to the right, and the leftmost to
9     position 1
10 Alphat = circshift(Alphat,1);
11
12 variance = sigma^2;
13 Alphat(1,1) = variance*u; %normally distributed white noise
14
15 Yt(1,1) = AR(1)*Yt(1,2)+AR(2)*Yt(1,3)+AR(3)*Yt(1,4)+AR(4)*Yt(1,5)+Alphat(1,1)+MA(1)
16     *Alphat(1,2)+MA(2)*Alphat(1,3)+MA(3)*Alphat(1,4);
17 return

```

D.3 ARMAyCor

```

1 function [Yt,Alphat] = ARMAyCor(Yt,Alphat,Rho,AR,MA,sigma)
2 %Receives a mx5 element Matrix YT and mx4 element Alphat, column 1 is for
3 %time = t, position 2 is for time = t-1 and so on. The lines correspond to
4 %different wind sites
5 %The Rho matrix is mxm and is the correlation matrix for the m
6 %wind sites.
7 %AR,MA and sigma is the ARMA model parameters
8 %Generates the next Y and Alpha and returns them
9 m = length(Rho); %Number of values to generate
10 mu = zeros(1,m);
11 R = mvnrnd(mu,Rho); %correlated number from the normal distribution (mean(mu) of 0
12     and var (sigma) of 1)

```

```

12 for i=1:m
13     [Yt(i,:),Alphat(i,:)] = ARMAy(Yt(i,:),Alphat(i,:),AR(i,:),MA(i,:),sigma(i),R(i)
14     );
15 end
16 return

```

D.4 ARMAywind

```

1 function v = ARMAwind(mean,sd,yt)
2 v = mean+sd*yt;
3 if v < 0
4     v = 0;
5 end
6 return

```

D.5 unifrnd_corr

```

1 function Y = unifrnd_corr(Rho)
2 % Function for generating correlated random uniform distributions. Based on
3 % an algorithm from http://comisef.wikidot.com/tutorial:correlateduniformvariates
4 %
5 % Input:
6 % Rho: The correlation matrix, needs to be positive definite
7
8 Dim1 = length(Rho);
9 Dim2 = 1;
10
11 % First generate standard normally distributed numbers
12 X = randn(Dim1, Dim2);
13
14 % adjust correlations for uniforms
15 for i = 1:Dim1
16     for j = 1:Dim1
17         if i ~= j
18             Rho(i, j) = 2 * sin(pi * Rho(i, j) / 6);
19             Rho(j, i) = 2 * sin(pi * Rho(j, i) / 6);
20         end
21     end
22 end
23
24 % induce correlation
25 C = chol(Rho);
26 Y = C * X;
27
28 % create uniforms
29 Y=normcdf(Y);

```

D.6 weibull

```

1 function [v] = weibull(U_wind,alpha,beta)
2 v = alpha*(-log(U_wind))^(1/beta);
3 end

```


D.7 Solver_excerpt

```

1 % WIG
2
3 wtg_up = 0;
4 gen_wind = zeros(n_buses,1); %power generation from each bus from wtg
5 P_wind = zeros(n_buses,1); % powercurve value for each bus
6 k = find(bus_w_wind); % array with the bus nr with WIG
7
8 % Determining wind conditions
9 if n_sites == 1 % if there is only one bus with wind (k is a single number)
10     if windmodel %ARMA model
11         [Yt, Alphas] = ARMAyCor(Yt, Alphas, Rho, AR, MA, sigma);
12         v = ARMAwind(mean_wind, SD_wind, Yt(1,1));
13     else %Weibull model
14         U_wind = rand(); % generate uniformly distributed random number
15         v = weibull(U_wind, alpha, beta); % wind speed
16     end
17     P_wind(k) = wtg_poweroutput(v, A, B, C, V_ci, V_r, V_co); % determine available
        capacity of rated value
18 % Considering correlation:
19 elseif n_sites > 0 && n_sites <= 4 % if there are correlated wind sites
20     v = zeros(n_sites,1);
21     if windmodel %ARMA model
22         [Yt, Alphas] = ARMAyCor(Yt, Alphas, Rho, AR, MA, sigma);
23         for j=1:n_sites
24             v(j) = ARMAwind(mean_wind(j), SD_wind(j), Yt(j,1));
25         end
26     else %Weibull model
27         U_wind = unifrnd_corr(Rho); % generate a set of correlated random numbers
            with correlation from 0 to 1
28         for j=1:n_sites
29             v(j) = weibull(U_wind(j), alpha(j), beta(j)); % wind speed at location j
30         end
31     end
32     for j=1:n_sites
33         P_wind(k(j)) = wtg_poweroutput(v(j), A(j), B(j), C(j), V_ci(j), V_r(j), V_co(j));
            % determine available capacity of rated value at location j
34     end
35 end

```

D.8 WTGSamplingSS

```

1 for j = 1:n_wtg
2     x = rand();
3     if x >= generation_wind(j,7)
4         gen_wind(generation_wind(j,2),1) = gen_wind(generation_wind(j,2),1) +
            generation_wind(j,1)*P_wind(generation_wind(j,2),1);
5         wtg_up = wtg_up + 1;
6     end
7 end

```

D.9 WTGSamplingST

```
1 for j = 1:n_wtg
2     if comp_states(j+n_generators,3) == 0 %WIG states stored after the regular
3         generators
4             gen_wind(generation_wind(j,2),1) = gen_wind(generation_wind(j,2),1) +
5                 generation_wind(j,1)*P_wind(generation_wind(j,2),1);
6             wtg-up = wtg-up + 1;
7         end
8     end
9 end
```

E LOLE-estimates

The result section of this thesis focused on the estimates of the EENS-index. The estimates of the LOLE-index are presented in this section to provide additional information about the results. The presented estimates were obtained by 1000 simulation years for the State Sampling approach, and 7500 simulation years for the State Transition approach.

E.1 MRBTS: 20MW WECS with the Swift Current wind-regime

E.1.1 DC

E.1.1.1 State Sampling

Table E.1: Obtained LOLE-estimates for the MRBTSSW-4 State Sampling DC-case study, corresponding to Table 4.3.

Bus nr.	Priority order	LOLE (hours/year)		
		MRBTS	MRBTSSW-ARMA	MRBTSSW-WB
2	1	0.0030	0.0010	0.0020
3	5	1.1300	0.8890	0.8830
4	3	0.0010	0.0000	0.0000
5	2	0.0100	0.0100	0.0120
6	4	0.0180	0.0200	0.0210
System	-	1.1480	0.9090	0.9060

E.1.1.2 State Transition

Table E.2: Obtained LOLE-estimates for the MRBTSSW-4 State Transition DC-case study, corresponding to Table 4.4

Bus nr.	Priority order	LOLE (hours/year)		
		MRBTS	MRBTSSW-ARMA	MRBTSSW-WB
2	1	0.0000	0.0013	0.0039
3	5	1.1243	0.8067	0.8901
4	3	0.0000	0.0002	0.0019
5	2	0.0067	0.0104	0.0159
6	4	0.0252	0.0222	0.0339
System	-	1.1495	0.8293	0.9257

E.1.2 AC**E.1.2.1 State Sampling**

Table E.3: Obtained LOLE-estimates for the MRBT SW-4 State Sampling AC-case study, corresponding to Table 4.5.

Bus nr.	Priority order	LOLE (hours/year)		
		MRBTS	MRBT SW-ARMA	MRBT SW-WB
2	1	0.0010	0.0030	0.0020
3	5	1.8110	1.4400	1.4800
4	3	0.0000	0.0020	0.0000
5	2	0.0120	0.0100	0.0120
6	4	0.3120	0.2340	0.2660
System	-	1.9360	1.5210	1.5810

E.1.2.2 State Transition

Table E.4: Obtained LOLE-estimates for the MRBT SW-4 State Transition AC-case study, corresponding to Table 4.6.

Bus nr.	Priority order	LOLE (hours/year)		
		MRBTS	MRBT SW-ARMA	MRBT SW-WB
2	1	0.0019	0.0007	0.0012
3	5	1.8685	1.4543	1.3860
4	3	0.0000	0.0000	0.0004
5	2	0.0104	0.0139	0.0123
6	4	0.2921	0.2289	0.2556
System	-	1.9952	1.5375	1.4816

E.2 RTS: 600MW WECS with the Swift Current wind-regime

The following estimates are from the DC-based contingency solver.

E.2.1 State Sampling

Table E.5: Obtained LOLE-estimates for the RTSW-19 State Sampling case study, corresponding to Table 4.9.

Bus nr.	LOLE (hours/year)		
	RTS	RTSW-19-ARMA	RTSW-19-WB
2	0.0000	0.0000	0.0000
3	0.0000	0.0000	0.0000
4	0.0013	0.0000	0.0010
5	0.0027	0.0020	0.0000
6	0.0053	0.0060	0.0070
7	2.9960	3.0190	3.0720
8	0.0013	0.0020	0.0040
9	9.3267	5.8060	5.7400
10	0.1373	0.0670	0.0580
11	0.0000	0.0000	0.0000
12	0.0000	0.0000	0.0000
13	0.0000	0.0000	0.0000
14	2.8573	1.6660	1.7100
15	0.0000	0.0000	0.0000
16	0.0000	0.0000	0.0000
17	0.0000	0.0000	0.0000
18	0.0120	0.0050	0.0050
19	0.6493	0.3550	0.3790
20	0.0000	0.0000	0.0000
System	12.3240	8.8320	8.8160

E.2.2 State Transition

Table E.6: Obtained LOLE-estimates for the RTSW-19 State Transition case study, corresponding to Table 4.10.

Bus nr.	LOLE (hours/year)		
	RTS	RTSW-19-ARMA	RTSW-19-WB
2	0.0000	0.0000	0.0000
3	0.0000	0.0000	0.0005
4	0.0000	0.0012	0.0037
5	0.0000	0.0017	0.0003
6	0.0171	0.0032	0.0064
7	2.9495	2.9633	3.0991
8	0.0005	0.0003	0.0011
9	9.4100	5.6648	5.6215
10	0.1263	0.0628	0.0460
11	0.0000	0.0000	0.0000
12	0.0000	0.0000	0.0000
13	0.0000	0.0000	0.0000
14	2.8861	1.6264	1.5979
15	0.0000	0.0000	0.0000
16	0.0000	0.0000	0.0000
17	0.0000	0.0000	0.0000
18	0.0119	0.0095	0.0048
19	0.6507	0.3216	0.3084
20	0.0000	0.0000	0.0005
System	12.3695	8.6305	8.7257

E.3 RBTS: 20MW WECS with the Ørland wind-regime

E.3.1 State Sampling

Table E.7: Obtained LOLE-estimates for the Ørland RBTSW-4 State Sampling case study, corresponding to Table 4.23.

Bus nr.	LOLE (hours/year)		
	RBTS	RBTSW-4-ARMA	RBTSW-4-WB
2	0.0010	0.0020	0.0000
3	1.1010	0.5940	0.6330
4	0.0000	0.0010	0.0000
5	0.0070	0.0110	0.0150
6	9.9970	9.9780	9.9930
System	11.0980	10.5730	10.6260

E.3.2 State Transition

Table E.8: Obtained LOLE-estimates for the Ørland RBTSW-4 State Transition case study, corresponding to Table 4.24.

Bus nr.	LOLE (hours/year)		
	RBTS	RBTSW-4-ARMA	RBTSW-4-WB
2	0.0017	0.0012	0.0007
3	1.0747	0.5505	0.5885
4	0.0005	0.0000	0.0000
5	0.0161	0.0088	0.0111
6	9.9795	9.8519	9.6475
System	11.0540	10.4023	10.2367

E.4 RTS: 600MW WECS with the Ørland wind-regime

E.4.1 State Sampling

Table E.9: Obtained LOLE-estimates for the Ørland RTSW-19 State Sampling case study, corresponding to Table 4.25.

Bus nr.	LOLE (hours/year)		
	RTS	RTSW-19-ARMA	RTSW-19-WB
2	0.0000	0.0000	0.0000
3	0.0000	0.0000	0.0000
4	0.0013	0.0010	0.0020
5	0.0027	0.0000	0.0000
6	0.0053	0.0030	0.0040
7	2.9960	3.0080	3.0540
8	0.0013	0.0070	0.0040
9	9.3267	3.6830	3.9980
10	0.1373	0.0380	0.0500
11	0.0000	0.0000	0.0000
12	0.0000	0.0000	0.0000
13	0.0000	0.0000	0.0000
14	2.8573	1.1020	1.1730
15	0.0000	0.0000	0.0000
16	0.0000	0.0000	0.0000
17	0.0000	0.0000	0.0000
18	0.0120	0.0060	0.0020
19	0.6493	0.2290	0.2460
20	0.0000	0.0000	0.0000
System	12.3240	6.6970	7.0550

E.4.2 State Transition

Table E.10: Obtained LOLE-estimates for the Ørland RTSW-19 State Transition case study, corresponding to Table 4.26.

Bus nr.	LOLE (hours/year)		
	RTS	RTSW-19-ARMA	RTSW-19-WB
2	0.0000	0.0000	0.0000
3	0.0000	0.0000	0.0000
4	0.0000	0.0012	0.0150
5	0.0000	0.0008	0.0000
6	0.0171	0.0073	0.0000
7	2.9495	2.9489	3.2380
8	0.0005	0.0029	0.0060
9	9.4100	3.6099	3.8150
10	0.1263	0.0445	0.0070
11	0.0000	0.0000	0.0000
12	0.0000	0.0000	0.0000
13	0.0000	0.0000	0.0000
14	2.8861	1.0844	1.0640
15	0.0000	0.0000	0.0000
16	0.0000	0.0000	0.0000
17	0.0000	0.0000	0.0000
18	0.0119	0.0037	0.0000
19	0.6507	0.2385	0.1850
20	0.0000	0.0000	0.0000
System	12.3695	6.5701	7.0630

E.5 Wind Speed Correlation

Table E.11: Obtained LOLE-results for wind speed correlation at RTS using Ørland wind data, corresponding to Table 4.27

R	RTS	RTSW-1&3
0.0	12.3240	5.6060
0.2		5.7700
0.5		5.9220
0.8		6.2330
1.0		6.5570

F Standard Deviation of EENS-estimates

The standard deviation of the EENS-estimates, presented in section 4, is presented in this section to provide additional information about the results.

F.1 MRBTS: 20MW WECS with the Swift Current wind-regime

F.1.1 DC

F.1.1.1 State Sampling

Table F.1: EENS standard deviation for the MRBT SW-4 State Sampling DC-case study, corresponding to Table 4.3.

Bus nr.	Priority order	EENS SD (MWh/year)		
		MRBTS	MRBT SW-ARMA	MRBT SW-WB
2	1	0.6810	0.5343	0.4257
3	5	13.5082	12.1806	11.9310
4	3	0.5801	0.0000	0.0000
5	2	1.2708	1.3420	1.5600
6	4	1.6137	1.8254	1.8952
System	-	14.1863	12.6276	12.2844

F.1.1.2 State Transition

Table F.2: EENS standard deviation for the MRBT SW-4 State Transition DC-case study, corresponding to Table 4.4

Bus nr.	Priority order	EENS SD (MWh/year)		
		MRBTS	MRBT SW-ARMA	MRBT SW-WB
2	1	0.0000	1.1856	2.5061
3	5	48.8941	46.0419	51.0572
4	3	0.0000	1.1450	3.8160
5	2	2.9157	3.6694	5.7064
6	4	7.1086	5.4752	7.2019
System	-	49.6331	46.9933	53.0567

F.1.2 AC**F.1.2.1 State Sampling**

Table F.3: EENS standard deviation for the MRBTSSW-4 State Sampling AC-case study, corresponding to Table 4.5.

Bus nr.	Priority order	EENS SD (MWh/year)		
		MRBTS	MRBTSSW-ARMA	MRBTSSW-WB
2	1	0.2838	0.7833	0.6165
3	5	17.2479	16.0706	15.5962
4	3	0.0000	1.0379	0.0000
5	2	1.4691	1.3170	1.3733
6	4	3.4780	3.2999	3.1794
System	-	17.7626	17.3291	16.3566

F.1.2.2 State Transition

Table F.4: EENS standard deviation for the MRBTSSW-4 State Transition AC-case study, corresponding to Table 4.6.

Bus nr.	Priority order	EENS SD (MWh/year)		
		MRBTS	MRBTSSW-ARMA	MRBTSSW-WB
2	1	0.9692	0.3983	0.9099
3	5	69.1212	60.8691	63.6478
4	3	0.0000	0.0000	0.0035
5	2	4.7244	5.5774	3.7582
6	4	8.9503	9.0716	8.6036
System	-	70.6272	63.2220	65.2534

F.2 RTS: 600MW WECS with the Swift Current wind-regime

The following results are from the DC-based contingency solver.

F.2.1 State Sampling

Table F.5: EENS standard deviation for the RTSW-19 State Sampling case study, corresponding to Table 4.9.

Bus nr.	EENS SD (MWh/year)		
	RTS	RTSW-19-ARMA	RTSW-19-WB
2	0.0000	0.0000	0.0000
3	0.0000	0.0000	0.0000
4	1.6407	0.0000	1.5297
5	2.5008	2.0777	0.0000
6	5.9711	5.5154	6.3840
7	139.6530	131.2178	141.5159
8	4.6609	5.1848	6.5938
9	329.1633	260.9371	249.9112
10	33.2556	23.3307	20.8728
11	0.0000	0.0000	0.0000
12	0.0000	0.0000	0.0000
13	0.0000	0.0000	0.0000
14	187.2805	143.4107	143.2692
15	0.0000	0.0000	0.0000
16	0.0000	0.0000	0.0000
17	0.0000	0.0000	0.0000
18	11.2353	3.7269	5.3222
19	81.2594	60.6113	59.4109
20	0.0000	0.0000	0.0000
System	543.3354	434.9150	421.0708

F.2.2 State Transition

Table F.6: EENS standard deviation for the RTSW-19 State Transition case study, corresponding to Table 4.10.

Bus nr.	EENS SD (MWh/year)		
	RTS	RTSW-19-ARMA	RTSW-19-WB
2	0.0000	0.0000	0.0000
3	0.0000	0.0000	2.2712
4	0.0000	3.3389	7.1793
5	0.0000	3.9945	1.2412
6	48.0552	11.2977	25.5380
7	602.5205	606.5070	618.4287
8	4.9519	3.6391	6.8938
9	1831.0792	1215.3086	1198.4664
10	130.7653	82.2651	50.2299
11	0.0000	0.0000	0.0000
12	0.0000	0.0000	0.0000
13	0.0000	0.0000	0.0000
14	937.3787	606.6591	560.7682
15	0.0000	0.0000	0.0000
16	0.0000	0.0000	0.0000
17	0.0000	0.0000	0.0000
18	29.5982	22.6606	26.5209
19	368.9624	220.1699	171.7167
20	0.0000	0.0000	5.5294
System	3092.5412	2056.3529	1961.5700

F.3 RBTS: 20MW WECS with the Ørland wind-regime

F.3.1 State Sampling

Table F.7: EENS standard deviation for the Ørland RBTSW-4 State Sampling case study, corresponding to Table 4.23.

Bus nr.	EENS SD (MWh/year)		
	RBTS	RBTSW-4-ARMA	RBTSW-4-WB
2	0.5405	0.6691	0.0000
3	13.6680	9.2314	10.0642
4	0.0000	1.0483	0.0000
5	0.9528	1.3680	1.5893
6	39.5297	40.0334	39.6479
System	41.3728	41.0921	40.6953

F.3.2 State Transition

Table F.8: EENS standard deviation for the Ørland RBTSW-4 State Transition case study, corresponding to Table 4.24.

Bus nr.	EENS SD (MWh/year)		
	RBTS	RBTSW-4-ARMA	RBTSW-4-WB
2	1.3282	1.1252	0.3398
3	51.0038	31.9836	38.7043
4	0.8594	0.0000	0.0000
5	4.5669	3.1741	5.3663
6	174.5738	174.8356	173.6524
System	182.3240	177.5581	177.6530

F.4 RTS: 600MW WECS with the Ørland wind-regime

F.4.1 State Sampling

Table F.9: EENS standard deviation for the Ørland RTSW-19 State Sampling case study, corresponding to Table 4.25.

Bus nr.	EENS SD (MWh/year)		
	RTS	RTSW-19-ARMA	RTSW-19-WB
2	0.0000	0.0000	0.0000
3	0.0000	0.0000	0.0000
4	1.6407	1.0288	1.3334
5	2.5008	0.0030	0.0000
6	5.9711	4.4012	5.8573
7	139.6530	136.0924	134.8930
8	4.6609	8.0612	0.0000
9	329.1633	200.1587	205.8979
10	33.2556	19.4506	20.1699
11	0.0000	0.0000	0.0000
12	0.0000	0.0000	0.0000
13	0.0000	0.0000	0.0000
14	187.2805	112.8568	110.2488
15	0.0000	0.0000	0.0000
16	0.0000	0.0000	0.0000
17	0.0000	0.0000	0.0000
18	11.2353	9.7898	7.2374
19	81.2594	45.2319	48.9526
20	0.0000	0.0000	0.0000
System	543.3354	342.1445	343.0130

F.4.2 State Transition

Table F.10: EENS standard deviation for the Ørland RTSW-19 State Transition case study, corresponding to Table 4.26.

Bus nr.	EENS SD (MWh/year)		
	RTS	RTSW-19-ARMA	RTSW-19-WB
2	0.0000	0.0000	0.0000
3	0.0000	0.0000	0.0000
4	0.0000	2.9311	14.8635
5	0.0000	3.4865	0.0000
6	48.0552	30.2664	0.0000
7	602.5205	591.1358	621.1638
8	4.9519	11.7202	18.5738
9	1831.0792	891.8497	766.5484
10	130.7653	57.1881	3.1849
11	0.0000	0.0000	0.0000
12	0.0000	0.0000	0.0000
13	0.0000	0.0000	0.0000
14	937.3787	461.8822	322.8944
15	0.0000	0.0000	0.0000
16	0.0000	0.0000	0.0000
17	0.0000	0.0000	0.0000
18	29.5982	12.4990	0.0000
19	368.9624	174.5497	78.7133
20	0.0000	0.0000	0.0000
System	3092.5412	1579.3601	1261.4750

F.5 Wind Speed Correlation

Table F.11: EENS standard deviation for wind speed correlation at RTS using Ørland wind data, corresponding to Table 4.27

R	RTS	RTSW-1&3
0.0	543.3354	294.9610
0.2		306.1436
0.5		313.0472
0.8		325.8158
1.0		340.5673

G Standard Deviation of LOLE-estimates

The standard deviation of the LOLE-estimates, presented in Appendix E, is presented in this section to provide additional information about the results.

G.1 MRBTS: 20MW WECS with the Swift Current wind-regime

G.1.1 DC

G.1.1.1 State Sampling

Table G.1: LOLE standard deviation for the MRBTSW-4 State Sampling DC-case study, corresponding to Table E.1.

Bus nr.	Priority order	LOLE SD (hours/year)		
		MRBTS	MRBTSW-ARMA	MRBTSW-WB
2	1	0.0547	0.0316	0.0447
3	5	1.0441	0.9474	0.9446
4	3	0.0316	0.0000	0.0000
5	2	0.0995	0.0995	0.1089
6	4	0.1330	0.1401	0.1435
System	-	1.0579	0.9611	0.9550

G.1.1.2 State Transition

Table G.2: LOLE standard deviation for the MRBTSW-4 State Transition DC-case study, corresponding to Table E.2

Bus nr.	Priority order	LOLE SD (hours/year)		
		MRBTS	MRBTSW-ARMA	MRBTSW-WB
2	1	0.0000	0.0905	0.1792
3	5	4.2863	3.5002	3.5851
4	3	0.0000	0.0404	0.1317
5	2	0.2513	0.2979	0.4313
6	4	0.5586	0.4580	0.5856
System	-	4.3218	3.5271	3.6339

G.1.2 AC**G.1.2.1 State Sampling**

Table G.3: LOLE standard deviation for the MRBTSW-4 State Sampling AC-case study, corresponding to Table E.3.

Bus nr.	Priority order	LOLE SD (hours/year)		
		MRBTS	MRBTSW-ARMA	MRBTSW-WB
2	1	0.0316	0.0547	0.0447
3	5	1.3134	1.2206	1.2701
4	3	0.0000	0.0447	0.0000
5	2	0.1089	0.0995	0.1089
6	4	0.5648	0.4811	0.5172
System	-	1.3527	1.2582	1.3066

G.1.2.2 State Transition

Table G.4: LOLE standard deviation for the MRBTSW-4 State Transition AC-case study, corresponding to Table E.4.

Bus nr.	Priority order	LOLE SD (hours/year)		
		MRBTS	MRBTSW-ARMA	MRBTSW-WB
2	1	0.1007	0.0416	0.0841
3	5	5.4772	4.7393	4.4780
4	3	0.0000	0.0000	0.0346
5	2	0.3440	0.4031	0.3276
6	4	1.3145	1.2498	1.2899
System	-	5.5356	4.8047	4.5284

G.2 RTS: 600MW WECS with the Swift Current wind-regime

The following estimates are from the DC-based contingency solver.

G.2.1 State Sampling

Table G.5: LOLE standard deviation for the RTSW-19 State Sampling case study, corresponding to Table E.5.

Bus nr.	LOLE SD (hours/year)		
	RTS	RTSW-19-ARMA	RTSW-19-WB
2	0.0000	0.0000	0.0000
3	0.0000	0.0000	0.0000
4	0.0365	0.0000	0.0316
5	0.0516	0.0447	0.0000
6	0.0729	0.0773	0.0834
7	1.7702	1.6270	1.8083
8	0.0365	0.0447	0.0632
9	3.0542	2.4654	2.2400
10	0.3670	0.2580	0.2464
11	0.0000	0.0000	0.0000
12	0.0000	0.0000	0.0000
13	0.0000	0.0000	0.0000
14	1.6957	1.3192	1.3243
15	0.0000	0.0000	0.0000
16	0.0000	0.0000	0.0000
17	0.0000	0.0000	0.0000
18	0.1090	0.0706	0.0706
19	0.8370	0.6192	0.6275
20	0.0000	0.0000	0.0000
System	3.5222	2.9874	2.8280

G.2.2 State Transition

Table G.6: LOLE standard deviation for the RTSW-19 State Transition case study, corresponding to Table E.6.

Bus nr.	LOLE SD (hours/year)		
	RTS	RTSW-19-ARMA	RTSW-19-WB
2	0.0000	0.0000	0.0000
3	0.0000	0.0000	0.0462
4	0.0000	0.0739	0.1624
5	0.0000	0.0986	0.0231
6	0.5831	0.1673	0.2856
7	7.7456	7.7604	7.8857
8	0.0462	0.0231	0.0712
9	16.5727	11.2552	11.2092
10	1.3763	0.7921	0.5433
11	0.0000	0.0000	0.0000
12	0.0000	0.0000	0.0000
13	0.0000	0.0000	0.0000
14	8.2527	5.4404	5.2141
15	0.0000	0.0000	0.0000
16	0.0000	0.0000	0.0000
17	0.0000	0.0000	0.0000
18	0.3426	0.2679	0.1818
19	3.5487	2.1707	1.8599
20	0.0000	0.0000	0.0462
System	18.3845	13.6941	13.6127

G.3 RBTS: 20MW WECS with the Ørland wind-regime

G.3.1 State Sampling

Table G.7: LOLE standard deviation for the Ørland RBTSW-4 State Sampling case study, corresponding to Table E.7.

Bus nr.	LOLE SD (hours/year)		
	RBTS	RBTSW-4-ARMA	RBTSW-4-WB
2	0.0316	0.0447	0.0000
3	1.0516	0.7481	0.7918
4	0.0000	0.0316	0.0000
5	0.0834	0.1044	0.1296
6	3.0927	3.1924	3.1485
System	3.2660	3.2872	3.2194

G.3.2 State Transition

Table G.8: LOLE standard deviation for the Ørland RBTSW-4 State Transition case study, corresponding to Table E.8.

Bus nr.	LOLE (hours/year)		
	RBTS	RBTSW-4-ARMA	RBTSW-4-WB
2	0.1039	0.0739	0.0383
3	4.0493	2.6894	2.8009
4	0.0462	0.0000	0.0000
5	0.4032	0.2437	0.3885
6	14.0421	14.1324	14.0866
System	14.6005	14.3759	14.2994

G.4 RTS: 600MW WECS with the Ørland wind-regime

G.4.1 State Sampling

Table G.9: LOLE standard deviation for the Ørland RTSW-19 State Sampling case study, corresponding to Table E.9.

Bus nr.	LOLE (hours/year)		
	RTS	RTSW-19-ARMA	RTSW-19-WB
2	0.0000	0.0000	0.0000
3	0.0000	0.0000	0.0000
4	0.0365	0.0316	0.0447
5	0.0516	0.0030	0.0000
6	0.0729	0.0547	0.0632
7	1.7702	1.7225	1.7158
8	0.0365	0.0834	0.0000
9	3.0542	1.9587	1.9844
10	0.3670	0.1913	0.2270
11	0.0000	0.0000	0.0000
12	0.0000	0.0000	0.0000
13	0.0000	0.0000	0.0000
14	1.6957	1.0142	1.0650
15	0.0000	0.0000	0.0000
16	0.0000	0.0000	0.0000
17	0.0000	0.0000	0.0000
18	0.1090	0.0773	0.0447
19	0.8370	0.4741	0.4957
20	0.0000	0.0000	0.0000
System	3.5222	2.5518	2.6753

G.4.2 State Transition

Table G.10: LOLE standard deviation for the Ørland RTSW-19 State Transition case study, corresponding to Table E.10.

Bus nr.	LOLE (hours/year)		
	RTS	RTSW-19-ARMA	RTSW-19-WB
2	0.0000	0.0000	0.0000
3	0.0000	0.0000	0.0000
4	0.0000	0.0663	0.3419
5	0.0000	0.0589	0.0000
6	0.5831	0.3841	0.0000
7	7.7456	7.5457	7.8690
8	0.0462	0.1479	0.1897
9	16.5727	8.2201	7.3676
10	1.3763	0.6472	0.1047
11	0.0000	0.0000	0.0000
12	0.0000	0.0000	0.0000
13	0.0000	0.0000	0.0000
14	8.2527	4.0460	3.1796
15	0.0000	0.0000	0.0000
16	0.0000	0.0000	0.0000
17	0.0000	0.0000	0.0000
18	0.3426	0.1583	0.0000
19	3.5487	1.7001	1.0039
20	0.0000	0.0000	0.0000
System	18.3845	11.0923	10.6305

G.5 Wind Speed Correlation

Table G.11: LOLE standard deviation for wind speed correlation at RTS using Ørland wind data, corresponding to Table E.11

R	RTS	RTSW-1&3
0.0	3.5222	2.3787
0.2		2.4538
0.5		2.4045
0.8		2.5146
1.0		2.6431

